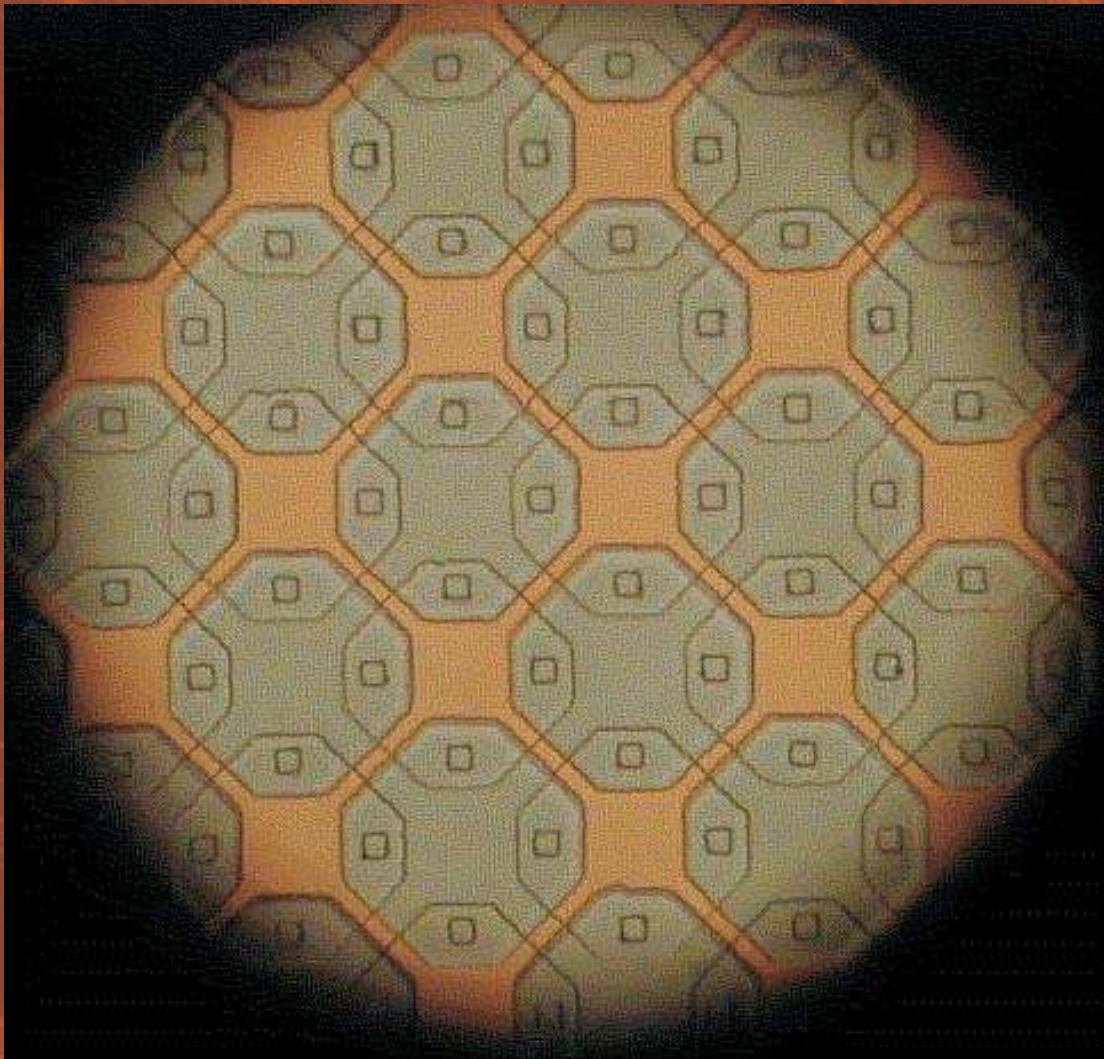


NEW DEVELOPMENTS IN JOSEPHSON JUNCTIONS RESEARCH

Editor
Sergei Sergeenkov



TRANSWORLD RESEARCH NETWORK

Contents

DC magnetic moments of SIS and SNS type Josephson junction arrays	1
E.V. Matizen and S.M. Ishikaev	
Experimental and theoretical study on 2D ordered and 3D disordered SIS type arrays of Josephson junctions	25
F.M. Araujo-Moreira and S. Sergeenkov	
Magnetization states in annular π-junction arrays	45
G. Rotoli	
Josephson junction as a prototype for synchronization of nonlinear oscillators	83
G. Filatrella	
Current-voltage characteristics and breakpoint phenomenon in intrinsic Josephson junctions	107
Yu.M. Shukrinov and F. Mahfouzi	

Transworld Research Network
37/661 (2), Fort P.O., Trivandrum-695 023, Kerala, India



New Developments in Josephson Junctions Research, 2010: 1-23
ISBN: 978-81-7895-328-1 Editor: Sergei Sergeenkov

DC magnetic moments of SIS and SNS type Josephson junction arrays

S.M. Ishikaev and E.V. Matizen

Nikolaev Institute of Inorganic Chemistry, Siberian Branch of the Russian Academy of Sciences, 630090 Novosibirsk, Russia

Abstract

Here we review our latest results on DC magnetic behavior of large SIS and SNS type Josephson junction arrays paying special attention to the influence of disorder on establishment of the so-called Self-Organized Criticality (SOC) regime in the magnetic flux distribution within the arrays. Our experiments clearly demonstrated that, contrary to some theoretical predictions, a local distortion of SNS-type arrays does not necessarily lead to formation of SOC states with flux avalanches. Besides, we have observed a substantial asymmetry in

Correspondence/Reprint request: Dr. E.V. Matizen, Nikolaev Institute of Inorganic Chemistry, Siberian Branch of the Russian Academy of Sciences, 630090 Novosibirsk, Russia. E-mail: matizen@che.nsk.su

magnetic dynamics with pronounced hysteretic behavior of the magnetization loops in SNS-type arrays..

1. Introduction

Josephson structures have given rise to a new scientific and technological trend and their study (both experimental and theoretical) remains one of the most interesting and actual problems of the modern solid state and low-temperature physics. The phenomenon of Josephson generation in these structures makes it possible to fill in the gap in a frequency range of tens and hundreds of MHz with a tunable coherent submillimetric radiation. These structures can be used to preserve and process information based on magnetic flux quanta – RSFQ-logic and ultimately realize the idea of quantum computing. In this regard, it is interesting to mention that a heterodyne radiation detector with a working frequency of 500 GHz able to receive very weak signals ($\sim 10^{-13}$ W) has been already produced and successfully tested [1].

The magnetic dynamics of Josephson junction array (JJA), as the basis for a practical application of these structures, has been reported in numerous theoretical studies (see, e.g., [2-15] and further references therein) while the experimental investigations of Josephson arrays and Josephson stacks are still limited mainly to the study on voltage-current characteristics. It is worth noting that the behavior of magnetic moments has been the subject of study in just a few experimental works [16-24] including our own efforts [20-24].

The experimental results for the magnetic properties and the processes of JJA magnetization clearly indicate that the magnetic dynamics in regular networks differs substantially from the theoretical predictions. First of all, according to theoretical calculations, in the absolutely regular JJA, no dynamic state of Self-Organized Criticality (SOC) type can be realized as far as its magnetization is concerned. However, such a state has been recorded experimentally. Besides, the asymmetry of magnetization processes observed in JJAs is also at odds with the current theory. Let us consider these two phenomena in much detail, including their experimental observation and comparison with theoretical predictions.

2. Josephson arrays: Topology and preparation

Schematically, the studied JJAs are the regular square superconducting networks with Josephson junctions inserted into their edges. The arrays of two main designs (with SIS and SNS type junctions) and different forms of superconducting islands (octagon and cross) were studied (see Figures 1-3). Configuration in the form of a cross displayed a greater cell inductance and a four times larger junction area which allowed for higher critical currents, in comparison with the octagon configuration.

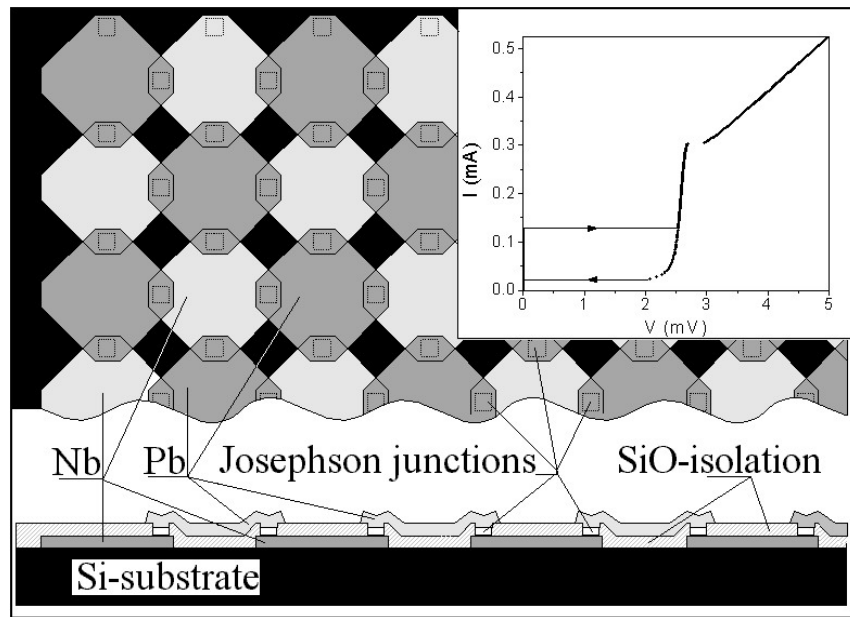


Figure 1. Geometry of Josephson SIS-type junction network. The insert shows a voltage-current characteristics of an individual SIS-junction at $T=4.2$ K.

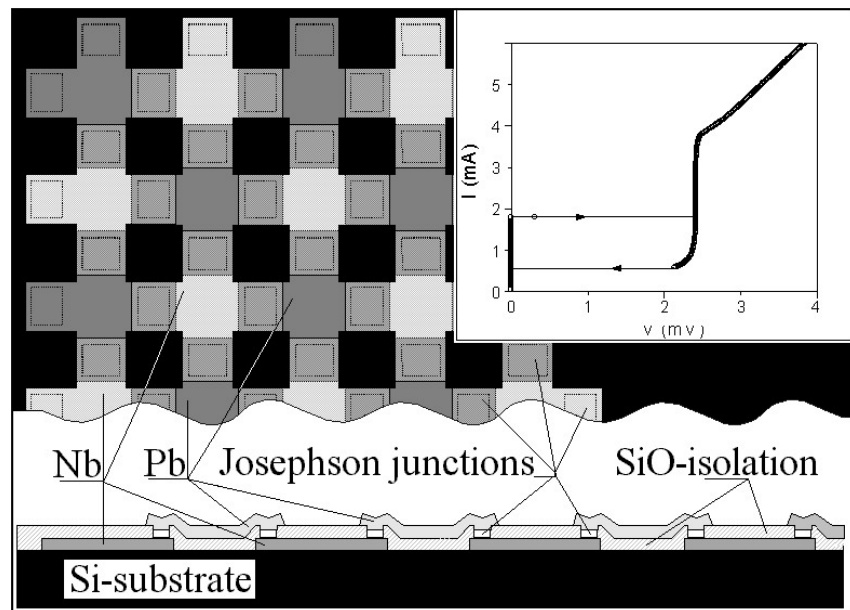


Figure 2. Geometry of Josephson SNS-type junction networks. The insert shows a voltage-current characteristics of an individual SNS-junction at $T=4.2$ K.

The arrays were produced using conventional film technologies. First, the Nb film of a thickness of ~ 100 nm was precipitated by the method of magnetron sputtering in the constant current discharge in the argon atmosphere with a pressure of about 10^{-2} mbar. Then, photolithography with subsequent chemical etching in a mixture of hydrofluoric and nitrogen acids was used to prepare a lower superconducting layer structure. The insulating layer of silicon

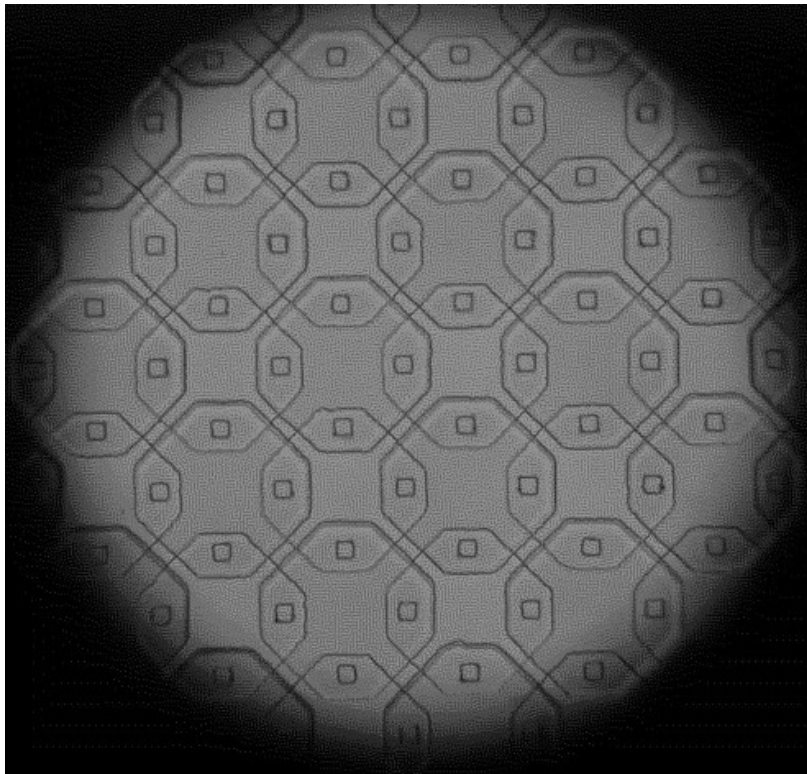


Figure 3. A fragment of the photo of SIS-type junction network.

oxide (silicon monoxide SiO) of a thickness of ~ 150 nm was precipitated using the thermal vacuum evaporation method. The lift-off photolithography was employed to produce windows in the SiO film in which a Josephson junction was then formed. The opening of windows, the spreading of photoresistive layer and the formation of image for subsequent lift-off were followed by ionic surface cleaning. The controlled oxidation of Nb surface in a mixture of argon with oxygen resulted in the formation of the tunnel NbO_x interlayer for SIS junctions, and in the case of the SNS ones, the interlayer of “dirty” Cu_{0.95}Al_{0.05} metal was used. The upper lead layer was obtained using a method similar to vacuum evaporation, that is right after the formation of the tunnel interlayer (in one vacuum cycle) with subsequent structure formation by means of lift-off photolithography. Unfortunately, it is impossible to directly apply Nb to the upper layer because of the very high temperature necessary for its deposition on a substrate. At this temperature, a complete degradation of the preliminarily produced NbO layer was registered.

The technology of SNS-type array production is almost identical to the aforementioned technology for producing SIS-type arrays. However, there are two important distinctions. The formation of windows in the layer of silicon oxide was not followed by the oxidation of Nb surface. Instead, the magnetron sputtering was used to produce a layer of a thickness of about 160 nm from Cu_{0.95}Al_{0.05}. The last layer, in this case, consisted of Nb (instead of lead) in order

Table 1. Comparative characteristics of the of SIS (Nb–NbO_x–Pb) and SNS (Nb–Cu_{0.95}Al_{0.05}–Nb) type Josephson junction arrays.

Type of junction	SIS1	SIS2	SISk	SNS
Number of meshes in array	100 × 100	100 × 100	64 × 64	100 × 100
Mesh size, μm ²	20 × 20	20 × 20	20 × 20	20 × 20
Junction area, μm ²	~7	~7	~25	~7
Critical current at 4.2 K, A	~80	~150	~1800	1500
Normal resistance, Ω	10	20	~0.7	10 ⁻³
Mesh inductance, H	~2.5 × 10 ⁻¹²	~2.5 × 10 ⁻¹²	~10 ⁻¹¹	~2.5 × 10 ⁻¹²
Junction capacity, pF	~1	~1	~3	~0.01

to provide a high stability of samples and a slightly higher temperature of a superconducting junction.

Table 1 summarizes the comparative characteristics of our SIS-type and SNS-type arrays. It is worth mentioning that the SIS-type arrays were short-lived and the changes in parameters were noticeable already after two months. In contrast, the SNS-type arrays were rather stable and preserved their properties for more than two years.

3. Experimental technique

The magnetic moment of the JJA is rather small due to the smallness of Josephson currents. Its value at temperatures of about 6 – 6.5 K does not exceed 10⁻¹¹ A·m². Hence, only sensitive enough SQUID-magnetometers can measure such small moments and their variations with magnetic field. This magnetometer is based on a high-frequency SQUID (see Figure 4). Our home-made magnetometer manifests a series of peculiarities in the design of pickup coils of flux transformer, in the method of compensating their astaticism, and in the design of a solenoid. Conventional pickup flux transformer coils are usually symmetric first-order gradiometers. Our design differs in that it was produced in the form of a symmetric second-order gradiometer [25,26]. As distinct from the classical circuit, the central coil was divided into two identical separated coils, resembling the Helmholtz ones. This offered some preferences. Namely, the microphone noise was decreased, a parasite signal of a sample rod was effectively compensated by the second-order gradiometer, and the dependence of the signal on the position of the sample was weaker.

The solenoid consisted of two superconducting parts, i.e., the outer one was short-circuit and the inner one was non-circuit. A certain field value was frozen in the short-circuit solenoid and the non-circuit one was used for continuous

Overview of SQUID-magnetometers

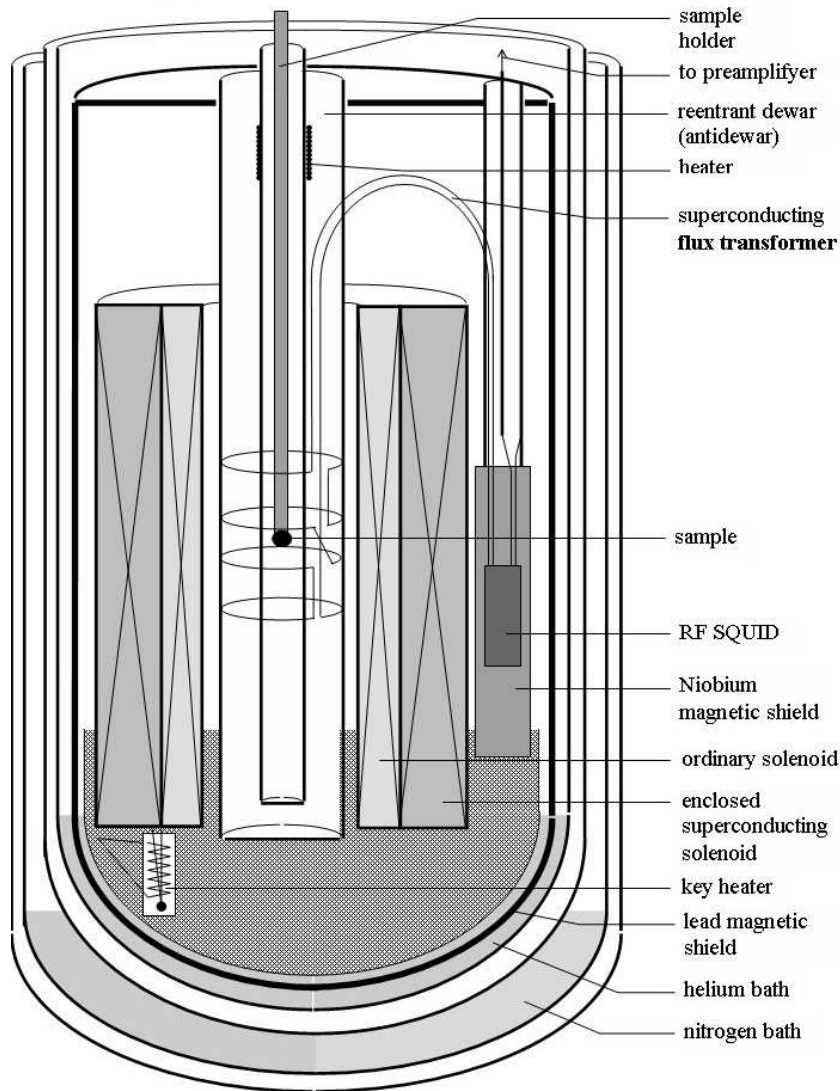


Figure 4. Overview of SQUID-magnetometers.

field variations within some limits. The astaticism of the carefully produced pickup coils was about $3 \cdot 10^{-4}$. To reach additional compensation, we introduced a small coil of several copper wire turns wound around the same mandrel as the flux transformer with mutual inductance. This coil was switched on sequentially with the non-circuit solenoid. The number of turns in it (in our case, six) was taken to compensate, to a maximum extent, the astaticism of the system of the pickup coils. During the work, the current was passed through the additional coil which differed from the solenoid one and was proportional to it with some coefficient which could be varied within certain limits. Thus, the slope of the magnetization curves can be varied by adding the field-proportional value to the sample signal which almost fully compensated the contribution of the screening currents of superconducting Nb

Table 2. SQUID – magnetometer characteristics.

Temperature range	1.5 – 270 K
Temperature measurement accuracy	0.2 K
Magnetic fields range	$10^{-3} - 5 \times 10^2$ Oe
Magnetic moment sensitivity	10^{-13} Am ²
Sample size	4 mm diameter, 5 mm length
Helium expenditure	3.5 liters per 10 hours

and Pb film electrodes. As a result, only the contribution from the currents passing through the Josephson array remained in the magnetic moment measured. Note that without this apparatus compensation, it is almost impossible to distinguish a weakly pronounced signal structure against the background of the large general slope of the magnetization curve during further treatment of the recorded signal.

To decrease drifts and interferences, the liquid helium containing the flux transformer, the solenoid, and a superconducting magnetic screen, was transferred to a superfluid state by pumping the vapor out. To this end, the measurements were performed mainly at night. The temperature was measured using a Cu+0.1%Fe - Cu+0.1%Ge thermocouple with a sensitivity of about 10 μ V/K at helium temperatures. In this case, the superconducting transitions in both Nb and Pb and the point at which helium converted into the superfluid state (which was seen as a sharp decrease in low-frequency magnetometer noise) served as the reference points.

The SQUID-magnetometer was calibrated using the samples with the magnetic moments of well-known values. When the magnetic moment sensitivity is of the order of 10^{-13} Am², the magnetometer allows measurements not only under the conditions for measuring the temperature dependence of the moment with the field frozen in the superconducting solenoid, but also at constant temperature in the regime of the field sweep. Thus, we could steadily obtain the full hysteresis loops with a good reproducibility of results. Table 2 summarizes the basic parameters of our SQUID-magnetometer.

4. Experimental results

The magnetic behavior of the JJAs with SIS and SNS type junctions is quite different [22]. The magnetic properties of the JJAs are mainly determined by flux quantization in a superconductor, which makes a vivid description in terms of fluxon dynamics more convenient. Fluxons are the magnetic flux quanta. The interaction of fluxons with a periodic potential of the array as well as their interaction with each other determine most of the peculiarities of the magnetic dynamics of the JJA.

Figures 5-8 show the typical results of the measurement of the magnetic moments of two SIS- type arrays with a continuously (at constant rate) changing field (hysteresis loops) within about ± 1 Oe and at temperatures 2 - 7 K. Before the measurements, the arrays were cooled down in a field of less than 0.1mOe which provided the absence of the Abrikosov vortices in superconducting films. Figures 5 and 6 demonstrate the hysteresis loops of the SIS-type arrays for two samples with various critical currents of the junctions at various temperatures. A change in the direction of the field sweep makes the screening currents in the array reverse their direction and the array rapidly acquires its critical state. As a result, a smoothed field configuration in the array resembles the profile obtained from the conventional Bean model: a pit at

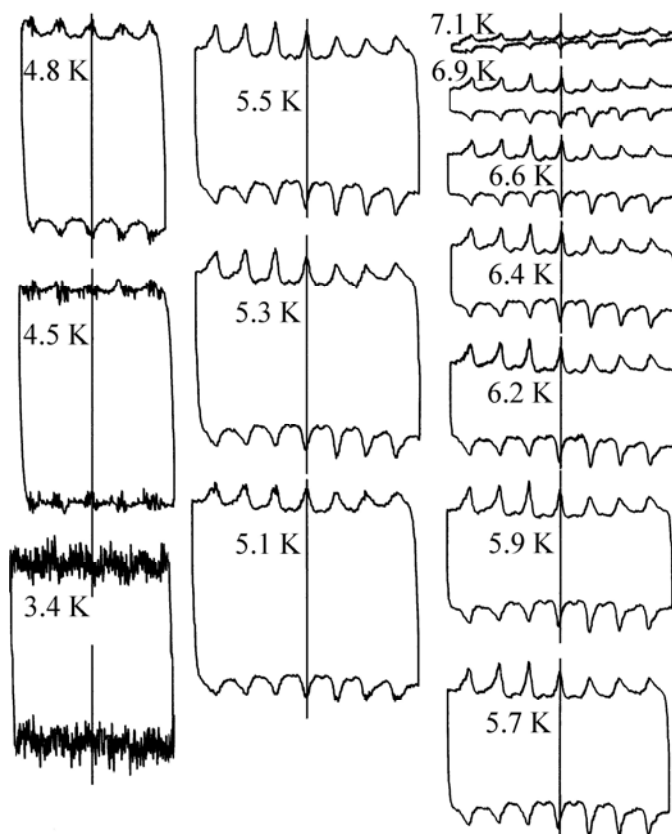


Figure 5. Magnetization curves for the SIS2 array for various temperatures.

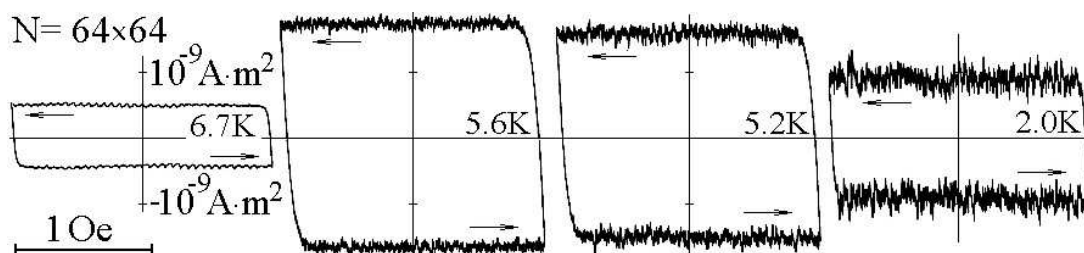


Figure 6. Magnetization curves for the SISk array for various temperatures.

the center is obtained with increasing field while a pile of fluxons is obtained with decreasing field. However, this pattern is observable only in fairly low fields. For higher fields (above 1 Oe), the magnetic moment of the array decreases (ultimately reaching a zero value) due to field-induced suppression of the critical current of the junction. In the upper part of the temperature range studied, the periodic peaks are observed in the hysteresis loops of the array (see Figures 5 and 6). The distance between the peaks corresponds to the penetration of one flux quantum through one cell, namely $\Delta H = \Phi_0/a^2$. Note that the periodicity of the magnetic array properties follows from the corresponding symmetry of the Hamiltonian of the array related to the transformation $\hat{H} \rightarrow \hat{H} + \Phi_0/a^2$. Exactly in-between the high peaks, small tubercles are observed, i.e., a unique second harmonics which corresponds to a change in the flux in the array, on the average, in one fluxon per each two cells. This obviously corresponds to the distribution of added flux quanta in the array in the form of quite stable staggered rows [27,28]. The array is supposed to contain also harmonics of higher orders related to a periodic formation of fluxon superarrays (with corresponding periods) which, however, were not observable against noise due to their smallness. As follows from Figure 5, the hysteresis loop displays minor asymmetry. In this case the peaks are smaller with decreasing field than those observed in the curve with increasing field.

In the lower part of the temperature range from 2K to 5K (depending on the critical junction current), the hysteresis loops manifest the noise-like jumps of the magnetic moment whose amplitude (unlike temperature fluctuations) increases with decreasing temperature. First, these jumps are observed at the vertices of periodic peaks of the magnetic moment and then they propagate laterally to form first compact periodic groups with a period identical to that observed in high-temperature curves. As the temperature continues to drop, these groups join to form a continuous “chatter”. Figure 7 depicts an enlarged fragment of the magnetization curve. According to this figure, the noisy behavior is actually a monotonous increase in the magnetic moment with decreasing field, interrupted by sharp staggered falls. On the other hand, as the field increases, a continuous decrease in the moment is suddenly interrupted by its staggered increase. After these jumps, the array gains (or loses) the flux quanta (whose number in our case reached hundreds of fluxons) resulting in the evident electromagnetic radiation. A characteristic time for successful monitoring of the avalanche evolutionary process should be of the order of the characteristic Josephson times for the junctions under the study (which is of the order of 10^{-12} s). We have failed to resolve such fast processes because the working frequency band for our SQUID magnetometer was about 10 Hz, meaning that a drastic change in the moment appeared as an exponential relaxation with a characteristic response time of just about 0.1 s.

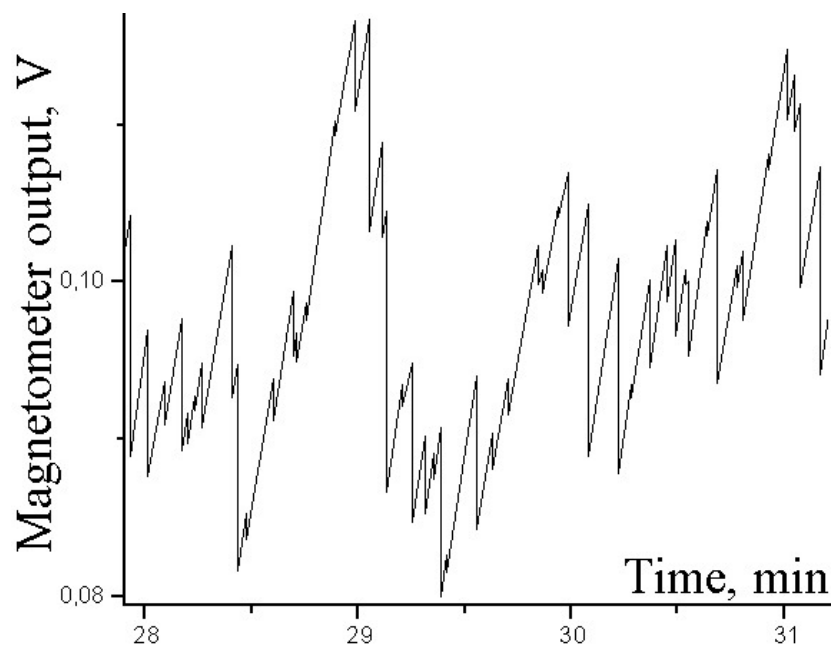


Figure 7. A fragment of magnetization curves of the SISk array at 4.1K; magnetic moment jumps (magnetic flux avalanches) are clearly seen.

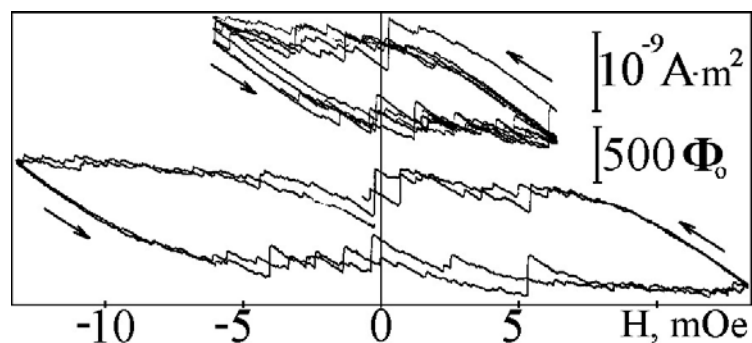


Figure 8. Hysteresis loops for the SIS1 array (containing 100x100 cells) at $T=4.15$ K in fields up to ± 15 mOe.

Figure 8 shows the random jumps (avalanches) that are independent of the field sweep. More precisely, this figure presents the magnetization curves for a continuous change in the external field within small limits ± 15 mOe at 2.15K.

The upper curve consists of four complete cycles following each other. The lower curve consists of two cycles. All the curves have the regions in which a monotonous change in the magnetic moment is interrupted by spontaneous sharp falls followed by a monotonous dependence up to the next jump. These jumps are well observed. They occur at random values of the field and demonstrate significant scattering in their amplitudes. Of special interest is the existence of monotonous and fairly reproducible regions of 5-6 mOe in the curves in which the transition to another branch of the loop occurs after turning the field direction.

5. Self-Organized Criticality (SOC) and avalanche statistics

A statistic analysis of jumps in the magnetization curves indicates the existence of SOC in the studied arrays. Due to a constant sweep rate, the field can be identified with the time also fixed during experiment.

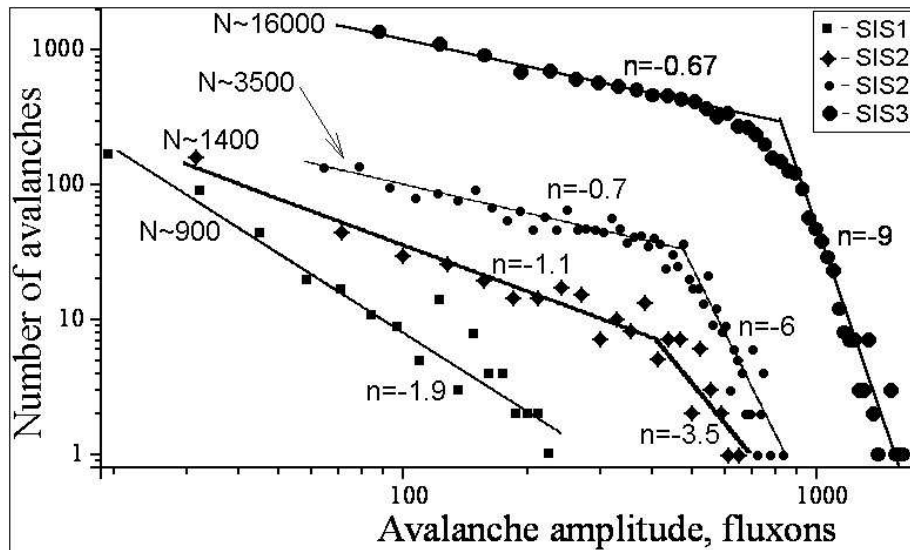


Figure 9. Distribution of magnetic moment jumps (flux avalanches) with respect to the amplitude in SIS-type junction network at $T=4.1$ K; n is a slope of straight line (with exponent $n1$), N is the number of avalanches.

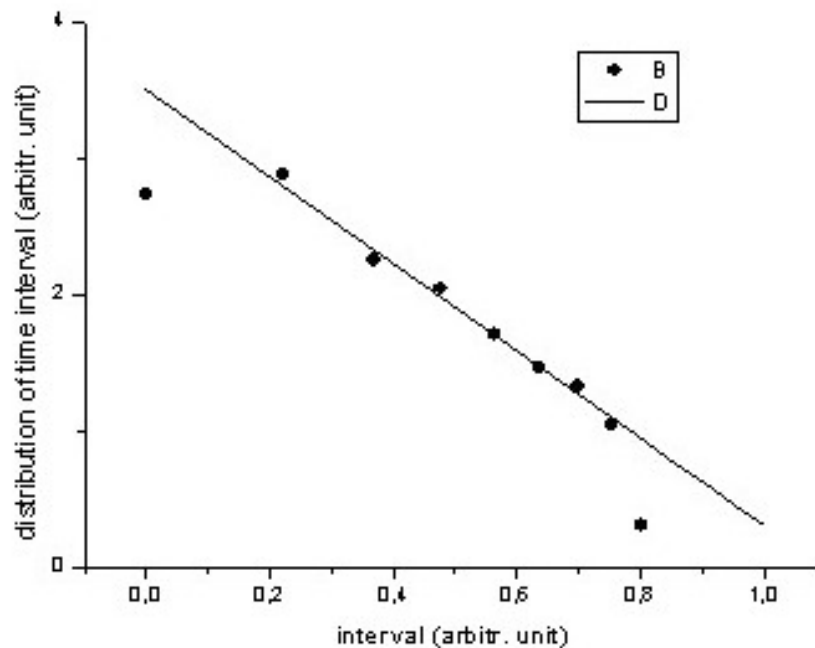


Figure 10. Distribution of time intervals with respect to time interval in Log scale; dots (experiment), solid line (fit with the slope $n2 = -3.2$).

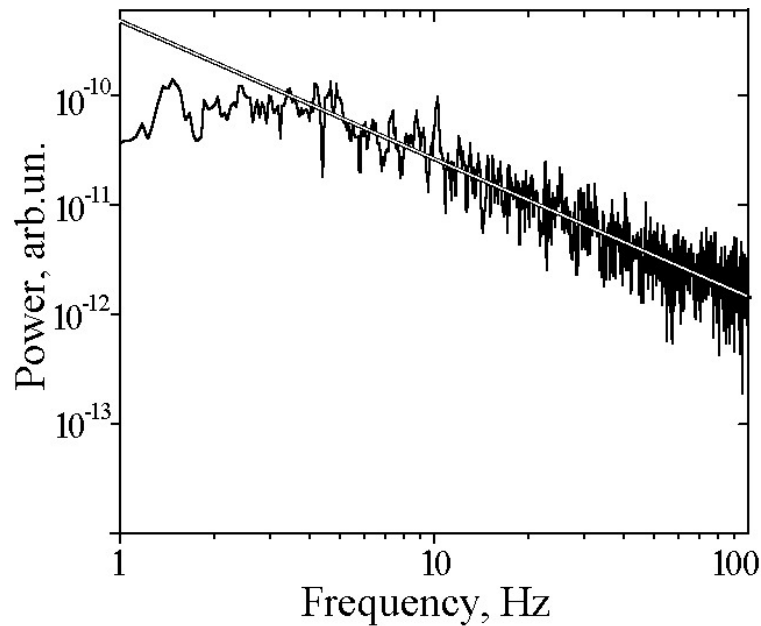


Figure 11. The Fourier spectrum for fragments in the magnetization curve corresponding to flux avalanches.

Figure 9 shows the density of the probability for appearance of avalanches depending on their amplitude on a double logarithmic scale. For low amplitudes we observe a power-like distribution $P_1(A) = P_1 A^{n_1}$. The same form is also observed for high amplitudes but with another exponent $P_2(A) = P_2 A^{n_2}$. The exponent is negative and fractional, and $|n_1| < |n_2|$. Thus, as follows from this figure, the dependence of distribution density on the avalanche amplitude has a crossover which is most pronounced in the case of a fairly large body of the data.

The density of time distribution among neighboring avalanches, and identical avalanches display a power character with nonintegral exponents (see Figure 10). It is interesting to point out that the Fourier spectrum for fragments of the magnetization curve in which the avalanches manifest themselves has a Flicker-noise type $1/f^\alpha$ – character (see Figure 11).

6. Discussion of results on SIS type arrays

It is worth mentioning that the self-organized criticality (SOC), observed in our experiments on SIS-type arrays (via avalanche relaxation) along with the obtained power dependences are widely available in the nature. To mention just a few examples, they are observed in the dynamics of granular materials, biological evolution, earthquakes, forest fires, landscape formation, solar flare, river networks, mountain ranges, volcanic activity, traffic jams, plasmas, superconductors, stock markets, brain functions, spreading epidemics etc. However, these dependences have first become the subject of study only

recently. Namely, in 1987 Bak, Tang and Wisenfeld [29] proposed a phenomenological model describing a thermodynamic system with avalanches. The phenomenon of the dynamic state of a thermodynamic system resulting in the formation of such avalanches was called the Self-Organized Criticality (SOC). The latter is related to the fractal properties of the spatial distribution of objects, displays scaling with varying system parameters, and possesses characteristic correlation functions related to avalanche spectrum. It is worth noting that the appearance of avalanches does not depend on the value of either external effect or fluctuations, and even a small action can provoke a huge avalanche (catastrophe). Another peculiarity is the fact that, despite chaotic motion, the system is self-organized, that is on average it acquires a constant parameter (e.g., the slope of the sand pile or the magnetic moment of the Josephson array). Thus, the system can sustain its own critical state which means that the SOC and the other parameters of the system do not require any adjustment. Note that the amplitude distribution of avalanches exhibits a power like character. Thus, the probability of large avalanches whose scale is limited only by system dimensions is rather high. The aforementioned objects (similar to the ones in the SOC state) can be considered as discrete systems with a great number of energy levels which are moved out of balance under the action of external factors. At some moment, these systems acquire a particular critical dynamic state which is more stable than equilibrium state and thus has lower entropy. The stationary state in such systems is sustained by avalanches. Notice that this general approach (based on nonlinear Lorentzian equations [30]) is purely phenomenological. It does not take into account any real interactions and hence, though useful for some qualitative predictions, this theory has little in common with reality. During the last 15 years after the pioneering studies on SOC [29,31,32], many different theoretical models have appeared that imitate, quite successfully, various natural phenomena, such as earthquakes [33,34], intercrossing phase transitions [35-39], quark-hadron phase transitions [40], rain phenomena [41], the propagation of forest fires [42,43], the crises in economy [44], the development of populations in biology [45], etc. Since the systems of this type include biosphere, society, infrastructures of various types, military and industrial complexes, and other hierarchical systems, the results from the studies on SOC are highly important for analyzing the potentials for control and development of the methods for protection against catastrophes.

In the scientific literature, some doubt has been cast on the adequacy of the Self-Organized Criticality theory as determined by the founders of the concept [29]. Hence, the term Self-Organized Complexity (SOCX) is often used instead of the Self-Organized Criticality (SOC). In particular, in some works, the distribution of avalanches with amplitude is different from the power like behavior typical for SOC. Both the examination based on the analysis of the statistic dependences of various processes (performed in [46]) and the

experiment on the study of the inner local avalanches of the magnetic flux in thin Nb films [47] clearly indicate that the dependence of the probability of avalanches on amplitude is often better described in terms of the stretched exponential function $P(x) \sim \exp(-(x/x_0)^\mu)$, where μ is a constant. In this case, there is a characteristic scale of avalanches x_0 , and an avalanche size distribution function is highly inhomogeneous. At present, the experimental data on SOC are obtained for a limited range of artificial objects, including the studies on the dynamics of growing sand pile [48], the motion of a piece of emery cloth over neylon carpet [49], the film boiling of nitrogen at the surface of high-temperature superconductor (HTSC) near the transition to a superconducting state [35-39], and the plastic deformation of a loaded metallic rod [50,51]. More recently, one of the creators of the SOC theory Kurt Wisenfeld together with John Linder suggested that the Josephson arrays are the ideal artificial objects for studying this universal phenomenon [52]. On one hand, this is due to the fact that the processes in the arrays can be calculated on the basis of fundamental physical laws that make it possible to deeply understand the origin of these processes, including the SOC nature. On the other hand, the arrays are convenient objects for experimental investigations. They can be modified starting from the change in the parameters of the interaction between the elements forming the array up to its total configuration.

The extensive theoretical studies on the dynamics of regular and irregular arrays were performed by Ginsburg and Savitskaya [7-15]. Their calculations for the behavior of array magnetization are based on a discrete sine-Gordon equation. Using the power character of avalanche distribution as a criterion, they have managed to determine the conditions under which the SOC can manifest itself in the arrays. Namely, they found that the condition under which the SOC state can be observed reduces to the inequality $\lambda(T) \ll a$ (or $k = \lambda/a \ll 1$), where $\lambda(T) = \Phi_0 / (\pi \mu_0 j_C(T))$ is the Josephson penetration depth of the field into the array, a is the array period, and $j_C(T)$ is the critical current of a single junction. The aforementioned inequality is equivalent to the inequality $LI_0(T) / \Phi_0 \gg 1$, where L is the inductance of one cell and $I_0(T)$ is the depinning current density.

As follows from these conditions, varying temperature (and thus, the critical current), one can pass to the region where the SOC state should exist (see Figs. 5 and 6). The criterion $LI_0(T) / \Phi_0 \gg 1$ was verified by direct measurements. The depinning current of fluxons was estimated from the half-width of magnetization hysteresis loops using a simplified assumption that the currents in the array pass over concentric square circuits. In this case, the width of the loop is proportional to the depinning current. According to this estimation, the temperature, at which the penetration depth of magnetic field into the array, $\lambda(T)$, becomes equal to the array parameter a , is $T_c \sim 6K$ (see Figure 5). This value corresponds to the temperature below which the random

jumps are observed in the magnetization curve. For the array shown in Figure 6, the depinning current is higher, so that this temperature becomes closer to the transition temperature of the upper lead junctions.

It is of interest to consider the dynamics of the motion of the system of fluxons in these two temperature domains. At high enough temperature, where $LI_C \ll \Phi_0$, one cell cannot retain a flux quantum and each fluxon is distributed over several cells. This corresponds to the condition $k \gg 1$ (weak pinning). In this case, the fluxons penetrate into the array in the form of hypervortices, covering many cells. The interaction between fluxons upon weak pinning leads to their deep penetration to the array with almost uniform distribution. The field profiles in the array in this case are maxima that are almost uniformly distributed over the array at the centers of the hypervortices (see, e.g., [53,54]). When $k \gg 1$, the fluxon extends over many cells, and the dynamics of the Josephson vortices can be described within a continuous (hydrodynamic) limit where the states with minimal energy are realized. This theoretical model is in excellent agreement with our observations because the curves shown in Figure 5 agree even in details with those calculated for the large values of the Josephson penetration depth (Cf. with Fig.14 from [3]).

On the other hand, when the value of the critical current is large, and $LI_C \gg \Phi_0$ (where L is the cell inductance, and I_C is the critical current in the Josephson junction), each cell can retain the flux of more than one quantum, and each cell can contain only the integer number of fluxons. The dynamics of fluxon motion in such a regime can be described as the motion of discrete quasiparticles localized within one cell and possessing a certain effective mass. This corresponds to $k \ll 1$ (the strong pinning state). An increase in the external magnetic field in cell contours (with initially zero current) causes an increase in the screening current and thus, in the magnetic moment of the cell. When the current reaches a critical value, a fluxon enters the cell and its magnetic moment decreases in jumps, the magnetic field penetrates the array almost discretely and synchronously over almost square contours. A system of fluxons is, in this case, in metastable states that are far from equilibrium. In this case, the field profile forms a quadrangular pit by steps from contour to contour and resembles the Bean field distribution in a volumetric type II superconductor. Recently, an interesting study on the penetration of magnetic flux into Nb films based on magneto-optics technique has been published [55,56]. A laborious analysis of the field profile performed there indicated the realization of the self-organized criticality in a given system.

7. Discussion of results on SNS type arrays

Figure 12 shows the hysteresis loops of the SNS-type array in the upper region of the temperature interval, where $\lambda(T) > a$. As compared with the SIS-type

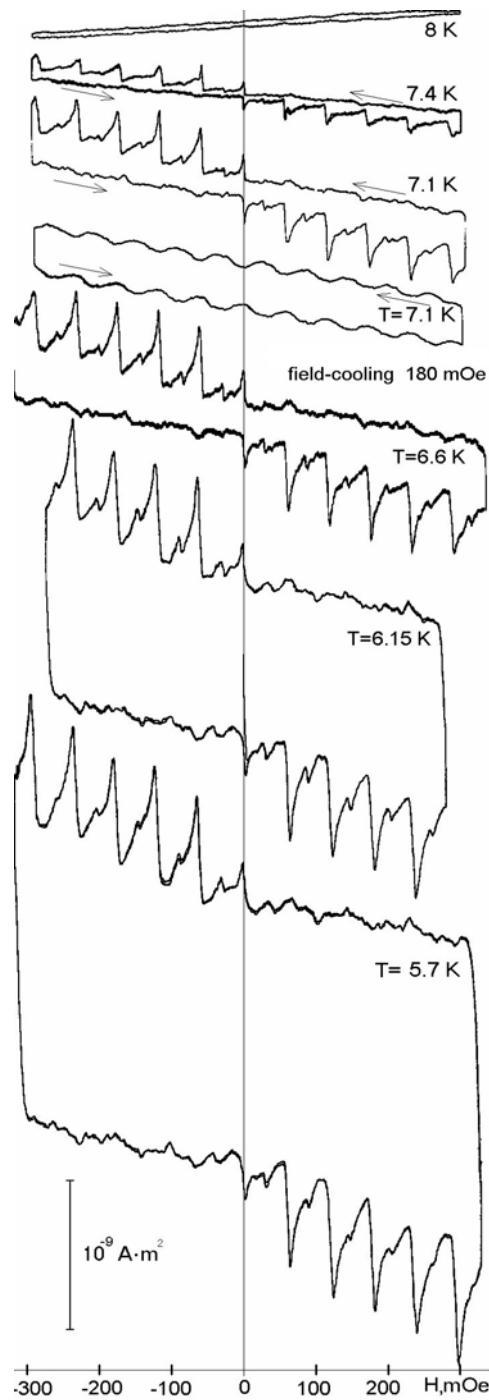


Figure 12. Magnetization curve of the SNS array at 5.7 – 8 K.

array, in this case we observe a substantial asymmetry in the magnetic flux dynamics. As the absolute value of the field increases, the character of the behavior of the magnetic moment in SNS-type array remains almost the same as the behavior of the SIS-type array moment. The magnetization curve also shows the periodic peaks located at the “pedestal” (Cf. with Figure 5 for the same temperature interval). As the absolute field value decreases, the characteristic peaks become less pronounced (in fact, they are actually absent).

The third upper hysteresis loop (shown in Figure 12) differs from the other loops. It displays neither sharp peaks nor asymmetry. In this case, the principle difference of the initial magnetic state of the system is that the array under study was cooled down below the superconducting transition temperature in a magnetic field of about 180 mOe, which caused the freezing of the Abrikosov vortices in Nb films. Obviously, the additional field created by these vortices interacts with the Josephson vortices and have a substantial effect on their motion. In Figure 13 the hysteresis loops are presented for temperatures at which $\lambda(T) < a$. In comparison with the SIS-type array, these loops show no jumps of the magnetic flux and the magnetic moment changes quite smoothly. More broad and relatively low maxima (in place of former sharp peaks) are observed in the magnetization curve because the self-fields of the currents in the SNS-type arrays (as the currents themselves) become rather important at low temperatures and have a considerable effect on fluxon distribution. In other words, the magnetic field in the array becomes, in this case, highly inhomogeneous, leading to the smearing of the peaks. The shape of the loops approaches in this case a classical form for a type II superconductor.

We have repeatedly studied the curve of the SNS-type array hysteresis in order to verify the fact that upon slow field sweep the regular peaks appear only with increasing absolute value of the field and are not observable with its decrease. Figure 14 shows the hysteresis curves obtained for various field sweep rates: 30, 150, and 100 in arbitrary units.

The middle curve (150) shows the particular hysteresis loops for various initial points: (1) an increase in the field from 0 field to point F, (2) a decrease in the field from F to G, (3) an increase in the field from G to F, (4) a decrease

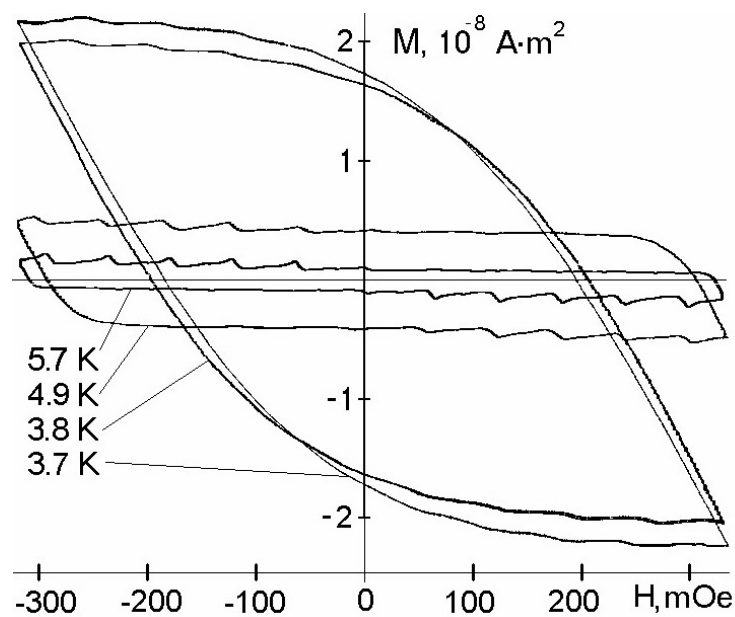


Figure 13. Magnetization curve of the SNS array at 3.7 – 5.7 K.

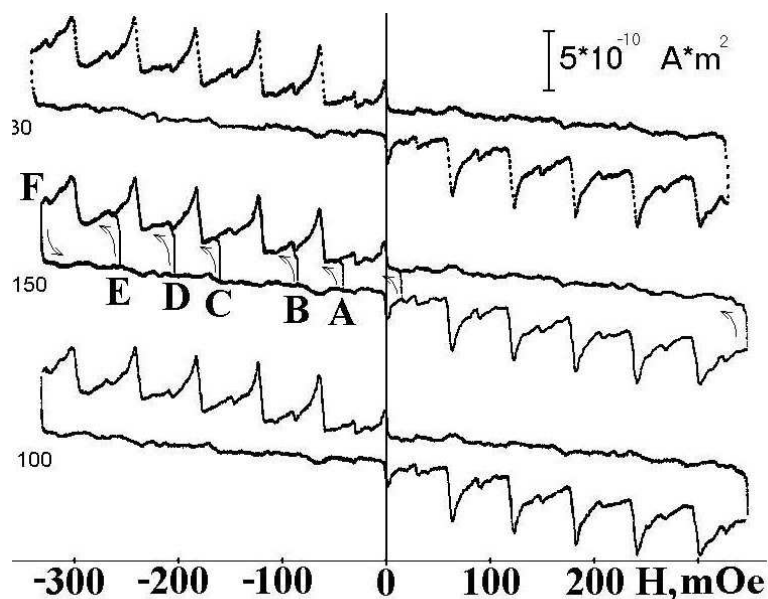


Figure 14. Magnetization curve of the SNS array for various sweep rates.

in the field from F to A, (5) an increase in the field from A to F, (6) an increase in the field from F to B, (7) an increase in the field from B to F, etc. All the curves superimpose well one another. Hence, we can conclude that at any initial field from which the measurements of the hysteresis curve are started, the peaks are observed with increasing field and are unobservable with decreasing field. Thus, we demonstrated that in the presence of a constant field, the magnetic dynamics asymmetry remains constant. This experiment proves that the penetration of the magnetic flux into the array causes periodic formation of regular spatial configurations of fluxons and the reverse process occurs randomly. In this case, the mean magnetic moment (which almost corresponds to the “pedestal” value) is symmetric.

To understand the reasons for the absence of SOC and the existence of the hysteresis loop asymmetry, we have tried to break the order of SNS-type array cell location, both within the array and along its edges. The first reason for doing this is the well-known fact that, according to the theory [7-15], the disorder in the location of the cells is enough to cause the SOC regime. Thus, by inducing the order breakdown, we expected to trigger this phenomenon. The second reason was the hope to change the regime of the motion of vortices upon their escape from the array.

Figure 16 shows the SNS-type array hysteresis loops with a different number of cells removed from the central region. In this case, the cells were removed mechanically by scribing. The removed region was in the form of a square with uneven sides that were, on average, parallel to the outer sides of the array. As it is clearly seen in the figure, the phenomenon of SOC does not manifest itself in this particular case.

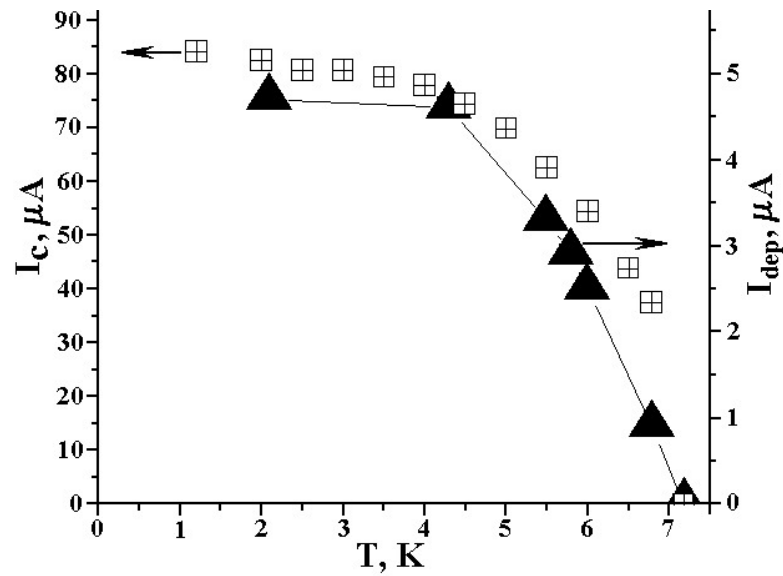


Figure 15. Temperature dependence of current in the SIS array. Triangles correspond to the estimates of current from the magnetic moment of the array, squares denote the data obtained from direct measurements of the critical current in a single junction.

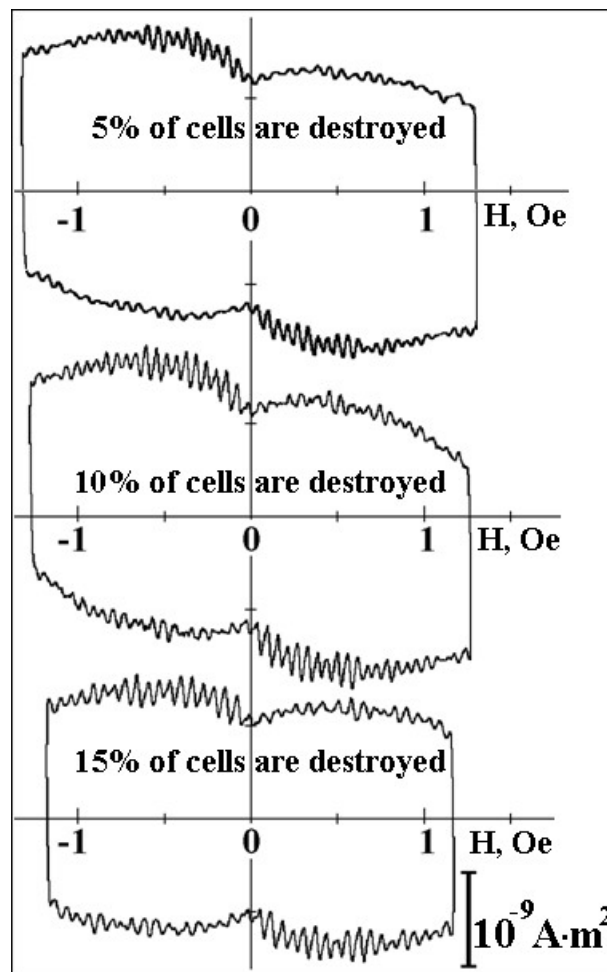


Figure 16. The SIS-type array with distorted cells in the center.

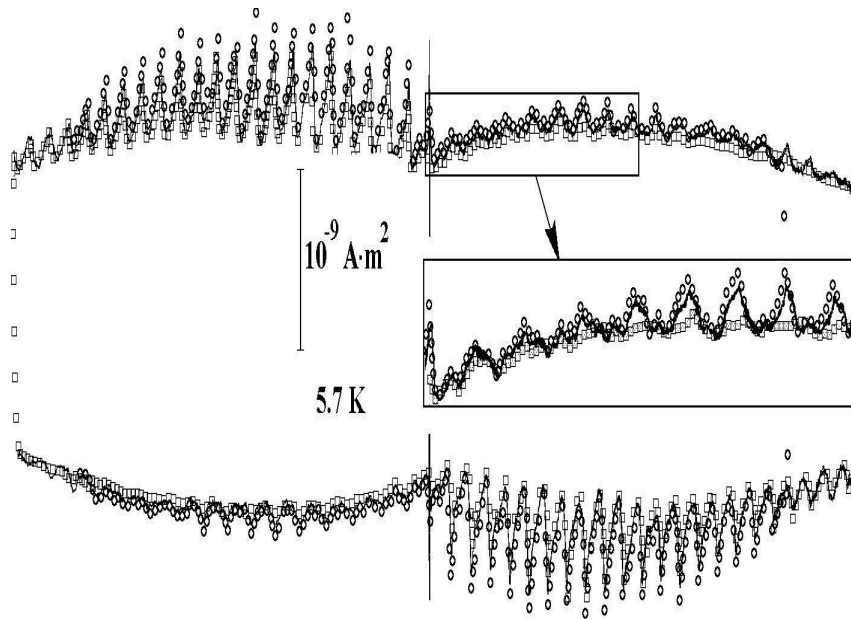


Figure 17. SIS array with distorted cells in the periphery: the initial array (circles), the removed angles (solid line), the removed angles and distorted cells at the boundary (squares).

Presumably, the asymmetry of the hysteresis curve is related to the conditions at the boundaries of the array under which some barrier layers can arise to prevent the flux quanta from moving. To verify this assumption, we have first removed the angles of the square network and then broken the cells at its periphery. Figure 17 clearly demonstrates that these distortions failed to decrease the magnetization curve asymmetry and even caused its slight increase. To better understand the problem regarding the influence of disorder in the arrays on SOC appearance, we have measured magnetic moment by magnetizing granular films and HTSC ceramics at 4.2 K in order to reveal an avalanche-like motion of the magnetic flux which was quite probable according to [7-15]. Our results have failed to reveal any signals of avalanches probably due to the fact that the intragrain junctions in the HTSC-ceramics consist mainly of SNS-type junctions.

8. Conclusion

In the present work, we have tried to pay special attention to the magnetic properties of the Josephson junction arrays under the action of relatively small magnetic fields (0-100 Oe) and over the available temperature range (2-10K).

Our experiments clearly indicate that in the arrays, the slowly varying magnetic field causes a specific dynamic situation that converts into the so-called Self-Organized Criticality (SOC) regime with decreasing temperature. Recall that in [16-19], the mutual-inductance technique was used to reveal the

uniformly separated peaks of the magnetic flux with increasing field and the scanning SQUID microscopy made it possible to reveal spontaneous (catastrophic) temperature-independent penetrations of the magnetic flux into the arrays with unshunted junctions. We have experimentally demonstrated that in the SIS-type arrays there are two temperature domains in which the behavior of the magnetic moment varies. In the first domain, the uniformly distributed peaks of the magnetic field are observed in the magnetization curve which almost coincides with a theoretical description [3]. In the second domain, we observed the random jumps of the magnetic moment that are the avalanches of the magnetic flux displaying specific statistics. The avalanche distribution in the values of their amplitudes and time between the neighboring avalanches has a power character with nonintegral exponents of order of unity. The density of the fluctuation spectrum of magnetization curve also exhibits a power-like Flicker noise type behavior ($\sim 1/f^\alpha$) with a negative nonintegral exponent of the order of unity. Even though this behavior is in fair agreement with the SOC theory, quantitatively the observed dependence markedly differs from the theoretical predictions [29]. Namely, the distribution of avalanches with amplitude displays a pronounced crossover. The distribution density of large avalanches decreases much faster with increasing amplitude than the distribution density of avalanches of minor amplitudes. It is interesting to point out that a somewhat similar phenomenon was detected by Gutenberg and Richter [57] in geophysics. As it is generally accepted, a fast decrease in the distribution density of large avalanches should occur due to the finite size of the Josephson array which means that the number of the field-induced fluxons in such an array is limited. Thus, a natural physical limitation is imposed on the size of large avalanches, which is in agreement with the calculations made by Ginsburg and Savitskaya [7-15], where such a drop of avalanche distribution density was predicted.

There is however a substantial disagreement between our experimental data and the theory of Ginsburg and Savitskaya. They claim [14] that the appearance of SOC in the magnetization of Josephson junction array depends not on the scattering in the critical currents of separate junctions but on the breakdown in the periodicity of the array parameter a . Moreover, this breakdown should exceed the errors in the technology of array production, which amount to less than 5%.

At the same time, our experimental studies on SNS-type arrays have revealed a series of peculiarities that do not follow from the available theoretical works. Let us mention the most important ones. First of all, we have failed to reveal any magnetic flux avalanches in the SNS-type array despite the fact that the main criterion for the existence of SOC (with $\lambda(T) \ll a$) was satisfied. Besides, we have observed a substantial asymmetry in magnetic dynamics which indicates a different character of motion at which the

penetration of the magnetic flux into the array actually occurs. More precisely, the flux penetration was found to have a more ordered character as compared with a fairly disordered process during its escape.

Acknowledgment

This work was financially supported by the Siberian Branch of the Russian Academy of Sciences within the Interdisciplinary Integration project N81 and by the Russian Foundation for Basic Research, project N06-08-00456-a.

References

1. Barbara, P., Cawthorne, A.B., Shitov, S.V., and Lobb, C.J. 1999, *Phys. Rev.Lett.*, 82, 1963.
2. Chen, D.-X., Moreno, J.J., Hernando, A., and Sanchez, A. 1996, *Phys. Rev.B*, 53, 6579.
3. Dominguez, D. and Jose, J.V. 1996, *Phys. Rev.B*, 53, 11692.
4. Luca, R.D., Matteo, T.O., Tuohimaa, A., and Paasi, J. 1998, *Phys. Rev.B*, 57, 1173.
5. Bryksin, V.V., Goltsev, A.V., and Dorogovtsev, S.N. 1990, *J. Phys. Condens. Matter*, 2, 6789.
6. Sergeenkov, S., Rotoli, G., Filatrella, G., and Araujo-Moreira, F.M. 2007, *Phys. Rev. B*, 75, 01406.
7. Ginzburg, S.L. 1994, *JETP*, 106, 607.
8. Ginzburg, S.L. and Savitskaya, N.E. 1998, *JETP Letters*, 68, 719.
9. Ginzburg, S.L., Pustovoit, M.A., and Savitskaya, N.E. 1998, *Phys. Rev.E*, 57, 1319.
10. Ginzburg, S.L. and Savitskaya, N.E. 1999, *JETP Letters*, 69, 133.
11. Ginzburg, S.L. and Savitskaya, N.E. 2000, *JETP*, 90, 202.
12. Ginzburg, S.L. and Savitskaya, N.E. 2001, *JETP Letters*, 73, 145.
13. Ginzburg, S.L. and Savitskaya, N.E. 2000, *Phys. Rev.E*, 66, 026128.
14. Ginzburg, S.L., Nakin, A.V., and Savitskaya, N.E. 2006, *JETP*, 103, 747.
15. Ginzburg, S.L. and Savitskaya, N.E. 2007, *Magnetic Flux Avalanches and Self-Organized Criticality in Discrete Superconductors*, Saint-Petersburg Nuclear Physics Institute, Gatchina (in Russian).
16. Araujo-Moreira, F.M., Barbara, P., Cawthorne, A.B., and Lobb, C.J. 1997, *Phys. Rev.Lett.*, 78, 4625.
17. Maluf, W., Cecato, G.M., Barbara, P., et.al. 2001, *J. of Magnetism and Magnetic Materials*, 226-230, 290.
18. Araujo-Moreira, F.M., Maluf, W., and Sergeenkov, S. 2005, *Eur. Phys.J. B*, 44, 33.
19. Maluf, W. and Araujo-Moreira, F.M. 2007, *Braz. J. Phys.*, 32, 1.
20. Ishikaev, S.M., Matizen, E.V., Ryazanov, V.V., et. al. 2000, *JETP Lett.*, 72, 26.
21. Ishikaev, S.M., Matizen, E.V., Ryazanov, V.V., et al. 2002, *JETP Lett.*, 76, 160.
22. Ishikaev, S.M., Matizen, E.V., Ryazanov, V.V., and Oboznov, V.A. 2003, *Physica C*, 388-389, 583.
23. Matizen, E.V., Ishikaev, S.M., and Oboznov, V.A. 2004, *JETP*, 126, 1065.
24. Matizen, E.V. and Ishikaev, S.M. 2005, *J. of Molecular Liquids*, 120, 39.
25. Ishikaev, S.M. 2002, *Instruments and Experimental Techniques*, 3, 145.

26. Ishikaev, S.M. and Matizen, E.V. 1999, High Temperature Superconductivity: New Materials and Properties, Joint Symposium of SB RAS and the CNEAS TU, Tohoku University, Japan, 65.
27. Philips, J.R., van der Zant, H.S.J., White, J., and Orlando, T.P. 1993, Phys. Rev.B, 47, 5219.
28. Trias, E., van der Zant, H.S.J., and Orlando, T.P. 1996, Phys. Rev.B, 54, 6568.
29. Bak, P., Tang, C., and Wisenfeld, K. 1987, Phys. Rev. Lett. , 59, 381.
30. Olemskj, A.I. and Kattsenelson, A.A. 2003, Sinergetics of Condensed Matter, Editorial URSS, Moscow (in Russian).
31. Bak, P., Chen, K., and Creutz, M. 1989, Nature, 342,780.
32. Bak, P. and Sneppen, K. 1993, Phys. Rev.Lett., 71, 4083.
33. Olami, Z., Feder, H.J.S., and Christensen, K. 1992, Phys. Rev.Lett., 68, 1244.
34. Carlson, J.M. and Langer, J.S. 1989, Phys. Rev.Lett., 62, 2632.
35. Skokov, V.N., Reshetnikov, A.V., Vinogradov, A.V., et al. 2007, Acoustical Physics, 53, 136.
36. Koverda, V.P., Skokov, V.N., Reshetnikov, A.V., et al. 2005, Doklady Physics, 50, 502.
37. Skokov, V.N., Reshetnikov, and A.V., Koverda, V.P. 2000, High Temperatures, 38, 759.
38. Skokov, V.N. and Koverda, V.P. 2000, Technical Physics Letters, 26, 900.
39. Skokov, V.N., Koverda, V.P., and Reshetnikov, A.V. 1999, Physics Letters A, 263, 430.
40. Hwa, R.C. and Pan, J.. 1995, Nuclear Physics A, 590, 601.
41. Andrade, R.F.S., Pinho, S.T.R., Fraga, S.C., and Tanajura, A.P.M. 2002, Physica A, 314, 405.
42. Drossel, B. and Schwabl, F. 1992, Phys. Rev.Lett., 69, 1629.
43. Drossel, B. 1996, Phys. Rev.Lett., 76, 936.
44. Iori, G. and Jafarey, S. 2001, Physica A, 299, 205.
45. Bak, P. and Sneppen, K. 1993, Phys. Rev.Lett.,71, 4083.
46. Laherrere, E. and Sornette, D. 1998, Eur. Phys. B, 2, 525.
47. Behnia, K., Capan, C., Mailly, D., et al. 2000, Phys. Rev.B, 61, R3815.
48. Held, G.A., Solina, D.H., Keane, D.T., Haag, W.J., Horn, P.M., and Grinstein, G. 1990, Phys. Rev.Lett., 65, 1120.
49. Feder, H.J.S. and Feder, J. 1991, Phys. Rev.Lett.,66, 2669.
50. Lebyodkin, M.A., Brechet, Y., Estrin, Y., and Kubin, L.P. 1995, Phys. Rev.Lett., 74, 4758.
51. Lebyodkin, M.A. and Dunin-Barkowskii, L.R. 1998, JETP, 86, 993.
52. Wiesenfeld, K. and Linder, J. 2004, Physica A,340, 617.
53. Chen, D.-X., Sanches, A., and Hernando, A. 1994, Phys. Rev.B, 50, 10342.
54. Chen, D.-X., Moreno, J.J., Hernando, A., and Sanches, A. 1996, Phys. Rev.B, 53, 6579.
55. Vlasko-Vlasov, V.K., Welp, U., Metlushko, V., and Crabtree, G. W. 2004, Phys. Rev.B, 69, 140504(R).
56. Aranson, I.S., Gurevich, A., Welling, et al. 2004, arXiv.org:cond-mat/0407490.
57. Gutenberg, B. and Richter, C.F. 1956, Ann. Geophys., 9, 1.

Transworld Research Network
37/661 (2), Fort P.O., Trivandrum-695 023, Kerala, India



New Developments in Josephson Junctions Research, 2010: 25-44
ISBN: 978-81-7895-328-1 Editor: Sergei Sergeenkov

2

Experimental and theoretical study on 2D ordered and 3D disordered SIS-type arrays of Josephson junctions

Fernando M. Araujo-Moreira¹ and Sergei Sergeenkov²

¹Grupo de Materiais e Dispositivos, Centro Multidisciplinar para o Desenvolvimento de Materiais Cerâmicos, Departamento de Física Universidade Federal de São Carlos, 13565-905 São Carlos, SP, Brazil

²Departamento de Física, CCEN, Universidade Federal da Paraíba Cidade Universitária, 58051-970 João Pessoa, PB, Brazil

Abstract

By employing mutual-inductance technique and using a high-sensitive home-made bridge, we have thoroughly investigated (both experimentally and theoretically) the temperature and magnetic field dependence of complex AC susceptibility of artificially prepared highly ordered (periodic) two-dimensional

Correspondence/Reprint request: Dr. Fernando M. Araujo-Moreira, Departamento de Física, Universidade Federal de São Carlos, 13565-905 São Carlos, SP, Brazil. E-mail: faraujo@df.ufscar.br

Josephson junction arrays (2D-JJA) of both shunted and unshunted Nb–AlO_x–Nb tunnel junctions as well as disordered three-dimensional arrays (3D-JJA). This paper reviews some of our latest results regarding the influence of non-uniform critical current density profile on magnetic field behavior of AC susceptibility in 2D-JJA, and the origin of remanent magnetization in disordered 3D-JJAs.

1. Introduction

Many unusual and still not completely understood magnetic properties of Josephson junctions (JJs) and their arrays (JJAs) continue to attract attention of both theoreticians and experimentalists alike (for recent reviews on the subject see, e.g. [1-5] and further references therein). In particular, among the numerous spectacular phenomena recently discussed and observed in JJAs we would like to mention the dynamic temperature reentrance of AC susceptibility [2] (closely related to paramagnetic Meissner effect [3,4]) and avalanche-like magnetic field behavior of magnetization [5,6]. More specifically, using highly sensitive SQUID magnetometer, magnetic field jumps in the magnetization curves associated with the entry and exit of avalanches of tens and hundreds of fluxons were clearly seen in SIS-type arrays [6]. Besides, it was shown that the probability distribution of these processes is in good agreement with the theory of self-organized criticality [7]. It is also worth mentioning the recently observed geometric quantization [8] and flux induced oscillations of heat capacity [9] in artificially prepared JJAs as well as recently predicted flux driven temperature oscillations of thermal expansion coefficient [10] both in JJs and JJAs. At the same time, successful adaptation of the so-called two-coil mutual-inductance technique to impedance measurements in JJAs provided a high-precision tool for investigation of the numerous magnetoinductance (MI) related effects in Josephson networks [11-14]. To give just a few recent examples, suffice it to mention the MI measurements [12] on periodically repeated Sierpinski gaskets which have clearly demonstrated the appearance of fractal and Euclidean regimes for non-integer values of the frustration parameter, and theoretical predictions [13] regarding a field-dependent correction to the sheet inductance of the proximity JJA with frozen vortex diffusion. Besides, recently [14] AC magnetoimpedance measurements performed on proximity-effect coupled JJA on a dice lattice revealed unconventional behaviour resulting from the interplay between the frustration f created by the applied magnetic field and the particular geometry of the system. While the inverse MI exhibited prominent peaks at $f = 1/3$ and at $f = 1/6$ (and weaker structures at $f = 1/9, 1/12, \dots$) reflecting vortex states with a high degree of superconducting phase coherence, the deep minimum at $f = 1/2$ points to a state in which the phase coherence is strongly suppressed.

More recently, it was realized that JJAs can be also used as quantum channels to transfer quantum information between distant sites [15-17] through the implementation of the so-called superconducting qubits which take advantage of both charge and phase degrees of freedom (see, e.g., [18,19] for a review on quantum-state engineering with Josephson-junction devices).

Artificially prepared two-dimensional Josephson junctions arrays (2D-JJA) consist of highly ordered superconducting islands arranged on a symmetrical lattice coupled by Josephson junctions (figure 1), where it is possible to introduce a controlled degree of disorder. In this case, a 2D-JJA can be considered as the limiting case of an extreme inhomogeneous type-II superconductor, allowing its study in samples where the disorder is nearly exactly known. Since 2D-JJA are artificial, they can be very well characterized. Their discrete nature, together with the very well-known physics of the Josephson junctions, allows the numerical simulation of their behavior.

Many authors have used a parallelism between the magnetic properties of 2D-JJA and granular high-temperature superconductors (HTS) to study some controversial features of HTS. It has been shown that granular superconductors can be considered as a collection of superconducting grains embedded in a weakly superconducting - or even normal - matrix. For this reason, granularity is a term specially related to HTS, where magnetic and transport properties of these materials are usually manifested by a two-component response. In this scenario, the first component represents the *intragranular* contribution, associated to the grains exhibiting ordinary superconducting properties, and the second one, which is originated from *intergranular* material, is associated to the weak-link structure, thus, to the Josephson junctions network [20-25]. For single-crystals and other nearly-perfect structures, granularity is a more subtle

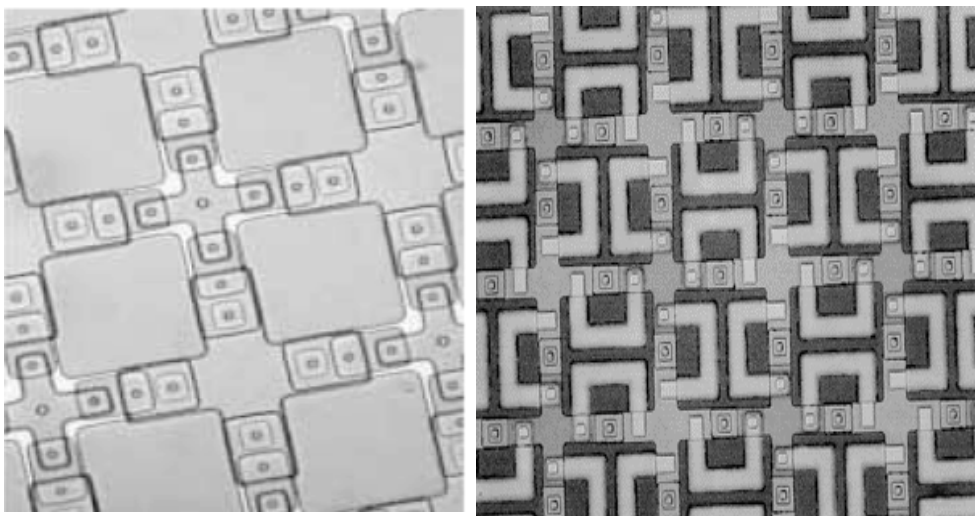


Figure 1. Photograph of unshunted (left) and shunted (right) Josephson junction arrays.

feature that can be envisaged as the result of a symmetry breaking. Thus, one might have granularity on the nanometric scale, generated by localized defects like impurities, oxygen deficiency, vacancies, atomic substitutions and the genuinely *intrinsic* granularity associated with the layered structure of perovskites. On the micrometric scale, granularity results from the existence of extended defects, such as grain and twin boundaries. From this picture, granularity could have many contributions, each one with a different volume fraction. The small coherence length of HTS implies that any imperfection may contribute to both the weak-link properties and the flux pinning. This leads to many interesting peculiarities and anomalies, many of which have been tentatively explained over the years in terms of the granular character of HTS materials. One of the controversial features of HTS elucidated by studying the magnetic properties of 2D-JJA is the so-called Paramagnetic Meissner Effect (PME), also known as Wohleben Effect. In this case, one considers first the magnetic response of a granular superconductor submitted to either an AC or DC field of small magnitude. This field should be weak enough to guarantee that the critical current of the intergranular material is not exceeded at low temperatures. After a zero-field cooling (ZFC) process which consists in cooling the sample from above its critical temperature (T_C) with no applied magnetic field, the magnetic response to the application of a magnetic field is that of a perfect diamagnet. In this case, the intragranular screening currents prevent the magnetic field from entering the grains, whereas intergranular currents flow across the sample to ensure a null magnetic flux throughout the whole specimen. This temperature dependence of the magnetic response gives rise to the well-known double-plateau behavior of the DC susceptibility and the corresponding double-drop/double-peak of the complex AC magnetic susceptibility [26-31]. On the other hand, by cooling the sample in the presence of a magnetic field, by following a field-cooling (FC) process, the screening currents are restricted to the intragranular contribution (a situation that remains until the temperature reaches a specific value below which the critical current associated to the intragrain component is no longer equal to zero). It has been experimentally confirmed that intergranular currents may contribute to a magnetic behavior that can be either paramagnetic or diamagnetic. Specifically, where the intergranular magnetic behavior is paramagnetic, the resulting magnetic susceptibility shows a striking reentrant behavior. All these possibilities about the signal and magnitude of the magnetic susceptibility have been extensively reported in the literature, involving both LTS and HTS materials [32-35]. The reentrant behavior mentioned before is one of the typical signatures of PME. We have reported its occurrence as a reentrance in the temperature behavior of the AC magnetic susceptibility of 2D-JJA [36,37]. Thus, by studying 2D-JJA, we were able to demonstrate that the appearance of PME is simply related to trapped flux and

has nothing to do with manifestation of any sophisticated mechanisms, like the presence of pi-junctions or unconventional pairing symmetry.

The paper is organized as follows. In Section 2 we briefly review the theoretical background for the numerical simulations based on a unit cell containing four Josephson junctions. In Section 3 we describe the influence of non-uniform critical current density profile on magnetic field behavior of AC susceptibility and discuss the obtained results. In Section 4 we study the origin of the so-called remanent magnetization in disordered 3D-JJAs based on both conventional and high-temperature superconductors. And finally, in Section 5 we summarize the main results of the present work.

2. Theoretical background for simulations

We have found that all the experimental results obtained from the magnetic properties of 2D-JJA can be qualitatively explained by analyzing the dynamics of a single unit cell in the array [36,37]. In our numerical simulations, we model a single unit cell as having four identical junctions, each with capacitance C_J , quasi-particle resistance R_J and critical current I_C . If we apply an external field of the form:

$$\mathbf{H}_{\text{ext}} = h_{\text{AC}} \cos(\omega t) \quad (2.1)$$

then the total magnetic flux, Φ_{TOT} , threading the four-junction superconducting loop is given by:

$$\Phi_{\text{TOT}} = \Phi_{\text{EXT}} + LI \quad (2.2)$$

where $\Phi_{\text{EXT}} = \mu_0 a^2 H_{\text{EXT}}$ is the flux related to the applied magnetic field with μ_0 being the vacuum permeability, I is the circulating current in the loop, and L is the inductance of the loop. Therefore the total current is given by:

$$I(t) = I_C(T) \sin \phi_i(t) + \frac{\Phi_0}{2\pi R_j} \frac{d\phi_i}{dt} + \frac{C_j \Phi_0}{2\pi} \frac{d^2 \phi_i}{dt^2} \quad (2.3)$$

Here, $\phi_i(t)$ is the superconducting phase difference across the i th junction, Φ_0 is the magnetic flux quantum, and I_C is the critical current of each junction. In the case of our model with four junctions, the fluxoid quantization condition, which relates each $\phi_i(t)$ to the external flux, reads:

$$\phi_i = \frac{\pi}{2} n + \frac{\pi}{2} \frac{\Phi_{\text{TOT}}}{\Phi_0} \quad (2.4)$$

where n is an integer and, by symmetry, we assume that [36,37] :

$$\phi_1 = \phi_2 = \phi_3 = \phi_4 \equiv \phi_i \quad (2.5)$$

In the case of an oscillatory external magnetic field of the form of Eq. (2.1), the magnetization is given by:

$$M = \frac{LI}{\mu_0 a^2} \quad (2.6)$$

It may be expanded as a Fourier series in the form:

$$M(t) = h_{AC} \sum_{n=0}^{\infty} [\chi_n' \cos(n\omega t) + \chi_n'' \sin(n\omega t)] \quad (2.7)$$

We calculated χ' and χ'' through this equation. Both Euler and fourth-order Runge-Kutta integration methods provided the same numerical results. In our model we do not include other effects (such as thermal activation) beyond the above equations. In this case, the temperature-dependent parameter is the critical current of the junctions, given to good approximation by [39,40]:

$$I_C(T) = I_C(0) \left[\frac{\Delta(T)}{\Delta(0)} \right] \tanh \left[\frac{\Delta(T)}{2k_B T} \right] \quad (2.8)$$

where

$$\Delta(T) = \Delta(0) \tanh \left(2.2 \sqrt{\frac{T_C - T}{T}} \right) \quad (2.9)$$

is the analytical approximation of the BCS gap parameter with $\Delta(0) = 1.76k_B T_C$.

We simulated χ_1 as a function of temperature and applied magnetic fields keeping in mind that χ_1 depends on the geometrical parameter β_L (which is proportional to the number of flux quanta that can be screened by the maximum critical current in the junctions), and the dissipation parameter β_C (which is proportional to the capacitance of the junction)

$$\beta_L(T) = \frac{2\pi LI_C(T)}{\Phi_0} \quad (2.10)$$

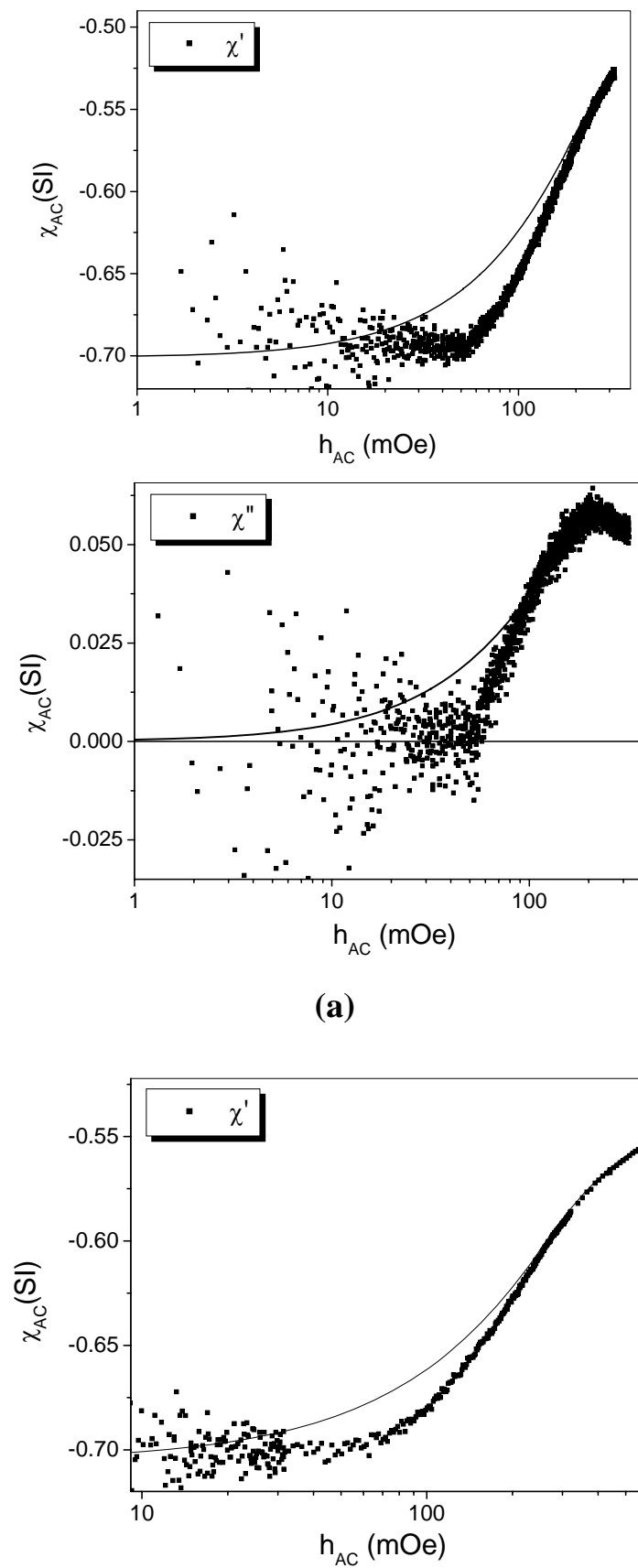
$$\beta_C(T) = \frac{2\pi I_C C_J R_J^2}{\Phi_0} \quad (2.11)$$

3. Influence of non-uniform critical current density profile on magnetic field response of AC susceptibility in ordered 2D-JJAs

So far, most of the investigations have been done assuming an ideal (uniform) type of array. However, it is quite clear that, depending on the particular technology used for preparation of the array, any real array will inevitably possess some kind of non-uniformity, either global (related to a random distribution of junctions within array) or local (related to inhomogeneous distribution of critical current densities within junctions). For instance, recently a comparative study of the magnetic remanence exhibited by disordered (globally non-uniform) 3D-JJA in response to an excitation with an AC magnetic field h_{AC} was presented [41]. The observed temperature behavior of the remanence curves for arrays fabricated from three different materials (Nb, $YBa_2Cu_3O_7$ and $La_{1.85}Sr_{0.15}CuO_4$) was found to follow the same universal law regardless of the origin of the superconducting electrodes of the junctions which form the array. In this section, through an experimental study of complex AC magnetic susceptibility $\chi(T, h_{ac})$ of the periodic (globally uniform) 2D-JJA of unshunted Nb–AlO_x–Nb junctions, we present evidence for existence of the local type non-uniformity in our arrays [42]. Specifically, we found that in the mixed state region $\chi(T, h_{ac})$ can be rather well fitted by a single-plaquette approximation of the over-damped 2D-JJA model assuming a non-uniform (Lorentz-like) distribution of the critical current density within a single junction.

Our samples consisted of 100×150 unshunted tunnel junctions. The unit cell had square geometry with lattice spacing $a = 46 \mu\text{m}$ and a junction area of $5 \times 5 \mu\text{m}^2$. The critical current density for the junctions forming the arrays was about 600 A/cm^2 at 4.2 K, giving thus $I_C = 150 \mu\text{A}$ for each junction. We used the screening method in the reflection configuration to measure the complex AC susceptibility $\chi = \chi' + i\chi''$ of our 2D-JJA (for more details on the experimental technique and set-ups see [36,37]). Figure 2 shows the obtained experimental data for the complex AC susceptibility $\chi(T, h_{ac})$ as a function of h_{ac} for a fixed temperature below T_C . As is seen, below 50 mOe (which corresponds to a Meissner-like regime with no regular flux present in the array) the susceptibility, as expected, practically does not depend on the applied magnetic field, while in the mixed state (above 50 mOe) both $\chi'(T, h_{ac})$ and $\chi''(T, h_{ac})$ follow a quasi-exponential field behavior of the single junction Josephson supercurrent (see below).

Figure 2



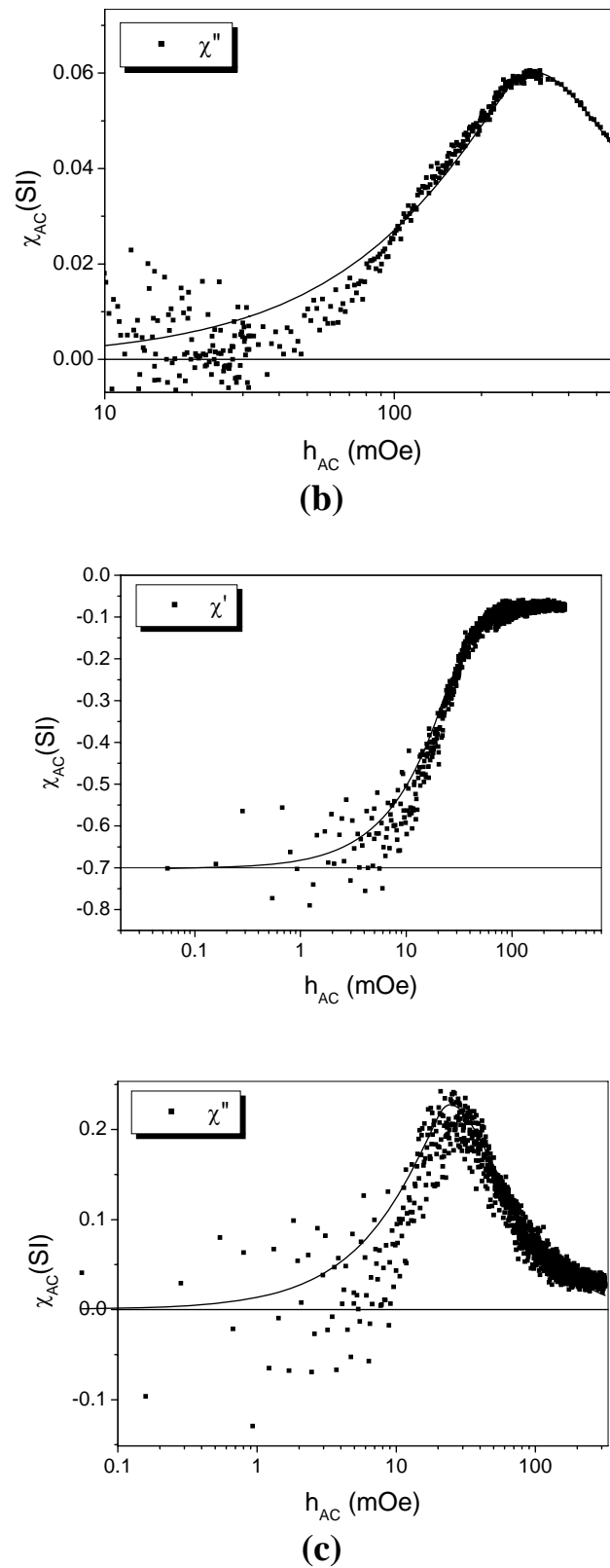


Figure 2. The dependence of both components of the complex AC magnetic susceptibilities on AC magnetic field amplitude h_{AC} for different temperatures: (a) $T = 4.2$ K, (b) $T = 6$ K, and (c) $T = 8$ K. Solid lines correspond to the fitting of the 2D-JJA model with non-uniform critical current profile for a single junction (see the text).

To understand the observed behavior of the AC susceptibility, in principle one would need to analyze the flux dynamics in our over-damped, unshunted 2D-JJA. However, given a well-defined (globally uniform) periodic structure of the array, to achieve our goal it is sufficient to study just a single unit cell (plaquette) of the array. (It is worth noting that the single-plaquette approximation proved successful in treating the temperature reentrance phenomena of AC susceptibility in ordered 2D-JJA as well as magnetic remanence in disordered 3D-JJA [29,41]. The unit cell is a loop containing four identical Josephson junctions. Since the inductance of each loop is $L = \mu_0 a = 64$ pH and the critical current of each junction is $I_C = 150$ μ A, for the mixed-state region (above 50 mOe) we can safely neglect the self-field effects because in this region the inductance related flux [43] $\Phi_L(t) = LI(t)$ is always smaller than the external field induced flux $\Phi_{\text{ext}}(t) = B_{\text{ac}}(t) \cdot S$. Here $I(t)$ is the total current circulating in a single loop, $S \approx a^2$ is the projected area of a single loop, and $B_{\text{ac}}(t) = \mu_0 h_{\text{ac}} \cos(\omega t)$ is an applied AC magnetic field. Besides, since the length \mathcal{L} and the width w of each junction in our array is smaller than the Josephson penetration depth $\lambda_j = \sqrt{\frac{\Phi_0}{2\pi\mu_0 d j_{c0}}}$ (where j_{c0} is the critical current density of the junction, Φ_0 is the magnetic flux quantum, and $d = 2\lambda_L + \xi$ is the size of the contact area with $\lambda_L(T)$ being the London penetration depth of the junction and ξ an insulator thickness), namely $\mathcal{L} \approx w \approx 5\mu\text{m}$ and $\lambda_j \approx 20\mu\text{m}$ (using $j_{c0} = 600$ A/cm² and $\lambda_L = 39$ nm for Nb at $T = 4.2$ K), we can adopt the small junction approximation [43] for the gauge-invariant superconducting phase difference across *ith* junction. Assuming by symmetry that $\phi_1 = \phi_2 = \phi_3 = \phi_4 = \phi_i$, we have:

$$\phi_i(x, t) = \phi_0 + \frac{2\pi B_{\text{ac}}(t)d}{\Phi_0} \cdot x \quad (3.1)$$

where ϕ_0 is the initial phase difference. The net magnetization of the plaquette is $M(t) = SI_S(t)$, where the maximum upper current (corresponding to $\phi_0 = \pi/2$) through an inhomogeneous Josephson contact reads:

$$I_S(t) = \int_0^{\mathcal{L}} dx \int_0^w dy j_c(x, y) \cos \phi_i(x, t) \quad (3.2)$$

For the explicit temperature dependence of the Josephson critical current density we use Eqs.(2.8) and (2.9) from the previous Section.

In general, the values of $\chi'(T, h_{AC})$ and $\chi''(T, h_{AC})$ of the complex harmonic susceptibility are defined via the time dependent magnetization of the plaquette as follows:

$$\chi'(T, h_{ac}) = \frac{1}{\pi h_{AC}} \int_0^{2\pi} d(\omega t) \cos(\omega t) M(t) \quad (3.3)$$

$$\chi''(T, h_{AC}) = \frac{1}{\pi h_{AC}} \int_0^{2\pi} d(\omega t) \sin(\omega t) M(t) \quad (3.4)$$

Using Eqs. (3.1)–(3.4) to simulate the magnetic field behavior of the observed AC susceptibility of the array, we found that the best fit through all the data points and for all temperatures is produced assuming the following non-uniform distribution of the critical current density within a single junction [43]

$$j_c(x, y) = j_{c0}(T) \left(\frac{L^2}{x^2 + L^2} \right) \left(\frac{w^2}{y^2 + w^2} \right) \quad (3.5)$$

It is worthwhile to mention that in view of Eq. (3.2), in the mixed-state region the above distribution leads to approximately exponential field dependence of the maximum supercurrent $I_S(T, h_{AC}) \approx I_S(T, 0) \exp(-h_{AC}/h_0)$ which is often used to describe critical-state behavior in type-II superconductors [27]. Given the temperature dependencies of the London penetration depth $\lambda_L(T)$ and the Josephson critical current density $j_{c0}(T)$, we find that:

$$h_0(T) = \frac{\Phi_0}{2\pi\mu_0\lambda_j(T)L} \approx h_0(0) \cdot \left(\frac{T_C - T}{T_C} \right)^{1/4} \quad (3.6)$$

for the temperature dependence of the characteristic field near T_C . This explains the improvement of our fits (shown by solid lines in figure 2) for high temperatures because with increasing the temperature the total flux distribution within a single junction becomes more regular which in turn validates the use of the small-junction approximation.

To further study the penetration of the magnetic field in our samples, we have analyzed the so-called susceptibility spectra (see Figs. 3-5). In this case χ'' is a function of χ' , taken at a fixed temperature. The analysis of this spectrum for different temperatures allows follow the evolution of the magnetic flux profile in a particular sample. Ishida and Mazaki [44] have proposed a critical state model based on a superconducting multiconnected

structure which has associated a symmetric curve of χ'' as a function of χ' with its maximum centered at $(-\chi') = 0.5$. On the other hand, Gotoh et al. [45] and Chen et al. [46] have shown that, for other critical states like Bean, exponential, and Kim models, the curve of χ'' as a function of χ' is asymmetric. The first authors have shown that, for the Bean case, $\chi''(\chi')$ has a maximum value of $\chi'' = 0.239$ at $(-\chi') = 0.375$. Figure 3 is related to an experiment performed at $T = 4.2$ K. It shows a curve that can be divided into two parts. The first one is symmetric and centered at $(-\chi') = 0.571$, as shown by the solid line. The second one is almost constant and oscillates around $\chi'' \approx 0$. Figure 4 is very similar to Fig. 3; its symmetric part (centered at $(-\chi') = 0.567$) is larger than that in Fig. 3. In both figures the symmetric curve represents the contribution of a multiconnected superconductor, as expected for a 2D-JJA. According to Chen et al. [46], Bean's model is the low- p limit of the exponential and Kim models. Figure 5, which corresponds to an experiment performed at $T = 8.0$ K, has its best fitting for $p = 0.13$, so at this temperature both models, Bean and exponential, are equivalents. This equivalence allows us to compare curve (5) to the result of Gotoh et al. [45] deduced for the Bean model, as follows. This figure shows an asymmetric curve with the expected shape for the exponential critical state model [46]. In this case, after its maximum value, $\chi''(\chi')$ should have a linear dependence. has its first part centered at $(-\chi') = 0.262$ and has a maximum value of $\chi'' = 0.239$. As explained before JJA samples never reach complete Meissner at $(-\chi') = 1$, which happens at $(-\chi') = 0.7$ (S.I. units). In this case, the value of

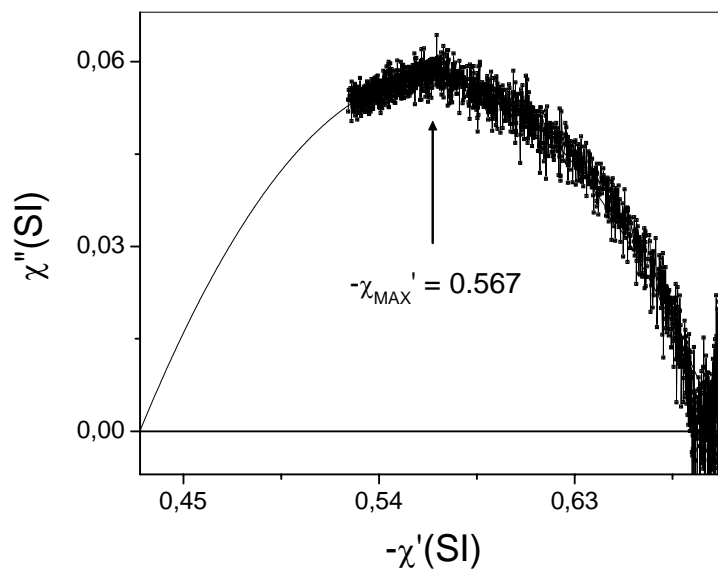


Figure 3. Curves for the susceptibility spectra, $\chi''(\chi')$, of an unshunted JJA for $T = 4.2$ K.

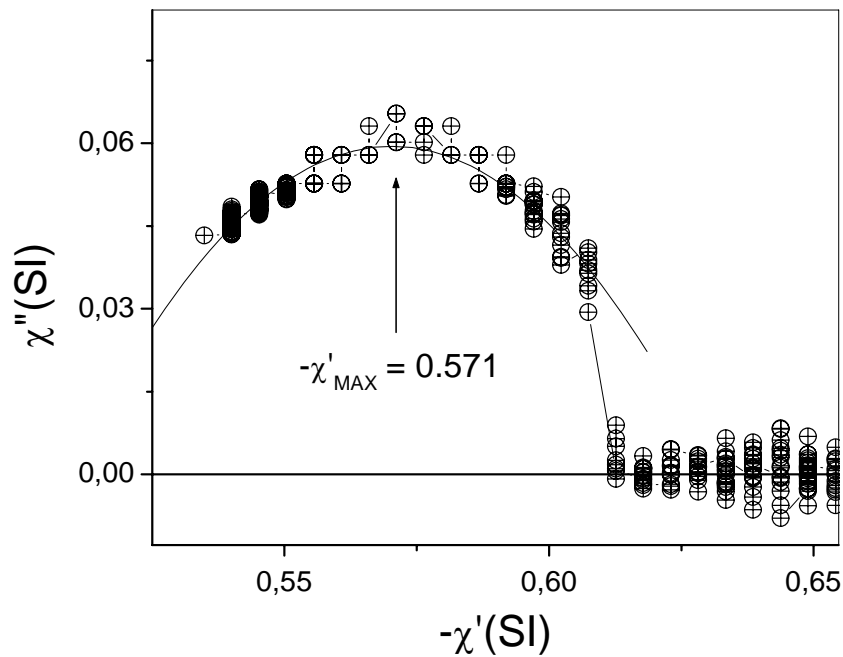


Figure 4. Curves for the susceptibility spectra, $\chi''(\chi')$, of an unshunted JJA for $T = 6.0$ K.

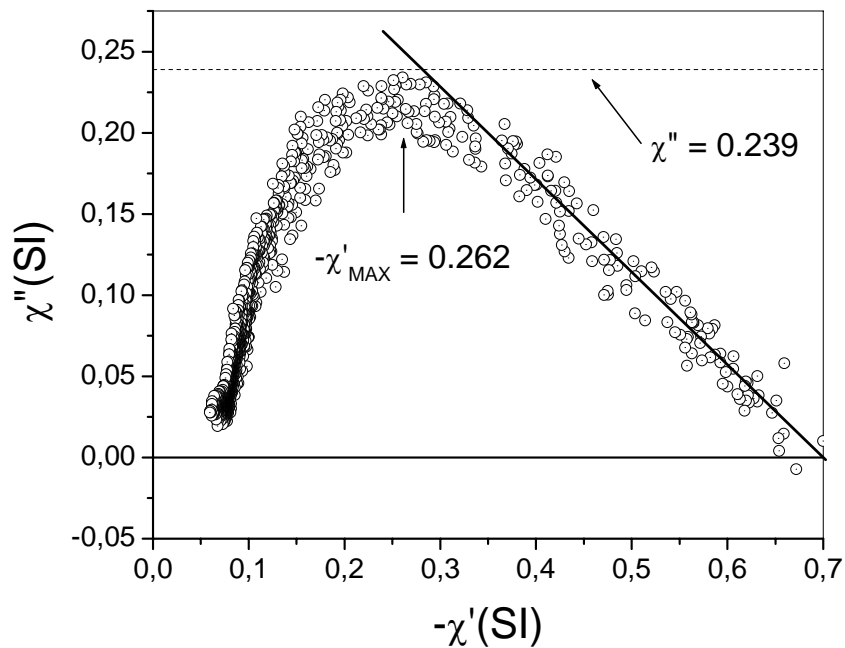


Figure 5. Curves for the susceptibility spectra, $\chi''(\chi')$, of an unshunted JJA for $T = 8.0$ K.

$(-\chi') = 0.262$ observed in JJA corresponds to a value of $(-\chi') = 0.374$ associated to superconducting materials in the Bean critical state. Thus, Figure 5 shows the evolution of the critical state from a multiconnected-like to the Bean (or the exponential) critical state model.

4. On the origin of the remanent magnetization in disordered 3D-JJAs

The tridimensional disordered Josephson junction arrays (JJAs) fabricated from either conventional (LTS) or high- T_c (HTS) superconductors are known [47,48] to exhibit the so-called temperature-dependent magnetic remanence, $M_R(T)$ upon excitation by a magnetic field. Typically [30], the magnetized state occurs in a rather narrow window of temperatures, the extent of which depends on the critical current, $I_C(T)$, of the junctions. Besides, there is a threshold value for the magnetic field in order to drive the JJA to the state where flux is retained after suppression of the field [30].

In this Section we present a comparative study of three different samples with a rather spectacular remanent behavior and suggest a possible interpretation of the observed temperature dependence of the remanent magnetization of both LTS and HTS tridimensional disordered JJAs. Our analysis shows that all the experimental data can be rather well fitted using the explicit temperature expressions for the activation energy and the inductance-dominated contribution to the magnetization of the array within the so-called phase-slip model [49-51]. Three samples were prepared from selected material, respectively of Nb, $\text{YBa}_2\text{Cu}_3\text{O}_7$ (YBCO) and $\text{La}_{1.85}\text{Sr}_{0.15}\text{CuO}_4$ (LSCO). All three exhibit the predicted remanence and other characteristic features of Josephson arrays. Fabrication routes as well as the experimental routines employed for the magnetic measurements are described elsewhere [47,48]. In short, the corresponding (e.g., niobium) powder was separated according to grain size (using a set of special sieves, with mesh gauges ranging from 38 to 44 μm), then uniaxially pressed in a mold to form a cylindrical pellet of 2.5 mm radius by 2.0 mm height. This pellet is a tridimensional disordered JJA in which the junctions are weakly-coupled grains, i.e., weak-links formed by a sandwich between (Nb) grains and a (Nb-oxide) layer originally present on the grain surface. The measurements were made using a Quantum Design MPMS-5T SQUID magnetometer featuring the regular DC extraction magnetometer and an AC-susceptibility module. The remanence was obtained measuring the sample magnetization after application and removal of a train of sinusoidal pulses. Using the field scan routine we measured the remanent magnetization as a function of the excitation field. For an ordinary superconductor of any kind, from a single crystal to a totally disordered granular sample, the only possibility of a remanence after the application of the AC field would be a residual magnetization due to flux eventually pinned inside the specimen. This contribution, however, is expected to be small and practically independent of the excitation field. We have verified the above characteristics measuring $M_R(h, T)$ for a variety of samples. In particular, the powder used to fabricate our arrays have the typical response of ordinary superconductors, so that the effects

described below are entirely due to the formation of the 3D-JJA. The typical experimental data for Nb samples are shown in Figure 6 which clearly demonstrate anisotropic character of the disordered 3D-JJA. The experimental results for all three samples (along with the model fits, see below) are summarized in Figure 7 which suggests that the observed behavior seems to follow a universal temperature pattern, irrespective of the type of superconductor of which the array is made. Let us turn to a possible interpretation of the obtained results. Since the observed remanent magnetization (RM) in our samples (JJAs) appears only below the so-called phase-locking temperature T_J (which marks the establishment of phase coherence between the adjacent grains in the array and always lies below a single grain superconducting temperature T_C), it is quite reasonable to assume that origin of RM is related to thermal fluctuations of the phases of the superconducting order parameters across an array of Josephson junctions (the so-called phase-slip mechanism [49-51]). In the present approach we consider the sample as a single plaquette with four Josephson junctions (JJs), each of which is treated via an effective single junction approximation. Within this approximation, the phase-slip scenario yields then

$$\Delta M_R(T) \equiv M(T) - M_R = M_0(T) I_0^{-2}[\gamma(T)/2] - M_R \quad (4.1)$$

for the observed remanent magnetization. Here, $M_0(T)$ is an inductance-induced contribution to the magnetization of the array (see below), $\gamma(T) = U(T)/k_B T$ is the normalized barrier height for thermal phase slippage, $I_0(x)$ is the modified Bessel function, and $M_R = M(T_J)$ is a residual temperature-independent contribution (notice that, according to Eq.(4.1), $\Delta M_R(T_J) = 0$).

For temperatures below T_J (where the main events take place, see Fig.7), the Bessel function can be approximated leading to a simplified version of Eq.(4.1):

$$M(T) = 2\pi M_0(T) [U(T)/k_B T] \exp[-U(T)/k_B T] \quad (4.2)$$

Figure 7 shows the temperature dependence (in reduced units, $\tau = T/T_J$) of the normalized remanent magnetization $m_r(T) = \Delta M_R(T)/\Delta M_R(T_p)$ where T_p is the peak temperature $\Delta M_R(T)$ is defined via Eqs. (4.1) and (4.2). The data for YBCO- and Nb-based JJAs are found to be well fitted with the following explicit expression for the array magnetization:

$$M(t) = A(1-t^4)^{5/2} \exp[-\alpha(1-t^4)] \quad (4.3)$$

where $t = T/T_C$. The best fits through all the data points (shown in Fig.7 by solid and dotted lines for YBCO- and Nb-based JJAs, respectively) using Eq.(4.3) and the known critical parameters:

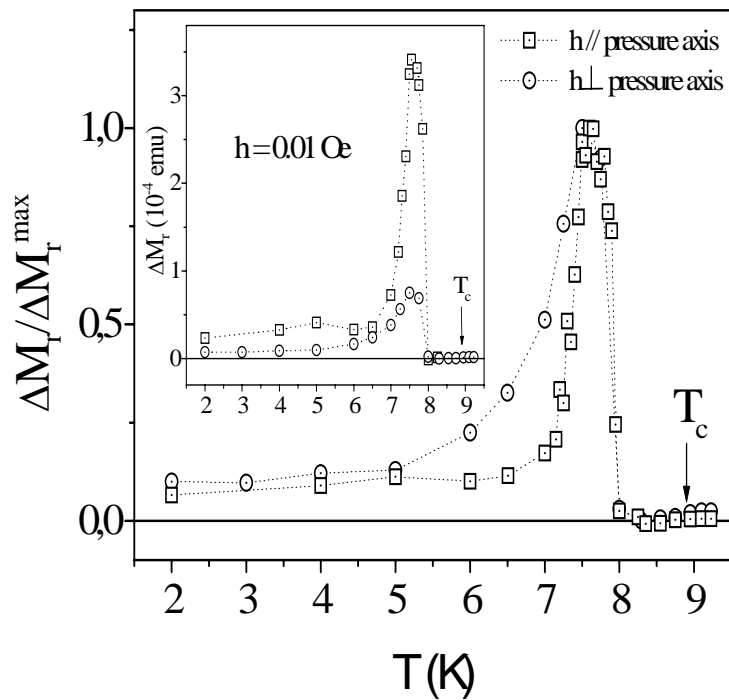


Figure 6. Sample anisotropy of a 3D-JJA of Nb, revealed in measurements of the remanence versus temperature for different orientations of the AC excitation field (h). Main graph: data normalized to peak values. Inset: “as measured” data.

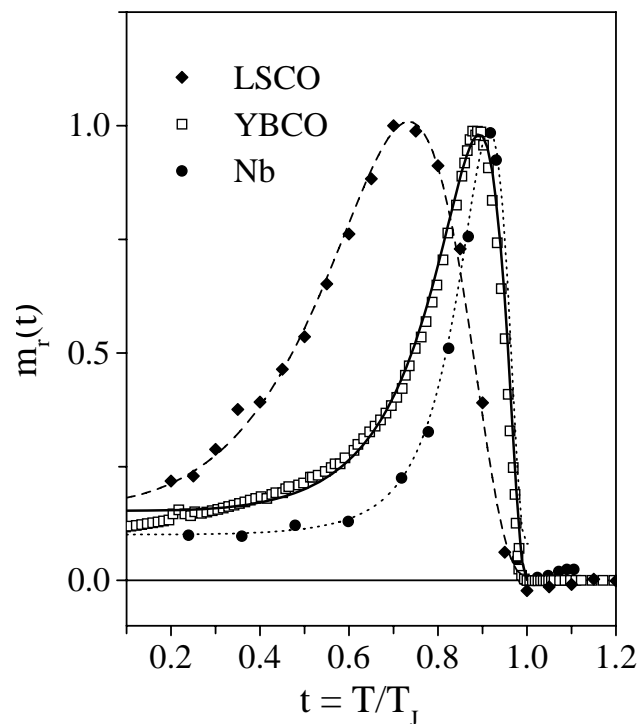


Figure 7. Temperature dependence of the normalized remanent magnetization $m_r(T)$, showing the experimental data for three different samples and the corresponding fittings (see text).

YBCO: $T_C = 90 \text{ K}$, $T_J = 82 \text{ K}$, $T_p = 0.88 T_J$;

LSCO: $T_C = 36.5 \text{ K}$, $T_J = 19.87 \text{ K}$, $T_p = 0.7 T_J$;

Nb: $T_C = 9.1 \text{ K}$, $T_J = 8.2 \text{ K}$, $T_p = 0.92 T_J$;

yield the following estimates of the model parameters: $\alpha_{\text{YBCO}} = 7$, $\alpha_{\text{LSCO}} = 2$, and $\alpha_{\text{Nb}} = 9$.

To understand the observed behavior of the remanent magnetization, we need to specify the temperature dependencies of the activation energy $U(T)$ and the inductance-dominated contribution $M_0(T)$ to the magnetization of the array. Starting with the YBCO- and Nb-based arrays, it is reasonable to assume that [36,37] $U(T) = \Phi_0 I_C(T)/2\pi$ and $M_0(T) = LI_C(T)/\mu_0 S$, where $I_C(T)$ is an average value of the critical current, L is an average inductance of the Josephson network, S is an effective (in general, temperature-dependent, see below) projected area of the contact, Φ_0 is the flux quantum, and μ_0 is the vacuum permeability. In turn, the temperature dependence of the critical current is dictated by the corresponding dependence of the London penetration depth, namely:

$$I_C(T) = I_C(0) \left[\frac{\lambda_L(0)}{\lambda_L(T)} \right]^2 \quad (4.4)$$

where

$$\lambda_L(T) = \lambda_L(0) \left[1 - \left(\frac{T}{T_C} \right)^4 \right]^{-1/2} \quad (4.5)$$

Finally, to arrive at the fitting expression given by Eq.(4.3), we have to assume that the projected area S is also temperature dependent (which is not unusual), viz. $S(T) = \pi d(T)l$ with $d(T)$ and l being the thickness and the length of a SIS-type sandwich, respectively ($d(T) = 2\lambda_L(T) + \xi$, where $\lambda_L(T)$ is the London penetration depth and ξ is the thickness of an insulating layer; in ceramics l plays the role of an average grain size r_g ; typically, $l \gg \lambda_L(T) \gg \xi$).

The above considerations bring about the following relationships between the fitting and the model parameters:

$$A = \left[\frac{LI_C(0)\alpha}{\mu_0 \lambda_L(0)l} \right] \quad \text{with} \quad \alpha = \left[\frac{\Phi_0 I_C(0)}{2\pi k_B T_C} \right] \quad (4.6)$$

At the same time, the phase locking temperature T_J , defined via the equation $U(T_J) = k_B T_J$, is related to the critical temperature T_C as follows:

$$T_J = T_c \left(\frac{\alpha}{1 + \alpha} \right) \quad (4.7)$$

5. Conclusion

In conclusion, in this review paper we presented some of our recent results on novel interesting phenomena related to the magnetic properties of ordered two-dimensional unshunted Nb–AlO_x–Nb Josephson junction arrays (2D-JJA) and disordered three-dimensional Josephson junction arrays (3D-JJA) based on conventional (Nb) and high-temperature (YBa₂Cu₃O₇ and La_{1.85}Sr_{0.15}CuO₄) superconductors. First of all, we demonstrated experimental evidence for the influence of the junction non-uniformity on magnetic field penetration into the periodic 2D array of ordered unshunted Josephson junctions. By using the well-known AC magnetic susceptibility technique, we have shown that in the mixed-state regime the AC field behavior of the artificially prepared array is reasonably well fitted by the single-plaquette approximation of the overdamped model of 2D-JJA assuming inhomogeneous (Lorentz-like) critical current distribution within a single junction. On the other hand, our experimental and theoretical results have demonstrated that the temperature dependence of the magnetic remanence in disordered 3D-JJA is universal, regardless of the origin of the superconducting electrodes of the junctions which form the array.

Acknowledgment

We thank P. Barbara, C.J. Lobb, A. Sanchez and R.S. Newrock for useful discussions and W. Maluf for his help in running some of the experiments. We gratefully acknowledge financial support from Brazilian Agencies FAPESP and CAPES.

References

1. Newrock, R.S., Lobb, C.J., Geigenmüller, U. and Octavio, M. 2000, *Solid State Physics*, 54, 263.
2. Araujo-Moreira, F.M., Bárbara, P., Cawthorne, A.B. and Lobb, C.J. 2002, *Studies of High Temperature Superconductors*, A. Narlikar (Ed.), Nova Science, New York 43, 227.
3. Li, M.S. 2003, *Phys. Rep.*, 376, 133.
4. Kirtley, J.R., Mota, A.C., Sigrist, M. and Rice, T.M. 1998, *J. Phys.: Condens.Matter*, 10, L97.
5. Altshuler, E. and Johansen, T.H. 2004, *Rev. Mod. Phys.*, 76, 471.
6. Ishikaev, S.M., Matizen, E.V., Ryazanov, V.V., Oboznov, V.A. and Veretennikov, A.V. 2000, *JETP Lett.*, 72, 26.

7. Jensen, H.J. 1998, *Self Organized Criticality: Emergent Complex Behavior in Physical and Biological Systems*, Cambridge University Press, Cambridge.
8. Sergeenkov, S. and Araujo-Moreira, F.M. 2004, *JETP Lett.*, 80, 580.
9. Bourgeois, O., Skipetrov, S.E., Ong, F. and Chaussy, J. 2005, *Phys. Rev. Lett.*, 94, 057007.
10. Sergeenkov, S., Rotoli, G., Filatrella, G. and Araujo-Moreira, F.M. 2007, *Phys. Rev. B*, 75, 014506.
11. Martinoli, P. and Leeman, C. 2000, *J. Low Temp. Phys.*, 118, 699.
12. Meyer, R., Korshunov, S.E., Leemann, Ch. and Martinoli, P. 2002, *Phys. Rev. B*, 66, 104503.
13. Korshunov, S.E. 2003, *Phys. Rev. B*, 68, 094512.
14. Tesei, M., Theron, R. and Martinoli, P. 2006, *Physica C*, 437–438, 328.
15. Ioffe, L.B., Feigel'man, M.V., Ioselevich, A., Ivanov, D., Troyer, M. and Blatter, G. 2002, *Nature*, 415, 503.
16. Born, D., Shnyrkov, V.I., Krech, W., Wagner, Th., Il'ichev, E., Grajcar, M., Hübner, U. and Meyer, H.G. 2004, *Phys. Rev. B*, 70, 180501.
17. Zorin, A.B. 2004, *JETP* 98, 1250.
18. Krive, I.V., Kulinich, S.I., Shekhter, R.I. and Jonson, M. 2004, *Low Temp. Phys.*, 30, 554.
19. Makhlin, Yu., Schon, G. and Shnirman, A. 2001, *Rev. Mod. Phys.*, 73, 357.
20. Clark, T.D. 1968, *Phys. Lett. A*, 27, 585.
21. Saxena, A.M., Crow, J.E. and Strongin, M. 1974, *Solid State Comm.*, 14, 799.
22. Yu, M.L. and Saxena, A.M. 1975, *IEEE Trans. Mag.*, 11, 674.
23. Resnick, D.J., Garland, J.C., Boyd, J.T., Shoemaker, S. and Newrock, R.S. 1981, *Phys. Rev. Lett.*, 47, 1542.
24. Sergeenkov, S. 2001, *Studies of High Temperature Superconductors*, A. Narlikar (Ed.), Nova Science, New York, 39, 117.
25. Sergeenkov, S. 2006, *Studies of High Temperature Superconductors*, A. Narlikar (Ed.), Nova Science, New York, 50, 85.
26. Araujo-Moreira, F.M., de Lima, O.F. and Ortiz, W.A. 1994, *Physica C*, 240-245, 3205.
27. Araujo-Moreira, F.M., de Lima, O.F. and Ortiz, W.A. 1996, *J. Appl. Phys.*, 80, 6.
28. Araujo-Moreira, F.M., de Lima, O.F. and Ortiz, W.A. 1999, *Physica C*, 311, 98.
29. Passos, W.A.C., Lisboa-Filho, P.N. and Ortiz, W.A. 2000, *Physica C*, 341-348, 2723.
30. Passos, W.A.C., Lisboa-Filho, P.N., Caparroz, R., Venturini, P.C., Araujo-Moreira, F.M., Sergeenkov, S. and Ortiz, W.A. 2001, *Physica C*, 354, 189.
31. Goldfarb, R.B., Lelental, M. and Thomson, C.A. 1992, *Magnetic Susceptibility of Superconductors and Other Spin Systems*, R. A. Hein, T. L. Francavilla and D. H. Liebenberg (Eds.), Plenum Press, New York, 49.
32. Wohlleben, D., Esser, M., Freche, P., Zipper, E. and Szopa, M. 1991, *Phys. Rev. Lett.*, 66, 3191.
33. Braunisch, W., Knauf, N., Neuhausen, S., Grutz, A., Koch, A., Roden, B., Khomskii, D. and Wohlleben, D. 1992, *Phys. Rev. Lett.*, 68, 1908.
34. Kostic, P., Veal, B., Paulikas, A.P., Welp, U., Gu, C., Geiser, U., Williams, J. M., Carlson, K.D. and Klemm, R.A. 1996, *Phys. Rev. B*, 53, 791.

35. Geim, A.K., Dubonos, S.V., Lok, J.G.S., Henini, M. and Maan, J.C. 1998, *Nature*, 396, 144.
36. Araujo-Moreira, F.M., Bárbara, P., Cawthorne, A.B. and Lobb, C.J. 1997 *Phys. Rev. Lett.*, 78, 4625.
37. Bárbara, P., Araujo-Moreira, F.M., Cawthorne, A.B. and Lobb, C.J. 1999, *Phys. Rev. B*, 60, 7489.
38. Jeanneret, J.L., Gavilano, G.A., Racine, A., Leemann, Ch. and Martinoli, P. 1989, *Appl. Phys. Lett.*, 55, 2336.
39. Meservey, R. and Schwartz, B.B. 1969, *Superconductivity*, R.D. Parks (Ed.), Marcel Dekker, New York, 1, 117.
40. Sergeenkov, S. 2002, *JETP Lett.*, 76, 170.
41. Sergeenkov, S., Passos, W.A.C., Lisboa-Filho, P.N. and Ortiz, W.A. 2001, *Phys. Lett. A*, 291, 311.
42. Araujo-Moreira, F.M., Maluf, W. and Sergeenkov, S. 2004, *Solid State Commun.*, 131, 759.
43. Barone, A. and Paterno, G. 1982, *Physics and Applications of the Josephson Effect*, Wiley, New York.
44. Ishida, T. and Mazaki, H. 1981, *J. Appl. Phys.*, 52, 6798.
45. Gotoh, S., Murakami, M., Fujimoto, H., Koshizuka, N. and Tanaka, S. 1993, *Physica C*, 166, 215.
46. Chen, D.X. and Sanchez, A. 1991, *J. Appl. Phys.*, 70, 5463.
47. Passos, W.A.C., Araujo-Moreira, F.M. and Ortiz, W.A. 2000, *J. Appl. Phys.*, 87, 5555.
48. Caparroz, R., Lisboa-Filho, P.N., Passos, W.A.C. and Ortiz, W.A. 2001, *Physica C*, 354, 284.
49. Ambegaokar, V. and Halperin, B.I. 1969, *Phys. Rev. Lett.*, 22, 1364.
50. Wright, A.C., Xia, T.K. and Erbil, A. 1992, *Phys. Rev. B*, 45, 5607.
51. Sergeenkov, S., Gridin, V. and Ausloos, M. 1996, *Z. Phys. B*, 101, 565.

Transworld Research Network
37/661 (2), Fort P.O., Trivandrum-695 023, Kerala, India



New Developments in Josephson Junctions Research, 2010: 45-81
ISBN: 978-81-7895-328-1 Editor: Sergei Sergeenkov

3

Magnetization states in annular Josephson π -junction arrays

G. Rotoli

Dipartimento di Ingegneria Meccanica, Energetica e Gestionale, and
CNISM, Università dell'Aquila, Località Monteluco, 67040 L'Aquila, Italy

Abstract

The so-called unconventional Josephson π -junctions can be used in a loop or in more complex arrays. If such loops contain an odd number of π -junctions, spontaneous currents arise in zero magnetic field. The two possible spinning modes give rise to two magnetization states which can be fine-tuned by local magnetic fields in experimentally manufactured high- T_c junction arrays. In this review, we present our latest results regarding a study of quite a simple unconventional

Correspondence/Reprint request: Dr. G. Rotoli, Dipartimento di Ingegneria Meccanica, Energetica e Gestionale and CNISM, Università dell'Aquila, Località Monteluco, 67040 L'Aquila, Italy
E-mail: giacomo.rotoli@gmail.com

array: a ring containing an even number of unconventional loops. From theoretical point of view, this device is analogous to an annular Josephson junction with a "built-in" natural degeneracy. Due to their peculiar topological and physical protection properties, such arrays could be used as natural qubit circuitry for basic building blocks of quantum computing design.

1. Introduction

Among many different types of superconducting devices, the so-called π -junctions [1] are probably the most intriguing ones. In a π -junction, a physical mechanism (such as a d -wave symmetry of high- T_c materials [2] or pairing interaction in Superconducting-FerromagneticSuperconducting (SFS) junctions [3]), will cause a π shift in the phase-current relation. These unconventional junctions are the necessary components for more complex π -circuitry devices like π -SQUIDS [4], π -loop arrays [5, 6, 7, 8, 9], and π junction based filters [10]. A π -SQUID is a single π -loop with one conventional and one π -junction. Generally speaking, a π -loop is an unconventional superconducting loop which contains an odd number of π -junctions. In zero field, the fundamental state of a π -loop has two energy degenerate magnetization states corresponding to two spontaneous current states: clockwise and counterclockwise [11]. In the limit of large loop inductance, these states appear as localized half-flux quanta $\Phi_0/2$, with $\Phi_0 = h/2e$ being the conventional flux quantum. Spontaneous currents have been observed in high- T_c films and grain boundaries [12] as well as in π -SQUIDS [13]. It can be shown that the fundamental state of an array of π -loops is an antiferromagnetic (AF) configuration of half-flux quanta [6, 8]. A closely related device is the so-called $0 - \pi$ long Josephson junction [15, 16, 17, 18, 19, 20] (here 0 means a conventional junction). It can be considered as a continuous "long junction" version of simpler π -loop. The simplest $0 - \pi$ junction is made of two sections (which are joined together), one conventional and one with a π -shift. The resulting discontinuity, $0 - \pi$ boundary, between conventional and π section is the place of spontaneous currents in $0 - \pi$ junction. It can be shown that half-flux quanta (or semifluxons), localize at $0 - \pi$ discontinuities in a long $0 - \pi$ junction [17]. It is also possible to study more complex $0 - \pi$ long junctions made of several conventional and π sections [18]. These systems will show magnetization states made up of chain of semifluxons with different polarity, analog of half-flux quanta state in discrete arrays [7]. These states have been observed in "engineered" [5, 9, 14] unconventional devices. Recently, using new fabrication techniques for $YBCO - I - Nb$ ramp-edge junctions, "zigzag" 1D and 2D arrays of mixed π /conventional junctions have been also realized and characterized [5, 16].

Such devices can be modeled as long $0 - \pi$ Josephson junction with many $0 - \pi$ boundaries [17] or 1D/2D Josephson junction arrays with randomly distributed π -loops. The local spontaneous magnetization was visualized using a SQUID microscope (SSM) [5]. The AF state was clearly seen in 1D case and a prevalent antiferromagnetism was observed also in 2D case [21, 11]. The antiferromagnetic fundamental state found in 2d system is nothing else but a checkerboard state which is found in zero field for 2d mutually coupled Josephson junction arrays with π -loops. Signature of this state is present also in mixed π conventional arrays as shown in [21, 11]. Unconventional devices have been realized also with SFS junctions [9] and local injection of current in a low- T_c device [14]. The interest for unconventional devices is related to the possibility of use the local magnetization in π -loops as the building blocks for a qubit device [22]. The search for a reliable superconducting qubit device has been a hot topic in recent years (see Ref. [41]). Until now the best decoherence times of the order of 100 ns have been reached with a 'mixed' device which use both 'charge' and 'flux' variables for the biasing of a decoupled optimal point in the parametric double well potential (see Ref. [44]). A similar technique was recently applied to a four-junction ring with decoherence measured via spin-echo technique, above $1\mu s$ [22]. The main advantage of an unconventional qubit device is that it works in absence of an external field bias. These systems and some of their variants have been named 'quiet' qubits [23]. In particular, for developing a qubit device, π -junctions based on SFS junctions have been proposed [24]. An important step toward 'quiet' high- T_c qubits, is the recent demonstration of Macroscopic Quantum Tunneling and Energy Level Quantization in a biepitaxial YBCO Josephson junction [25]. Also intrinsic BSSCO devices, formed by many nanoscopic junctions, have shown interesting quantum properties [26].

At the same time, in recent years, the search for a "protected qubit" has been intensified. It can be traced to the seminal works by Kitaev [27] and by Ioffe et al. [28], [29]. The basic idea is that a topological object, say a magnetic "flux" configuration over an array of Josephson junction, could have *at the classical level* (before the quantum effects come into play) the following properties: i) some solution sectors are excluded by assigning them different topological charges; ii) its Hamiltonian is decoupled from external perturbations in the limit of large N , where N is the array dimension (continuous case can be considered as N goes to ∞); iii) the system is insensitive to some perturbations which are topological invariants of the system. On the other hand, the application to large Josephson junction arrays of the concept of protected states is "at the limits of the present technology for such devices" [29]. Indeed, a "protected" qubit which uses 2D Josephson

junction arrays seems far from becoming a workable device. With respect to “protected” qubit, approach based on unbiased unconventional arrays seems more promising. In Ref. [5] is shown that control/read-out phase of half-flux quanta, which are the fundamental operation on a qubit system apart from isolated quantum evolution, can easily be realized using the local magnetic field induced by the SSM head. But, apart from their natural degeneration in zero magnetic field which rests on two degenerate AF configurations, they do not offer true advantages with respect to conventional devices, such as the simplest single-loop “flux” qubit or conventional arrays. Naturally, to fully exploit the topological protection, the unconventional arrays should be incorporated into the design developed in Ref. [29], which is not an easy task. The use of topology for making a *robust* qubit, insensitive to external world, has been also discussed by Wallraff et al. [30]. They have shown that fluxons in annular Josephson junctions can also behave as quantum objects at low temperature and could be used in principle as qubits when subject to a magnetic field induced potential [31]. This last approach can be considered as an extension of “flux” qubits in which a soliton (i.e., a fluxon) is carrying the bit signature. Among the advantages of this approach is that, contrary to traditional “flux” qubits, fluxons in annular junctions carry a topological “charge”, (the so-called winding number n identified as the number of flux quanta threading in annulus) which naturally selects only a family of solutions of the system and make them intrinsically stable against external perturbations.

In this Chapter, we would like to address an alternative simplest scheme which uses π -loop arrays but with the topology of an annular Josephson junction like in Ref. [30]. We will show that a (closed) ring of unconventional loops has both protection properties, induced by its non-trivial topology, and the natural degeneration needed for a qubit “flux” device. These properties are integrated in a single device giving arise to a robust scheme which can be scaled to multi-qubit devices. As low- T_c devices, they will be alternative to the use of long Josephson junction as in Ref. [31]. The remaining of the Chapter is organized as follows. In Section 2, we introduce a model for a ring of unconventional loops array and discuss its relation with unconventional arrays and junctions analyzed in Ref.s [17, 18, 7]. In Section 3, we consider the classical half-flux quanta states on the ring and classify them according to magnetization and winding number n . In Section 4, we evaluate the dependence of states and their energy on a static magnetic field. In particular, we will show how protection arises in the limit of large N . In Section 5, we discuss the obtained results along with a preliminary analysis of quantum behavior of ring arrays (which is currently in progress [32]). Some final conclusions are drawn in Section 6.

2. The model

The first and the simplest device based on π -junctions is the so-called π -SQUID, which is shown in Fig.1a. A π -SQUID is a loop with one π -junction and one 0 (conventional) junction. π -SQUID was realized and studied by many groups [4, 13]. From a formal point of view, the π -SQUID operation is equivalent to that of a conventional SQUID with a $\Phi_0/2$ flux trapped in its loop due to the π -shift introduced by the π -junction. The fundamental state of a π -SQUID is formed by two energy degenerate current states, clockwise and counterclockwise, around the loop. In Fig.1b a 1D Josephson junction annular array is formed by $N = 8$ loops with two junctions, alternatively π or 0. With respect to an open array [7], the loop line is closed on itself giving an annular configuration similar to an annular long Josephson junction [30]. We call this all- π Annular Josephson Junction Array (AJJA) because it is made exclusively by π -loops. All- π AJJA is the direct generalization of simple π -SQUID. The continuous analog of π -SQUID is the so-called 0 – π junction [15] which is

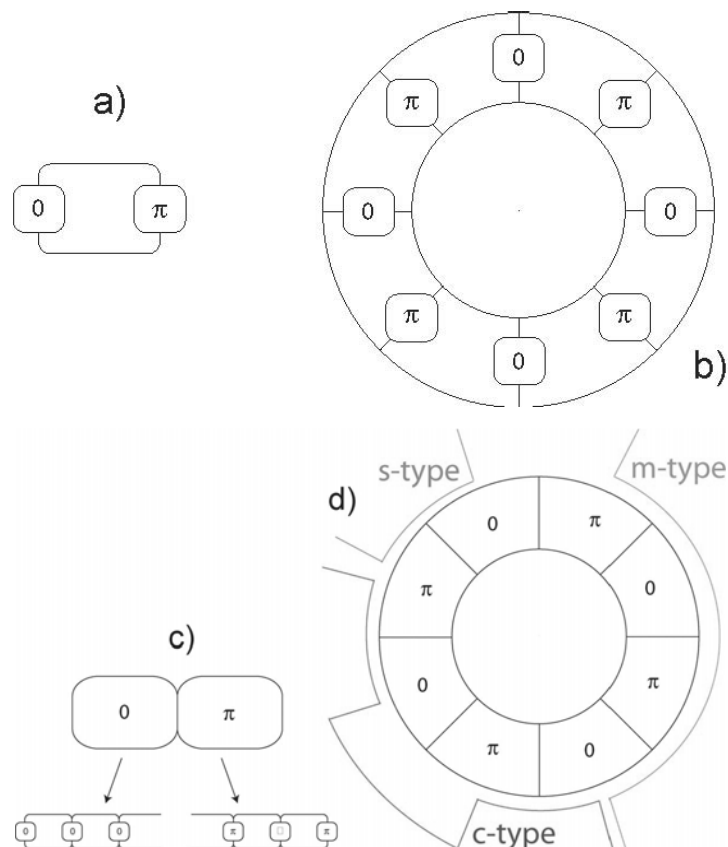


Figure 1. Examples of π Annular Josephson Junction Arrays (AJJA): a) a simple π -SQUID; b) a $N = 8$ ring all- π array; c) the 0 – π junction; d) a $k = 8$ ring k π -array with control lines. Notice that c-type is shown only partially because it should surround the whole array.

formed by two sections equivalent to a 0 (conventional) long Josephson junction and to a π long Josephson junction, respectively (see Fig. 1c). In view of the analogy between the long junctions and the small inductance 1D arrays, we can think of an $0 - \pi$ junction also as an 1D array of N conventional small inductance loops followed by an 1D array of N' small inductance π -loops (see the inset of Fig. 1c). This system will have a single π -loop at the boundary between 0 and π sections [7]. Using the $0 - \pi$ junctions as building blocks, a general version of π AJJA can be formed alternating 0 and π sections (i.e., a sequence of loops with all 0 or all π junctions with a π -loop at any boundary between the sections). We call these k - π AJJA, where k is the number of π -loops in the array (see Fig. 1d). It should be noted that, differently from the open π -arrays [7], the annular π -arrays will always have an even number of π -loops, by construction. The minimal annular $0 - \pi$ junction will necessarily have two π -loops along a diameter (for equal length of π and 0 section). This corresponds to a 2 - π AJJA. An asymmetric configuration with different length of sections can also be considered [18].

To model a ring π -array, we start from its classical energy. This can be written as the sum of Josephson energy and the magnetic field energy:

$$\mathcal{H} = \frac{E}{E_J} = \sum V(\varphi_j, \varphi_{j,t}) + \sum \frac{1}{2\beta} (\phi_j - \phi_{j,ext})^2 \quad (1)$$

where φ_j is the gauge invariant phase difference in the $j - th$ junction in the array (hereafter referred simply as the phase); $V(\varphi_j, \varphi_{j,t})$ is the generalized Josephson energy term of the $j - th$ junction and $\phi_j, \phi_{j,ext}$ are respectively the normalized total magnetic flux and the normalized external magnetic flux in the $j - th$ loop, i.e., $\phi_j = \Phi_j / \Phi_0$. As usual, $E_J = I_0 \Phi_0 / 2\pi$ is the Josephson energy per junction and $\beta = 2\pi I_0 L / \Phi_0$ with I_0 the junction critical current and L the loop inductance. Here we assume that all junctions have the same critical current I_0 and all loops the same self-inductance L . The effects of spread and difference in mean critical current for the conventional and π -junctions are discussed at the end of Section 5. The two sums in Eq. (1) are intended to N for a N -junctions ring array. In Eq. (1) we assume that there are no mutual inductance terms, this assumption is correct only if the array loops are not very large (i.e. self-inductance L is not too large), however the energy (1) can be used also for relatively large L by simply re-normalizing the self-inductance by next-neighbor mutual ones [33]. In any case, we assume that loops contain a maximum flux equal to a single flux quantum Φ_0 , so there are no situations in which more than a flux quantum can be found in the array loops. This will

exclude multi-quanta solutions (these solution will appear for large β and in simplest loops are known as metastable states) and set a limit on the self-inductances which depends on N , but practically means that β should not be much larger than 1. In the following we will give some estimates of the minimum value of $\beta = \beta_{mq}$ where multiquanta solution sets in. It is found that $\beta_{mq} \sim 6$ is the limit in all practical cases. Under these circumstances, the next-neighbor approximation can be safely used.

The generalized Josephson energy term is written as the charging energy over the junction capacity C (supposedly equal for each junction as for critical currents and self-inductances) plus a Josephson washboard potential:

$$V(\varphi_j, \varphi_{j,t}) = \frac{1}{2}\varphi_{j,t}^2 + 1 - (-1)^{k(j)} \cos \varphi_j - \gamma_j \varphi_j \quad (2)$$

where times are normalized to Josephson plasma frequency $\omega_J = \sqrt{2\pi I_0/C\Phi_0}$ and $\gamma_j = I_j/I_0$ is the normalized bias current in the j -th junction. The index $k(j)$ is 0 for conventional junction and 1 for π -junctions. The normalized flux ϕ_j can be written in term of the flux quantization in the j -th loop:

$$\phi_j = \Delta\varphi_j = \varphi_{j+1} - \varphi_j + 2\pi n_j \quad (3)$$

The quantum numbers n_j can be chosen to reduce the variation of phases within 2π in the loop by defining Δ as the difference operator mod 2π . This is generally acceptable for β not very large because the phase differences are small and n_j is almost always zero, with the notable exception of n_N . In fact, after one turn around the ring is completed, the build-up of the phases can end in a 2π multiple, so $n_N \equiv n$ can be identified as the *winding number* of the ring (i.e., the number of 2π phase slips around the ring). We use only integer winding numbers though it is possible in principle also consider situations in which the winding number is semi-integer (see Ref. [20]) closing the arrays at one of $0 - \pi$ boundaries. However, this will result in difficulty to realize practically a $0 - \pi$ boundary as a true discontinuity and besides, the "localization of a winding number" is a meaningless concept in a long annular junction. With these assumptions, the energy can be written in the form:

$$\mathcal{H} = \sum V(\varphi_j, \varphi_{j,t}) + \sum \frac{1}{2\beta} (\Delta\varphi_j^2 - 4\pi\Delta\varphi_j f_j + 4\pi^2 f_j^2) \quad (4)$$

where we have introduced the frustration $f_j = \phi_{j,ext}/2\pi$. We note that the sign of linear term in the loop frustration depends on the sign of phase differences

around the loop. This term will be responsible for removing the degeneration of the energy states in a paramagnetic and a diamagnetic state. If the frustration is uniform, $f_j = f$, we find: $-4\pi \Sigma \Delta \varphi_j f_j = -4\pi \Delta \varphi f$ which is *zero* for a ring with zero *winding number* $n = 0$. This implies that, differently from the open arrays [7], a uniform magnetic field (normal to the array plane) does not have effects on a ring array with $n = 0$. This is a property that can be traced to the topology of the ring array which does not have 'ends'. In the following we will discuss more carefully the field spatial configurations that are most effective in perturbing the fundamental state of the ring arrays. Naturally the same property is found in the annular long junctions, but the real difference is that in the annular junction the field is transverse, i.e., it is in the junction plane rather than orthogonal to it (see Ref. [30]). Depending on the geometry of the junctions in a ring π -array, a transverse component cannot be generally excluded but for a planar array it will act on the junctions if their barrier is normal to the array plane, rather than on the loops, which are in the array plane. Since the flux in the loops is the important quantity for a flux device, the perturbation induced by a transverse field can be considered as a higher order correction. When a non-uniform magnetic field is imposed over a ring π -array, its response is in general similar to single loop: paramagnetic and diamagnetic solutions are formed and the energy degeneration is removed. So for all π -arrays we assume that a local field can be put into the array loops, generated by a small coil in a loop, or more loops, of the array (see Fig. 1a). Alternatively a non-uniform field configuration can be generated in k - π -arrays by controlling the lines near the array (see Fig. 1b). From Eq. (4) the continuous limit can be derived taking $\Delta x = \beta^{1/2}$ and defining the normalized magnetic field as $\eta_j = 2\pi f_j / \beta^{1/2}$. This term will be equal to the normalized magnetic field at boundary: $\eta \equiv (2\pi / \Phi_0) \lambda_J \lambda B_{ext}$ (see Ref. [7]) with λ_J the array Josephson penetration length and λ equal to the penetration length in the direction perpendicular to the array. The exact value of λ depends on the geometry of the array, it can range from London length λ_L , for grain boundaries array [7], to roughly the loop (mean) diameter D . The above Δx can be identified as the normalized lattice space of the array, i.e., $\Delta x = D / \lambda_J$. The array normalized length can be written also as $l = N \Delta x = N \beta^{1/2}$ for N large. In the following we use also the normalized length of π or 0 sections defined as $a = (N/k) \beta^{1/2}$.

The "equations of motion" for the phases can be derived by the energy given by Eq. (4) by a standard variational approach. At the "classical" level we must include the dissipation due to the quasi-particle tunneling. This can be

modeled as an Ohmic dissipation corresponding to the standard RSJ model for a Josephson junction. This implies that the term containing the time derivatives of the phases is $\varphi_{j,tt} + \alpha\varphi_{j,t}$, where α is a normalized conductance. Finally, we obtain the modified Discrete Sine-Gordon equation (mDSG) for an N Josephson junction one-dimensional ring π -array:

$$\varphi_{j,tt} + \alpha\varphi_{j,t} + (-1)^{k(j)} \sin \varphi_j = \frac{1}{\beta} (\varphi_{j+1} - 2\varphi_j + \varphi_{j-1}) + \frac{2\pi}{\beta} (f_{j+} - f_{j-}) + \gamma_j \quad (5)$$

where $f_{j\pm}$ is the frustration in the j^{\pm} -th loop preceding (-) or following (+) the j -th junction and with the condition that $\varphi_N = \varphi_1 + 2\pi n$ (see Eq. (3)). As expected for ring arrays, there is no effect of a uniform (normal) magnetic field because last term of Eq. (5) is zero in all loops in this case. Some property of the continuous limit case can be deduced for system with very small β (< 0.01). The corresponding form of Eq. (5) for open arrays was deduced in the continuous limit by Goldobin et al. [17] in the context of analysis of 'zigzag' arrays. For a ring junction, the same continuous equation applies with the boundary condition $\varphi(0, t) = \varphi(l, t) + 2\pi n$. In the following we calculate the local magnetization using the solutions of Eq. (6). In particular for N loops system it can be calculated as:

$$m_j = \frac{\Delta\varphi_j}{2\pi} - f_j \quad (6)$$

where the last term is the mean frustration. So in a ring π -array for zero winding number the magnetization is always negative and reduces to the mean frustration.

3. Classical ring array states

Firstly, we study the zero-field classical solutions of Eq. (6). These can be classified in fundamental states and higher energy "excited" states. Following Ref. [18] we indicate the local magnetization state with an arrow indicating the "spin" of the associated magnetic moment to the π -loop, or $0 - \pi$ boundary, i.e., we set \uparrow (say) for the positive magnetization and \downarrow for the negative one. The magnetization will be near $\Phi_0/2$ (half flux quantum or semifluxon in long junctions) for large β or long sections, $a > 1$, and going to zero for small β or $a \ll 1$. For a single loop with identical junction the magnetization can be written as $m = \frac{1}{2\pi}\beta\gamma$ where γ is the normalized current. This implies that the

magnetization is going to zero for low β , being the current of the order of one. On the other hand, for large β we have $\gamma \sim \pi/\beta$ so magnetization is of the order of half flux quantum [11]. To understand the nature of Eq. (6) solutions we note that for large β the coupling is going to zero. (Practically, the value of β needed to fully develop half-flux quanta into an all π array, would be near $\beta \sim 10$. In this case also multi-quanta solutions appear and the simple next-neighbor approximation for loop interaction is questionable. However, we do not use these values of β in the following analysis, but discuss the large β case just to analyze the nature of mDSG solutions.) In this limit the loops are weakly interacting and the solution will be roughly the sum of the solutions for the single loops forming the array. This is especially true in the case of all π -arrays (Fig.1b) where the basic solutions of mDSG Eq. (6) for a large β consist of a collection of half-flux quanta localized in the array loops. Among these solutions with different energies, the minimum energy solution will be the fundamental state of the system. It is clear that for β going to infinity all the solutions with an arbitrary distribution of half-flux quanta over the array will have the same energy with no contribution from magnetic energy in Eq.(6) because the Josephson energy is the same whatever is the junction, 0 or π . However, for finite large β a residual interaction will split the energies. We have two possible solutions: the anti-ferromagnetic solution $\uparrow\downarrow \dots$ with a sequence of currents circulating in the opposite directions in the two loops, and the ferromagnetic solution $\uparrow\uparrow \dots$ with a sequence of currents circulating in the same direction. The magnetic energy is maximum for the ferromagnetic solution because in order to build this solution the phase differences have to be larger to form the sequence of \uparrow magnetic moments. Therefore, antiferromagnetic ordering will be preferred in the fundamental state of the system. The situation does not change for lower β because the energy split between ferromagnetic and antiferromagnetic solutions increases as $1/\beta$. Naturally, for any sequence of spins, another arrangement with the same energy exists with all spins flipped, so any state is at least double degenerate like the fundamental state of simple π -loop. A magnetic image of the fundamental state in an open 1d array is shown in Ref. [5]. When connection between loops was cut, the array did not show the antiferromagnetic state, but a random sequence of half-flux quanta. This implies that the circuit-type models shown in Fig. 1 are likely to provide the most correct description of π -arrays physics.

In a ring array only an even number of π -loops can exist, so there are only even number of spin arrangements, e.g., the minimum ring all π -array with $N = 2$ will have two π -loops with a fundamental state $\uparrow\downarrow$ or $\downarrow\uparrow$. For this array the

only other states are the ferromagnetic states $\uparrow\uparrow$ and $\downarrow\downarrow$, which are built up by a (delocalized) fluxon $\pi + \pi = 2\pi$ or an antifluxon $-\pi - \pi = -2\pi$. These ferromagnetic states carry a kink (like in annular junction case), so they need a winding number $n = \pm 1$ to set up. For k - π AJJA (see Fig.1d) the description of states is similar to all- π AJJA: the magnetization peaks localize at boundary between 0 and π sections [17]. In the k - π AJJA the width of magnetization peaks depends on equivalent normalized length a of the array sections. For $a \gtrsim 1$ or larger, half-flux quanta appears as an isolated cusp singularity localized at $0 - \pi$ boundaries [7]. For $a \lesssim 1$ the half-flux quanta merge and local magnetization is no longer equal to $\Phi_0/2$, but a description as a sequence of spins $\uparrow\downarrow \dots$ is still valid in many cases as we show below.

In general for a given k (N for all π) a ring π -array will have $2^k - 2$ different types of excited states that correspond to all arrangements of spin chains in the array. It should be noted that not all the excited states will be stable for $\beta \leq 1$ in all π -arrays. Due to larger distance between π -loops in k - π AJJA excited states are stable at smaller β . In the continuous limit the system sometimes can undergo antiferromagnetic-flat phase transition if its physical length becomes smaller than λ_J . In Ref. [17] this limit was evaluated for the continuous case in term of the minimal length of 0 (π) sections of the system. And for large k it was found that the limit is around $\beta = 1$ as is expected on intuitive grounds. The classification of magnetization states for $k = 4$ and $k = 6$ (or $N = 4$ and $N = 6$) is reported in Table 1 where also some critical values of β for the stability are given. Most excited states in ring π -arrays have solutions with a winding number different from zero (see Table 1). Winding number

Table 1. Classification of states in $k = 4$ and $k = 6$ ring arrays. n is the winding number. The number of states for topology is given in third and seventh columns. Critical β_c values are given for unstable solutions (when known). A j -spin solution is a solution with j contiguous spins over the ring. β_c^k is the critical value of β for k - β -AJJA (see text).

n	$k = 4$	16	type	$\beta_c (10^3 \beta_c^k)$	$k = 6$	64	type	$\beta_c (10^3 \beta_c^k)$
0	$\uparrow\downarrow\uparrow\downarrow$	2	AF		$\uparrow\downarrow\uparrow\downarrow\uparrow\downarrow$	2	AF	
0	$\uparrow\uparrow\downarrow\downarrow$	4	K-AK	2.52 (1.8)	$\uparrow\uparrow\downarrow\uparrow\downarrow\uparrow\downarrow$	12	K-AK	3.96 (2.4)
0					$\uparrow\uparrow\uparrow\downarrow\downarrow\downarrow$	6	triplet	4.41 (2.8)
1	$\uparrow\downarrow\uparrow\uparrow$	8	3-spin		$\uparrow\uparrow\downarrow\uparrow\uparrow\downarrow$	6	2-spin	
1					$\uparrow\uparrow\uparrow\downarrow\uparrow\downarrow$	12	3-spin	1.37
1					$\uparrow\uparrow\uparrow\uparrow\downarrow\downarrow$	12	4-spin	4.69
2	$\uparrow\uparrow\uparrow\uparrow$	2	FF		$\uparrow\uparrow\uparrow\uparrow\uparrow\downarrow$	12	5-spin	
3					$\uparrow\uparrow\uparrow\uparrow\uparrow\uparrow$	2	FF	

can be thought of as a kink localized at the end of spin sequence, e.g., for $N = 4$ $n = 1$ the state could be formally written as $\uparrow\uparrow\uparrow\downarrow^{(\downarrow)}$. The conservation of the spin sum, which is always zero, indicates the correct wrapping of the phase around the loop. A fully ferromagnetic solution will be written as, e.g., $\uparrow\uparrow\uparrow\uparrow^{(\downarrow)(\downarrow)}$ corresponding to a winding number $n = 2$ in this particular case.

To calculate the local magnetization and the energy of a given state we integrate numerically Eq.(6) to find the phases for all junctions. Initially the phases of conventional junctions are set to $2\pi l_j$, l_j integer, and the phases of π -junctions to $2\pi l_j \pm \pi$, which are the stable equilibrium points of the single junction potentials. For any choice l_j , a sequence of spontaneous currents circulating around the π -loops is selected. $\alpha = 1/\sqrt{\beta_C}$ was chosen in the interval $0.05 - 0.25$, which is comparable with the interval proposed in Ref. [17]. In some cases different α was used to generate the same static solution to check the stability of static solution against different initial conditions and numerical errors. We choose $\lambda_j = 0$ because we are interested in unbiased arrays driven by magnetic field only. In absence of bias currents, the system naturally sets in a static equilibrium solution after few plasma periods. Near critical β_c for excited states this process becomes slower, so longer integration times are needed.

3.1. All- π AJJA

The energy (per loop) of states in all π -arrays, as function of π and for $N = 2, 4, 6$, is reported in Fig. 2. For larger N the fundamental state and the ferromagnetic state tend to have the same energy and magnetization (see Fig. 2). On the other hand, we see that the energy gap between AF and FM states increases for small β as expected. The FM state energy is dominated by magnetic part that goes like $1/\beta$. In particular, it would be noted that ferromagnetic state with phases equal to $j\pi$ with $j \in [0, N - 1]$ and winding number $n = N$ is an exact solution of Eq.(6). The energy (per loop) is purely magnetic and it is simply equal to π^2/β .

The phases φ_j and the magnetizations m_j of the fundamental states $\uparrow\downarrow \dots$ are shown in Fig. 3 for the same values of N as in Fig. 2. They appear as discrete peaks each indicating the magnetization in any of the array loops. For low β the magnetization is going to zero and the phase tends to be flat. Anyway, the vanishing of magnetization is a smooth curve as shown in the inset of Fig. 2a. There is no abrupt transition to a flat phase in this case. AJJA have an even number of $0 - \pi$ boundaries, but formally they correspond to the case in which $a = b/2$ and $a_c = 0$ [34]. Both the phases and the magnetization in

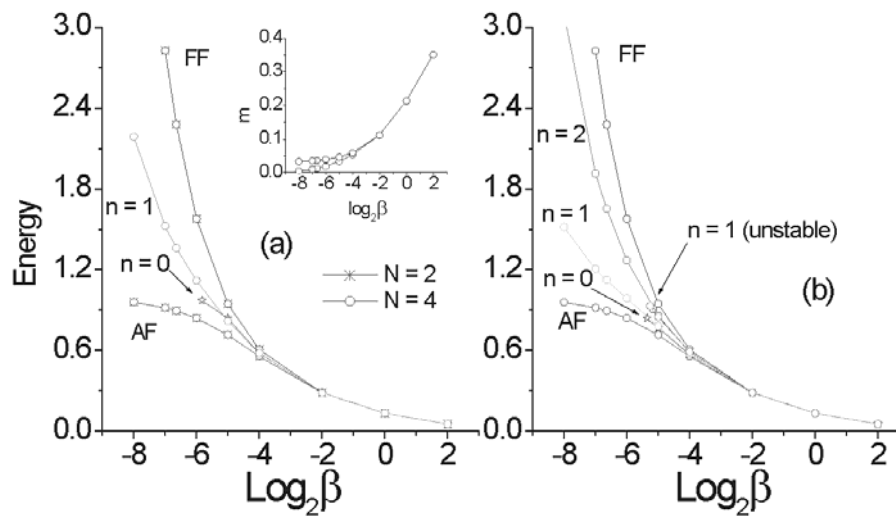


Figure 2. Energy per loop, E/N , of a $N = 2, 4, 6$ all- π AJJA, energy is normalized to $1/N$ and $\alpha = 0.25$: (a) $N = 2, 4$ with AF and FM states and $n = 0, 1$ states for $N = 4$; the inset shows the magnetization of π -loops; (b) $N = 6$ with the same states as in case (a) plus the $n = 2$ states. For unstable $n = 0, 1$ states \star the curve ends before reaching the lowest calculated β which is 0.001 in this case. Stable states exist for arbitrary low β values.

Fig.3 appear to be independent from N . This is a consequence of high symmetry of a ring array with no 'border', so that the $N = 2$ solution (Fig. 3a) replicates itself in the next loop pair (Fig.3b,c). This property is true for arbitrary N arrays.

The $N = 2$ ferromagnetic state can be also obtained by introducing a localized kink, in spin notation $\uparrow\uparrow$, added to second loop of AF state $\uparrow\downarrow$ for $\beta < 6.22$ and setting $n = 1$. Below this value the multi-quanta states are unstable and decay to a ferromagnetic one. For larger N this instability occurs at larger β (see below). This is a first example of the process $\uparrow\uparrow + \downarrow = \uparrow$ that, as we show in the following sections, is the main mechanism for changing magnetization states (see also [18, 19, 32]).

For $N > 2$ the energy spectrum of all- π AJJA will include also the excited states. The nearest states in energy to the fundamental state are $n = 0$ states. In Fig. 4a,b we report some $n = 0$ states for $N = 4, 6$. The k - ak pairs $\uparrow\uparrow\downarrow\downarrow$ become unstable for $\beta < \beta_c$. In analogy with an annular long junction, there exists a 'minimal distance' at which the pair can exist governed by 'equivalent length' given by $N\beta^{1/2}$. This means that, below the critical β_c , the k - ak is unstable and the only stable solution is the fundamental state. For $N = 4$ the k - ak is unstable for $\beta_c \lesssim 2.52$ as is reported also in Table I. The same happens for $\beta_c \lesssim 3.96$ and $\beta_c \lesssim 4.41$ for $N = 6$ depending on the type of $n = 0$ state considered (k - ak or triplet, see Table I). The higher values of β_c for $N = 6$ k - ak are likely due to presence of a spurious spin pair $\uparrow\downarrow$ which is not present for $N = 4$. The $n = 0$

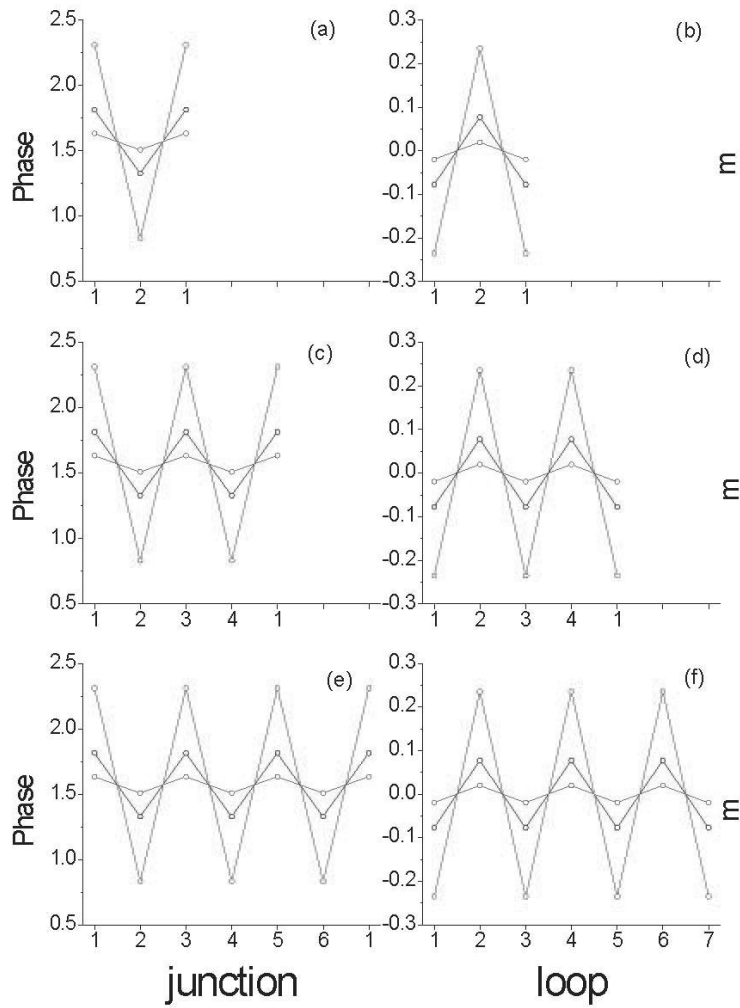


Figure 3. Simulated phase and magnetization of a $N = 2, 4, 6$ all- π AJJA with $\beta_L = 4, 1, 0.25$ and $\alpha = 0.25$, in all cases a last loop to be identified with first one has been added for better visualization of ring solution: (a) $N = 2$ phase; (b) $N = 2$ magnetization; (c) $N = 4$ phase; (d) $N = 4$ magnetization; (e) $N = 6$ phase; (f) $N = 6$ magnetization.

branches on energy vs β plot (see Fig. 2) end at the critical β_c . It is interesting to note that in this last case the only zero winding number stable solution of Eq. (6) is the fundamental state in a ring array, so if sectors with different n have proven to be excluded the only states are fundamental ones in this case. It is worthwhile to remember that this is not the case of open π -arrays, which can be subject to spin flips toward the higher energy states without a topological constraint.

The energy of $\uparrow\downarrow\uparrow\uparrow^{\downarrow\downarrow}$ state for $N = 4$ is also shown in Fig. 2b. Due to the ring symmetry all '3-spin' states for $N = 4$ have the same energy. The same happens for '2-spin', '3-spin' or '4-spin' states for $N = 6$. In Fig. 4c-f are shown the magnetization and the phases in some selected cases. For $N = 6$ the '3-spin' and '4-spin' states are unstable toward the minimum energy solution

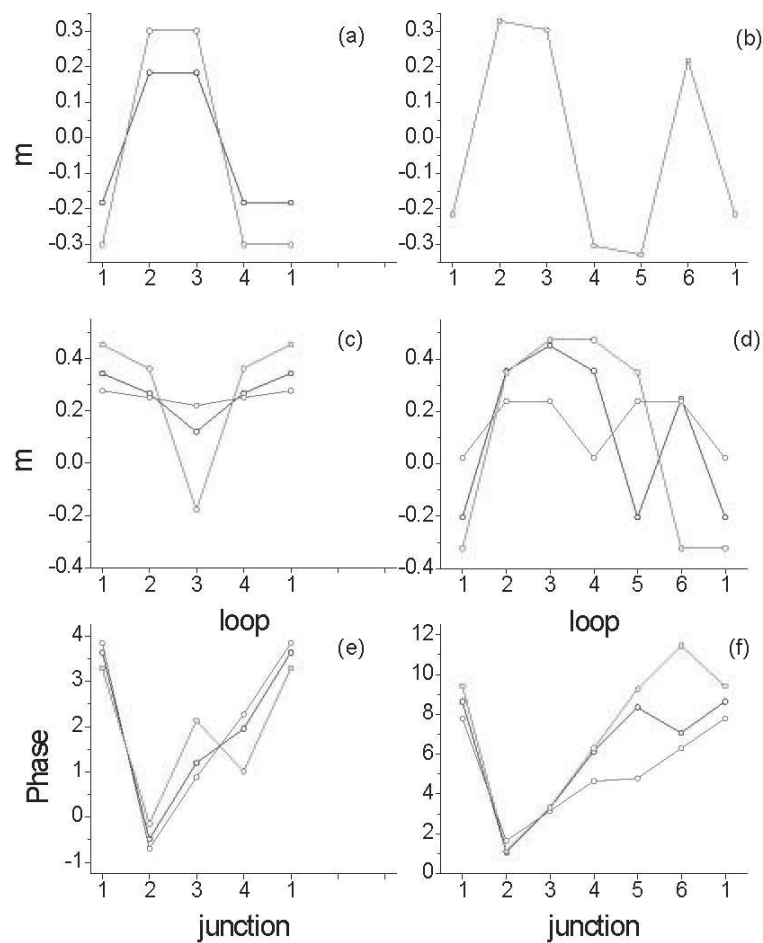


Figure 4. Simulated phase and magnetization of a $N = 4, 6$ all- π AJJA with $\alpha = 0.25$, in all cases a last loop to be identified with first one has been added for better visualization of ring solution: (a) $N = 4$ $n = 0$ magnetization with $\beta = 4, 1$; (b) $N = 6$ $n = 0$ magnetization with $\beta = 4$; (c) $N = 4$ $n = 1$ magnetization with $\beta = 4, 1, 0.25$; (d) $N = 6$ $n = 1$ magnetization with $\beta = 4, 1, 0.25$; (e) $N = 4$ $n = 1$ phase with $\beta = 4, 1, 0.25$; (f) $N = 6$ $n = 1$ magnetization with $\beta = 4, 1, 0.25$.

which is the '2-spin' below the critical β_c reported in Table I. In Fig.4d β is reduced from 4 to 0.25 and states sweep from '4-spin' to '2-spin'. It is seen that the magnetization of unpaired loop for small β becomes positive (see Fig. 4c), so the 'spin' interpretation becomes problematic for very small β in these cases. For $n \neq 0$ states the phase acquire a finite gradient for small β . This is necessary to fulfill the periodicity condition for the phase, i.e., $\varphi_N = \varphi_1 + 2\pi n$. Solutions with a constant phase gradient appears for very small β and the magnetization spreads over the whole ring. This is clearly shown in Fig. 4e,f where the phase corresponding to $n = 1$ states is reported. In Fig. 2b the energy of $n = 2$ '5-spin' state for $N = 6$ is also reported. This solution is stable due to the change in winding number.

The $n \neq 0$ states can be obtained adding a localized kink $\uparrow\uparrow$ in some loop. This changes winding number and generates the excited states. The addition of a kink in the fundamental state in larger ring π -arrays, beside the change in winding number, gives rise (for some interval of β) to fractionalization phenomenon [6], i.e., the kink splits in a '2+2-spin' configuration with $\dots \uparrow\uparrow\downarrow\uparrow\uparrow \dots$. The paired spins tends to repel each other with the lowering of β . This is shown in Fig. 5 where the case of a $N = 16$ array is reported. In AJJA the fractionalized state is identical to a $n = 1$ state when β is smaller than critical value for multi-quanta state (see Fig. 5). In fact, for large β , a multi-quanta solution exists in which the kink occupies a single loop of the array (actually this is not predicted by authors of Ref.[6] because they study lower β cases and their continuous-like approximation in the calculation of stability is not valid for very large β). This happens roughly for $\beta_{mq} \geq 9.3$ at $N \geq 4$ which represents the minimum β for the existence of stable multi-quanta solutions. We have shown just some $n \neq 0$ states for low N , but in the following we assume that the topological condition on winding number implies that only $n = 0$ states are involved in the flipping process from one fundamental state to other one. So we can avoid studying in detail the $n = 0$ states. For large N most

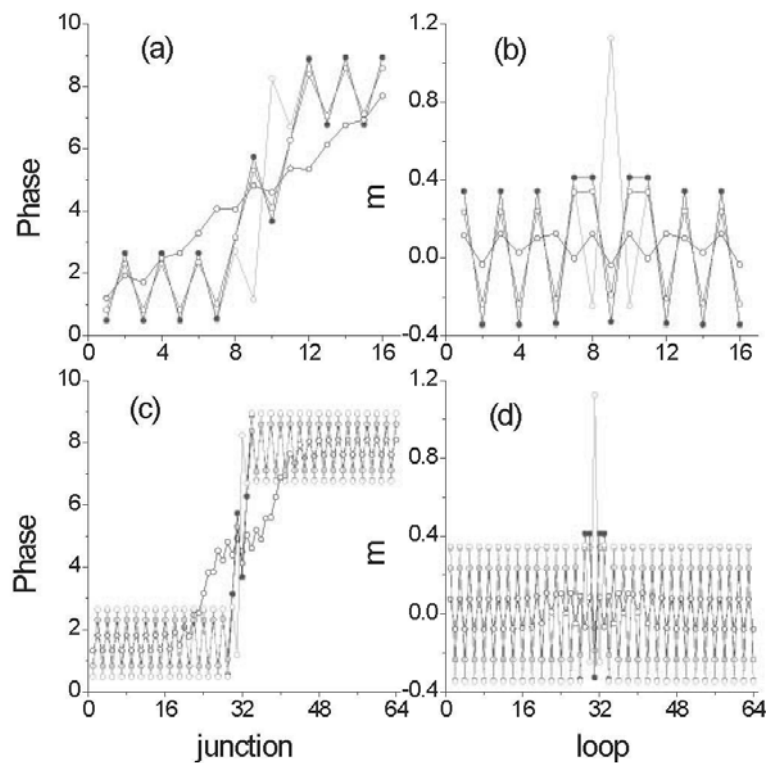


Figure 5. Simulated phase and magnetization of a $N = 16, 64$ all- π AJJA with $\alpha = 0.25$: (a) $N = 16$ $n = 1$ phase with $\beta = 10, 4, 1, 0.25$; (b) magnetization for (a); (c) $N = 64$ $n = 1$ magnetization with $\beta = 10, 4, 1, 0.25$; (d) magnetization for (c).

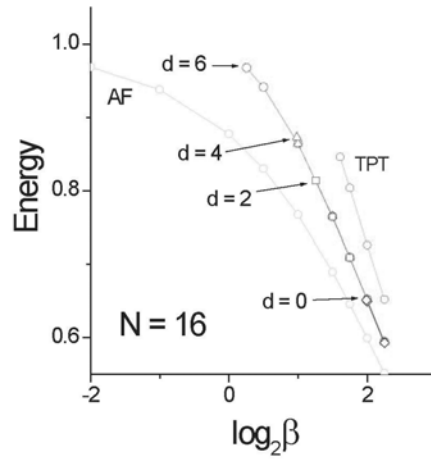


Figure 6. Energy of $n = 0$ states of a $N = 16$ all- π AJJA with $\alpha = 0.25$.

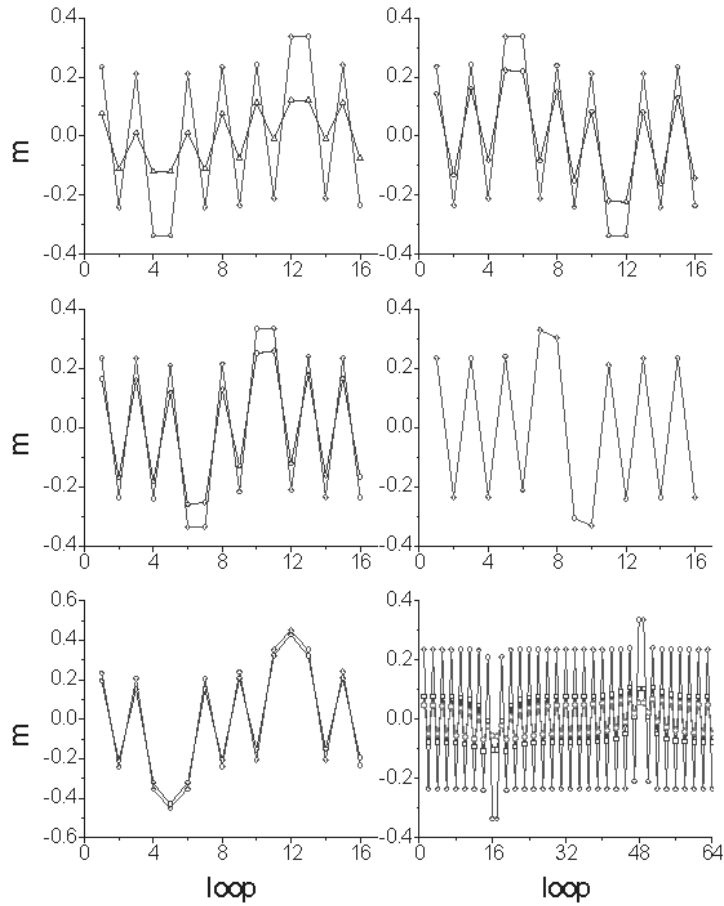


Figure 7. Simulated magnetization of a $N = 16, 64$ all- π AJJA with $\alpha = 0.25$: (a) $N = 16$ $n = 0$ phase with $\beta = 1.2$ and 4 at maximum distance of $k-ak$; (b) $N = 16$ $n = 0$ phase with $\beta = 1.9$ and 4 at distance 4 of $k-ak$; (c) $N = 16$ $n = 0$ phase with $\beta = 2.4$ and 4 at distance 2 of $k-ak$; (d) $N = 16$ $n = 0$ phase with $\beta = 4$ at minimum, distance of $k-ak$; (e) $N = 16$ $n = 0$ phase with $\beta = 3$ and 4 triplet state; (f) $N = 64$ $n = 0$ phase with $\beta = 0.6, 1$ and 4 at maximum distance of $k-ak$.

of the states will have non-zero winding number, whereas the $n = 0$ sector will have only relatively few solutions.

In Fig. 6 we show the energy of $n = 0$ sector for $N = 16$, the AF fundamental state branch is reported for comparison. Energy gaps always tend to increase, but the branches terminate at a critical β_c . In particular the lowest energy $n = 0$ state above the fundamental state involves a pair $k-ak \dots \downarrow\downarrow \dots \uparrow\uparrow \dots$ in which kinks are separated by an equal distance, in an annular configuration at the ends of a diameter. This $k-ak$ is unstable below $\beta = 1.19$ for $N = 16$ and below $\beta = 0.61$ for $N = 64$. In Fig. 7 magnetizations of $n = 0$ states for $N = 16$ and $N = 64$ are shown. These involve $k-ak$ pairs in which the separation is shorter and they are unstable also for large β ranging from 1.93 to 3.97 for the minimum distance. In this last case the kinks occur at the adjacent loops $\dots \downarrow\downarrow\uparrow\uparrow \dots$ and the critical $\beta_c \sim 4$ is essentially independent from loop number for $N \geq 6$. Other $n = 0$ configurations can exist involving more than half-flux or integer flux quanta, e.g. triplet like $\dots \downarrow\downarrow\downarrow \dots \uparrow\uparrow\uparrow \dots$ (see Fig. 7e) or state with more than a $k-ak$ pair, but their stability range is smaller than single $k-ak$ states and the energy is higher as we have just seen for the case $N = 6$.

3.2. $k-\pi$ AJJA

The energy for similar states in $k = 2, 4, 6$ arrays is shown Fig.8 where $N = 32, 64, 96$ with $N/k = 16$. Local magnetization and phase are reported in Fig. 9: similarly to all π -arrays the system replicates itself in the next period. On the other hand, the magnetization in $k \pi$ -arrays tends to be localized near the π -loops giving rise to the continuous like structure of half flux quanta reported in the literature [17]. This also implies that for FM state there is no longer a constant along the array. For large β half flux quanta appears like isolated spikes separated by flat phase regions. In this case the energy (Fig. 8) is simply the sum of isolated half-flux quanta and all states appear degenerate because there is no distinction between \uparrow and \downarrow states. Only for small values of β , practically corresponding to the continuous limit, the splitting of energies becomes relevant. In Fig.8 this occurs roughly at $\beta \simeq 1/16$ corresponding to a $= (N/k) \beta^{1/2} \simeq 4$ for the section length. For this value of β the total magnetization over the section a is $\sum_j^{N/k} m_j = 0.356$, i.e., 71% of half-flux quantum. The total magnetization vs β is reported in the inset of Fig.8a.

Again for $k > 2$ and low β the excited states are not all stable: there exist critical values β_c (see Table I and Fig. 8) where $k-ak$ and some of higher energy $n = 0$ excited states are unstable and decay respectively toward fundamental and lowest energy stable $n = 0$ excited states. The corresponding

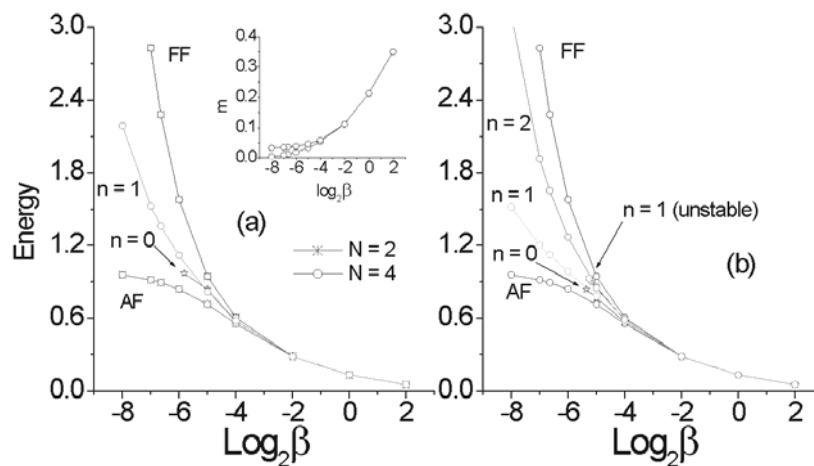


Figure 8. Energy of a $N = 2, 4, 6$ Josephson junction for a k - π AJJA $N/k = 16$, energy is normalized to $1/N$ and is $\alpha = 0.25$: (a) $k = 2, 4$ with AF and FM states and $n = 0, 1$ states for $k = 4$, the inset shows the magnetization of π -loops; (b) $k = 6$ with the same states as in case (a) plus the $n = 2$ state. For unstable $n = 0, 1$ states the curve ends before reaching the lowest calculated β . Stable solutions can be continued to arbitrary low β values.

branches in Fig. 8 end at some critical β_c . Plots of some excited states for $N = 4, 6$ are reported in Fig. 10a-d.

Localized kinks in the k - π AJJA also show the fractionalization phenomenon as is seen in Fig. 10e for intermediate values of β for the $k = 16$ case. We find that fractionalization occurs in the interval $2.87 < \beta < 5.95$. Larger β gives multi-quanta solutions (see Fig. 10e). In fact, on the small β side the solutions do not spread. This is different from the all- π AJJA case. The kink itself detaches from original π -loop and regains its shape moving in the flat phase region. Finally, for small $\beta < 0.76$ it annihilates on near half-flux quanta giving rise to a $n = 1$ solution (see Fig. 10f). This behavior is possible due to existence in k - β AJJA of flat phase regions in which conventional SG kinks can be added without (or weakly) interacting with the half-flux quanta structure of fundamental state if β is sufficiently large (and so is section length a). We again see how the annihilation of a full flux quantum (fluxon) involved in the spin flip mechanism of localized half-flux quanta [18, 19, 32].

In Fig. 11 we show the energy of $n = 0$ sector solutions for $k = 16, N/k = 16$. Apart from numerical differences the behavior is very similar to all- π arrays case: energy gaps increase and unstable branches terminate at a critical β_c . The maximum separation k - ak is unstable below $\beta \sim 0.008$ for $k = 16$ corresponding to $a \sim 1.43$ and below $\beta = 0.004$ for $k = 64$ corresponding to $a = 1.01$. In Fig. 12a lowest energy k - ak $n = 0$ solution for $N = 16$ is shown. As in

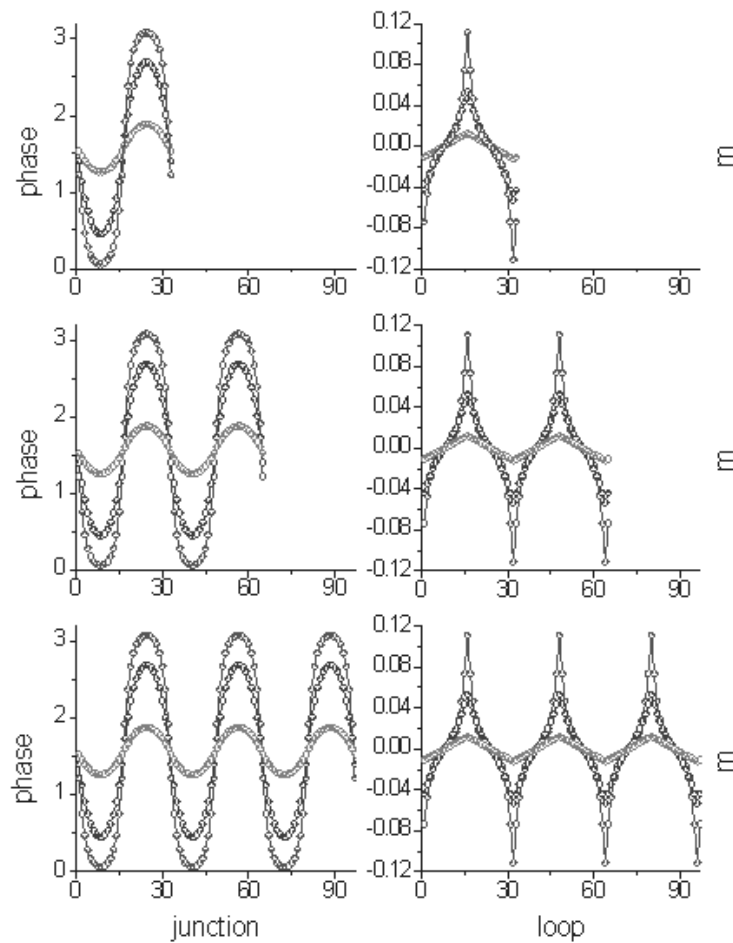


Figure 9. Simulated phase and magnetization of a $k = 2, 4, 6$ k - π AJJA with $\beta_L = 4, 1, 0.25$, $N/k = 16$ and $\alpha = 0.25$, in all cases a last loop to be identified with first one has been added for better visualization of ring solution: (a) $N = 2$ phase; (b) $N = 2$ magnetization; (c) $N = 4$ phase; (d) $N = 4$ magnetization; (e) $N = 6$ phase; (f) $N = 6$ magnetization.

all- π array higher energy solutions involve k - ak pairs in which the separation is shorter. They are unstable also for a larger β (see Fig. 11). In Fig. 12b a solution with higher energy is also shown, this corresponds to a localized $k - ak$ pair $\uparrow\uparrow\downarrow\downarrow$. In Fig. 12c the lowest energy k - ak $n = 0$ is shown for an array with $k = 64$, k and ak structures are separated by 30 alternating spins. As is mentioned above when the spin distance becomes smaller than Josephson length, i.e., $a \lesssim 1$, the k - ak pairs become unstable. In Fig. 12d the detail of first kink of Fig. 12c is shown. From Fig. 12d we see how the stability limit is approached: kinks, $\uparrow\uparrow$, or antikinks $\downarrow\downarrow$, tend to merge and surrounding spins show a strongly modified magnetization, i.e., the kinks locally disrupt the AF state by generation of screening currents before the annihilation occurs at shorter length. Below the stability limit these pairs move from one site to another

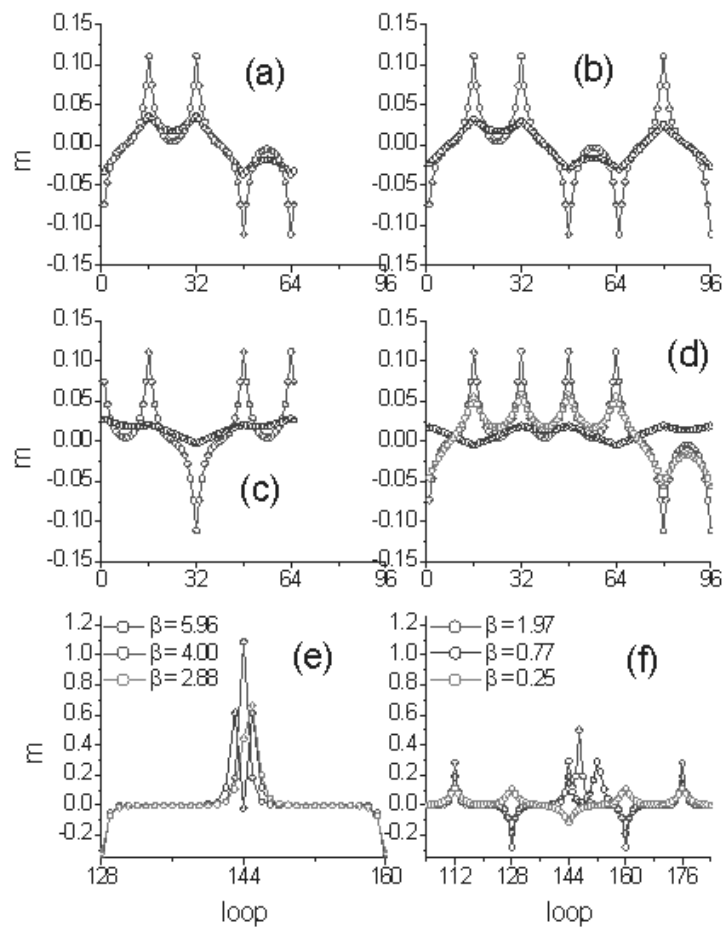


Figure 10. Simulated phase and magnetization of a $k = 4, 6, 16$ k - π AJJA with $\alpha = 0.25$ and $N/k = 16$, in all cases a last loop to be identified with first one has been added for better visualization of ring solution: (a) $k = 4$ $n = 0$ magnetization with $\beta = 0.25, 0.0625, 0.01$; (b) $k = 6$ $n = 0$ magnetization with $\beta = 0.25, 0.0625$; (c) $k = 4$ $n = 1$ magnetization with $\beta = 0.25, 0.0625, 0.01$; (d) $k = 6$ $n = 1$ magnetization with $\beta = 0.25, 0.0625, 0.01$; (e) $k = 16$ $n = 1$ magnetization with an added kink; (f) $k = 16$ $n = 1$ magnetization with an added kink.

in the array by flipping the surrounding flattened spins, until they annihilate each other. Also other $n = 0$ configurations can exist involving more half-flux or integer flux quanta, e.g. triplet like $\dots \downarrow\downarrow\downarrow \dots \uparrow\uparrow\uparrow \dots$ or solution with more than a k - ak pair, but again their stability range is smaller than k - ak pair solutions and the energy is higher.

4. Arrays in magnetic field

Apart from uniform field, which does not have effects on ring arrays at $n = 0$, there is a large number of different field configurations which can alter the energy of fundamental and excited states described above. As we will see below the degeneration of AF state is removed in field and an energy split occurs between

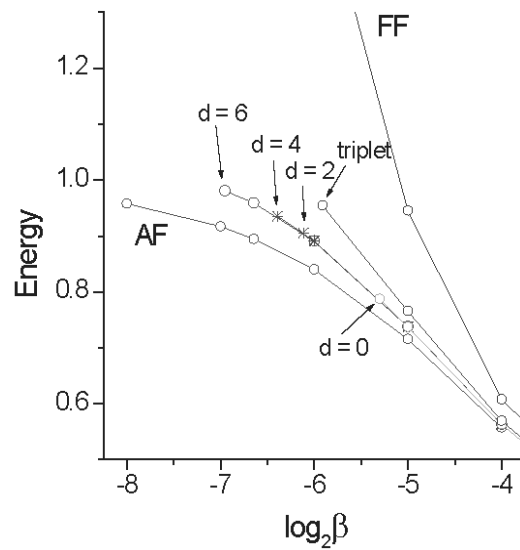


Figure 11. Energy of $n = 0$ solutions of a $k = 16$ k - π AJJA with $\alpha = 0.25$ and $N/k = 16$. The fundamental state branch is shown for comparison.

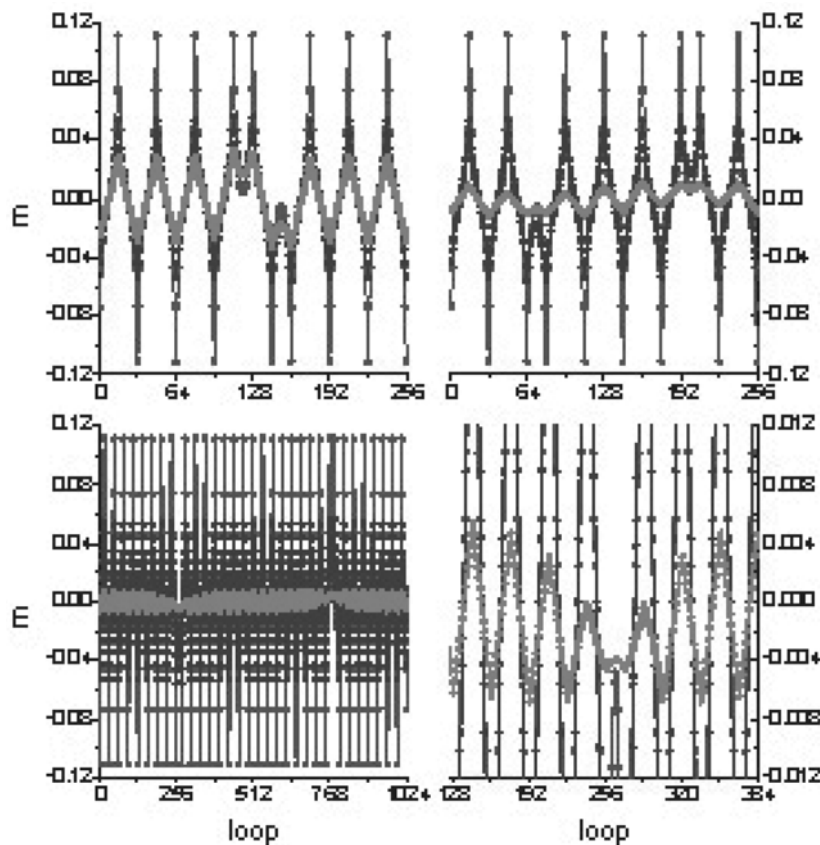


Figure 12. Simulated phase and magnetization of a $k = 16, 64$ k - π AJJA with $\alpha = 0.25$ and $N/k = 16$: (a) $k = 16$ $n = 0$ $d = 6$ magnetization with $\beta = 0.25, 0.0625, 0.025$; (b) $k = 16$ $n = 0$ $d = 0$ magnetization with $\beta = 0.25, 0.0625, 0.0081$; (c) $k = 64$ $n = 0$ $d = 30$ magnetization with $\beta = 0.25, 0.0625, 0.0047$; (d) detail of (c) near the first kink.

a paramagnetic solution (higher energy) and a diamagnetic solution (lower energy) [7]. It would be noted that in AJJA the lower energy solution, derived from AF fundamental state, will be always diamagnetic because there is an even number of half-flux quanta and so there is no net magnetic initial magnetic moment. From Eq.(6) we see that the field can act in any of N different loops of the array (see Fig. 1b). This picture applies to both all- π and k -arrays. However, if we assume that k -arrays are made of very small loops (as continuous limit would imply) the access to single loop is problematic and field is likely to act on the array via control lines (see Fig. 1d). In the following we study the effect of field on the fundamental AF states.

It is found that for any degeneration removing field spatial distribution a critical value of field exists at which the higher energy paramagnetic solution is unstable toward the diamagnetic solution. This occurs at relatively high values of field and it is the mechanism which permits the array to swap between the two fundamental states. As we will see below in the dynamics section this mechanism is very similar to that of current biased arrays [19, 14], which involves kink (anti-kink) in the flip mechanism.

4.1. All- π AJJA

For all- π AJJA we assume that the field act indirectly in N different loops, so in principle one should consider any arbitrary frustration vector f_j . Anyway here we want to separate the effect of a localized random field (LRF) from effect of an external imposed control field (CF). The first one may occur in any of the subsets of the array loops as a noise fluctuation. Flux noise is due to external sources and to intrinsic dissipative processes in the array itself, i.e., quasiparticle currents here schematically accounted for by dissipation α in Eq.(5). These currents circulating in the array loops also generate flux noise in the array which can simply be accounted for as a random fluctuating frustration vector f_j . As usual we can assume that intrinsic noise is a Gaussian uncorrelated noise. The simplest LRF is a frustration acting in a single array loop, i.e., a 00000 f 000..., or, shortly, LRF1. Below we study also the effect of LRF involving a larger number of loops with a spatial correlation longer than one loop. These can be described as 00000 f .. $\leftarrow^{n_f} \rightarrow$.. f 000..., or LRF n_f . They are obviously less unlikely to occur than single loop frustration if we think of noise fluctuations. It is interesting to note that only odd n_f correlation lengths really remove the degeneration of fundamental AF state. In fact, an even n_f correlation length frustration involves an even number of spins so the screening currents which are generated are identical for the two AF states. On the other hand, a CF can have a particularly symmetric configuration which is imposed from outside on the array. As typical CF configuration we can choose

a sequence of zero and f alternating in the array loops, i.e., f_j equal to $0f0f0f0f\dots$. This can be realized using a specially designed control coil which is mutually coupled to even number array loops (see also Discussion section below). CF is a rather unlikely configuration if compared with a generic LRF because implies an highly correlated static field with the spatial period of just two loops.

In Fig. 13 we show the effect of a LRF1 frustration f in the 8-th loop of a $N = 16$ all- π AJJA. In Fig. 13a the local magnetization is shown. The magnetic field adds to local one half-flux quanta, giving rise to a local paramagnetic, $m_{j \neq N/2} > m_{N/2} > 0$, or local diamagnetic solution, $m_{N/2} < m_{j \neq N/2} < 0$. Mean magnetization is negative as expected in both cases from Eq. (7) and is equal to $-f/N$. In Fig. 14 the energy of fundamental states of some ring arrays is reported as function of field η in the LRF1 case for different values of N . The energy of paramagnetic solution is higher than energy of diamagnetic solution. The two branches appear until the critical field η_c for stability of paramagnetic solution is reached as indicated by arrows in Fig. 14. At η_c a spin flip process occurs. Flip can be local involving only the frustrated loop and generating a $n = 0$ excited state, this occurs for values of β larger than critical β_c for the stability of $n = 0$ excited states. If β is smaller the whole array switches to

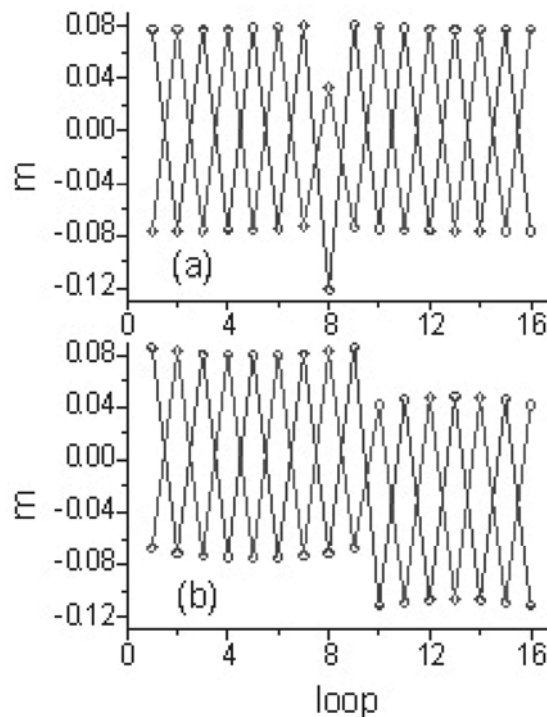


Figure 13. Simulated magnetization vs magnetic field for an all- π AJJA with $\beta = 0.25$ $N = 16$: a) local frustration in 8-th loop (LRF1); b) local frustration in the last seven loops (LRF7).

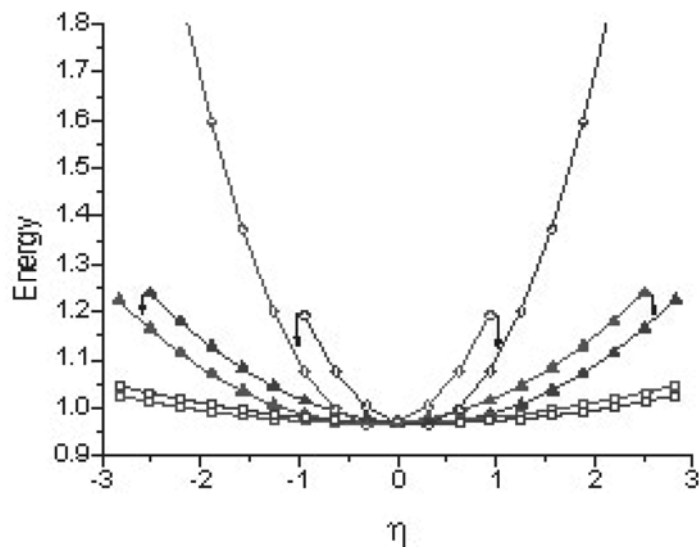


Figure 14. Energy vs magnetic field for an all- π AJJA with $\beta = 0.25$ with $N = 4$ (circles), $N = 16$ (triangles), $N = 64$ (squares) with a LRF1 spatial distribution.

diamagnetic lower energy solution (this is the case of Fig. 14). For a LRF1 frustration the critical field increase with N (see Fig. 14) because the complete flip needs more energy. We found $\eta_c = 0.94$ for $N = 4$ and $\eta_c = 2.52$ for $N = 16$. (For $N = 64$ the critical field is about 6.44 and is not shown in Fig. 14).

Moreover, the energy split is a decreasing function of N . In fact, for $N = 4$ the split is a relevant fraction of the energy ($> 8\%$) just at $\eta = 0.63$. But for $N = 64$ the split is only about 0.5 % at the same values of field. Doubling N the split roughly halves. So an energy 'protection' from LRF1 frustration will arise in the limit of large N . From noise point of view this implies that for large N the system is insensitive to simple uncorrelated field fluctuations in a single loop; a property well-known for conventional SQUID arrays [37]. Energy splits as function of β and frustration f for the LRF1 case are reported in Fig. 15a,b for $N = 16$ and 64 below critical field. Smaller β further reduce the split. For $N = 16$ the energy split goes to zero meaning that no higher energy states are present. The critical field η_c is practically independent from N due to AJJA topology which reproduces the symmetry of the elementary loops over the whole array.

A different case is shown in Fig. 13b where frustration was applied on a $N = 16$ in seven adjacent loops, i.e., a $n_f = 7$ frustration (LRF7). The corresponding energy splits are reported again in Fig. 15c,d. As is seen the split is not larger than the LRF1 split. This can be due to the fact that screening currents, which are responsible for the effective energy split, generate only locally where the frustration is changing, so a LRF7 is comparable with a LRF1 in terms of change in energy. If after critical field is reached and the

energy split is not zero, the system relaxes from an excited state, following other branches depending on β . However, this occurs almost everywhere for two higher β values, 1 and 4, where higher energy states are stable (we note that the limits described in the previous section are valid for zero field, in presence of field they can change). Only for a relatively large field in the $N = 64$ LRF7 case an excited state is generated.

Finally, we report in Fig. 16 the results of application of a control field to all- π arrays. The most relevant difference from Fig. 14 is that the split is practically independent from N . This is because control field is acting over the whole array, maximizing the effect of frustration in any loop. Also critical field

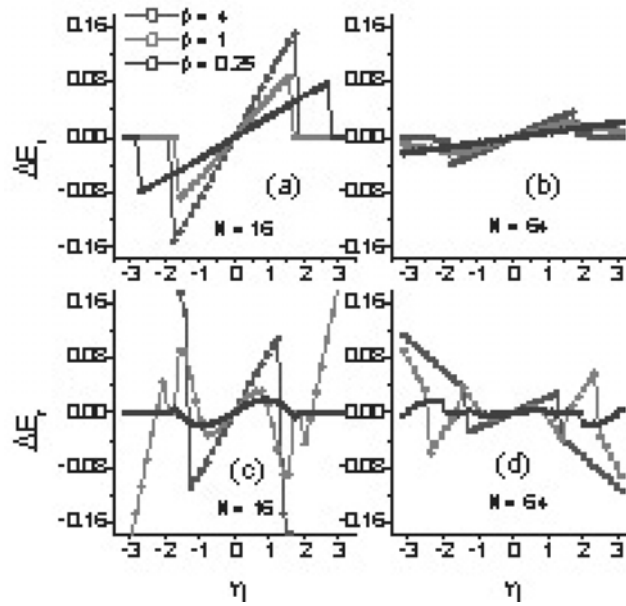


Figure 15. Energy split vs magnetic field for all- π arrays: a) LRF1 $N = 16$; b) LRF1 $N = 64$; c) LRF7 $N = 16$; d) LRF7 $N = 64$.

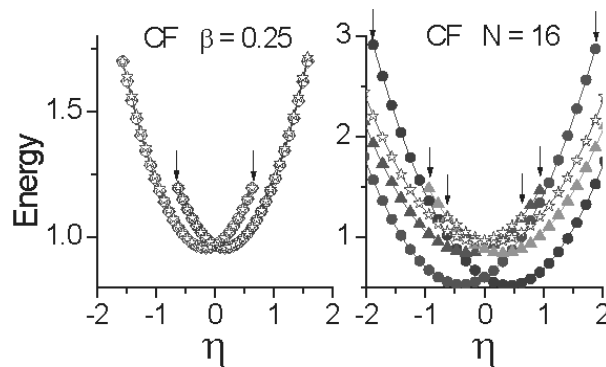


Figure 16. Energy vs magnetic field for all- π AJJA with $N = 16$ and $N = 64$ with control field (CF) spatial distribution: a) dependence on N at $\beta = 0.25$; b) dependence on β at $N = 16$.

is N independent and smaller than LRF cases critical field. This property of control field is useful in the practical design of devices because critical control field sets a relatively small, N -independent field which is the minimal field at which the system can flip due to an external influence. Using a square loop area of $4 \mu\text{m}^2$ and $\beta = 0.25$ we obtain $B_c \simeq 288\text{mG}$ with a critical current of about $30\mu\text{A}$ (using Ketchen approximate value of square washer inductance [38]). In comparison, the LRF1 critical field for the same parameters with $N = 16$ is $B_c \simeq 1037\text{mG}$.

4.2. k - π AJJA

In k - π AJJA we assume that spatial distribution of field is determined by control lines, which generate an external field. The details of spatial distribution of field can be not easy to derive in this case, but, we can assume that these do not have a significant role in determining the general response of system. Among different configurations of control lines the layouts most comparable to previous all- π array case are those plotted in Fig. 1d. The s -type is threading a single $0 - \pi$ boundary, so is similar to previous LRF1 case because it affects a single "spin". Similarly m -type can be compared to LRF n_f case because it spreads the field over a large number of "spins". Finally, the c -type is the analog of control field CF. Remembering that Eq. (5) is sensitive to "derivative" of field, we see that if the period $2N/k$ is relatively long the field can affect the system also where there are only 0 or π loops. This is not possible in simplest all- π AJJA.

The effect of a s -type control line on a $k = 2$ array with $N/k = 16$ and $\beta = 0.25$ is shown in Fig. 17 where three different spatial configurations of field have been chosen. In Fig. 17a (circles \circ) the frustration is not zero only in the control line whose length extends over 7 loops with the 0 - π boundary in the central loop. This rather abrupt field change causes the jumps in both 'paramagnetic' and 'diamagnetic' solutions. In Fig. 17a (stars \star) a smoothed magnetization is obtained using a smeared frustration with the same total frustration, i.e. $\sum_j f_j$. The frustration was assumed to vary linearly from 6 to 2 loops before the $0 - \pi$ crossing (see the inset in Fig. 17a). The smeared frustration solution is visually more appealing, but is not substantially different from the other solution. Difference in the mean magnetization is zero for equal total frustration. The chosen linear distribution is rather arbitrary because the exact distribution depends on exact layout of control lines. For this hereafter we use spatial configurations similar to that used in Fig. 17a (circles \circ) assuming that the differences with more realistic smeared configurations are not modifying the gross behavior of the k - π AJJA.

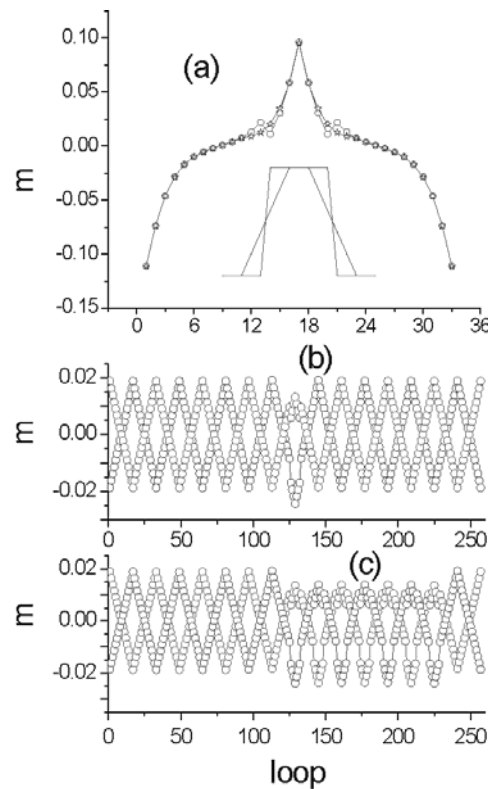


Figure 17. Simulated magnetization vs magnetic field for a $k\text{-}\pi$ AJJA with $\beta = 0.25$: a) $k = 2$ local magnetization for two different frustration vectors shown in the inset: the plot with circles represents not-zero frustration in seven loop around the $0\text{-}\pi$ boundary; the plot with squares is a smeared version with a linear growth around the central loops; in the inset the two frustration vectors are schematically shown out of scale; b) s-type control line around the 8th $\pi - 0$ boundary; c) m -type control line around seven $\pi - 0$ boundaries from 8th to 14th.

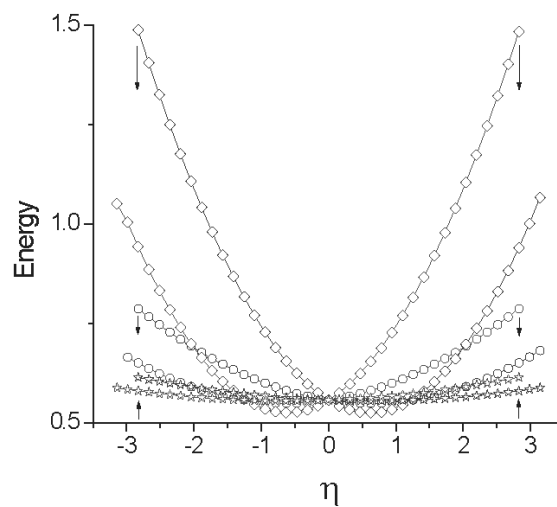


Figure 18. Energy vs magnetic field for a k -array with $\beta = 0.01$ with $k = 4$ (circles), $k = 16$ (triangles), $k = 64$ (squares).

In Fig. 17b,c the effect of a s -type and m -type control lines on a $k = 16$, $N/k = 16$, $\beta = 0.01$ AJJA is shown. The results are very similar to all- π arrays apart from jumps described above. A s -type control line seven loop long is used in Fig. 17b. For the s -type control line the energy of solutions for different k is reported in Fig. 18. Energy protection in the sense of a smaller energy split sensitivity to field is again obtained for large N . In particular we found that energy split is 15% at field of 0.62 for the $k = 4$ array and is 1% for $k = 64$ array. Details of energy split for $k = 16$, 64 are given in Fig. 19. Smaller β have been chosen because this implies a large energy split from higher energy excited states which otherwise can influence the fundamental state mixing. However, for larger fields the split does not become zero also for small β indicating that some excited states have been established in the system.

Finally, we report in Fig. 20 the results of application of a control field (c -type) to k - π AJJA. Again the split is practically independent from N , so that no protection effect arises using c -type control lines in k -arrays. In normalized units the critical field is about $\simeq 1.6$ at $\beta = 0.01$ and up to $\simeq 2.4$ for $\beta = 0.0625$. It is worthwhile to remember that field normalization implies that $\eta_c = 2$ is the so-called Josephson field [35] where the magnetic field completely penetrates a long Junction. The minimal critical field for flip is generally larger than corresponding field for all- π AJJA if the device dimension has to be the

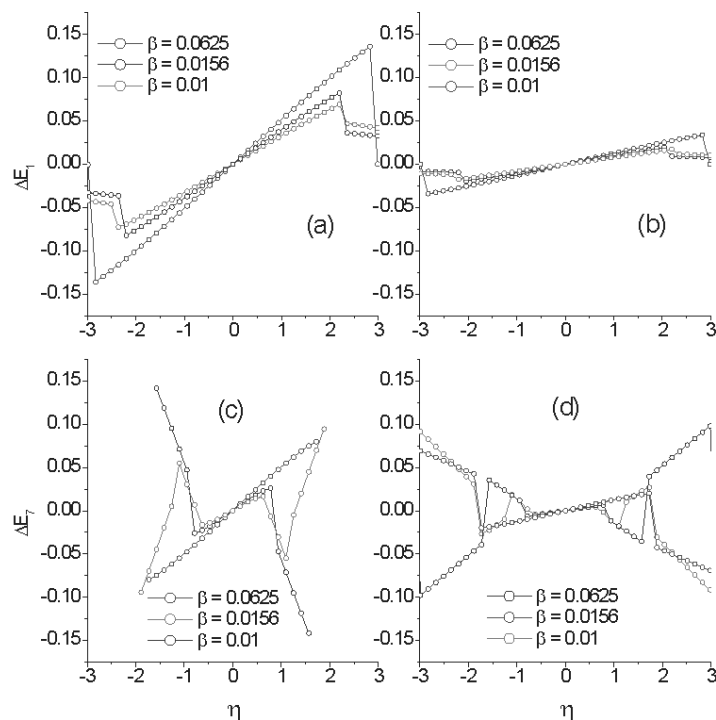


Figure 19. Energy split vs magnetic field for k -arrays: a) s -type $k = 16$; b) s -type $k = 64$; c) m -type $k = 16$; d) m -type $k = 64$.

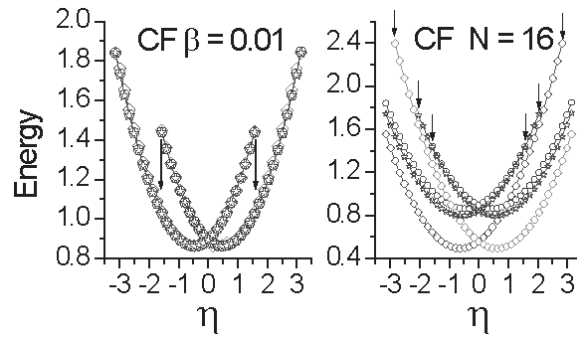


Figure 20. Energy vs magnetic field for k -arrays with $k = 16$ and $k = 64$ with c -type control line (CF): a) dependence on k at $\beta = 0.01$ for $k = 4, 16, 64$ no difference arises; b) dependence on β at $k = 16$ for $\beta = 0.0625$ (diamond), $\beta = 0.0156$ (stars), $\beta = 0.01$ (circles).

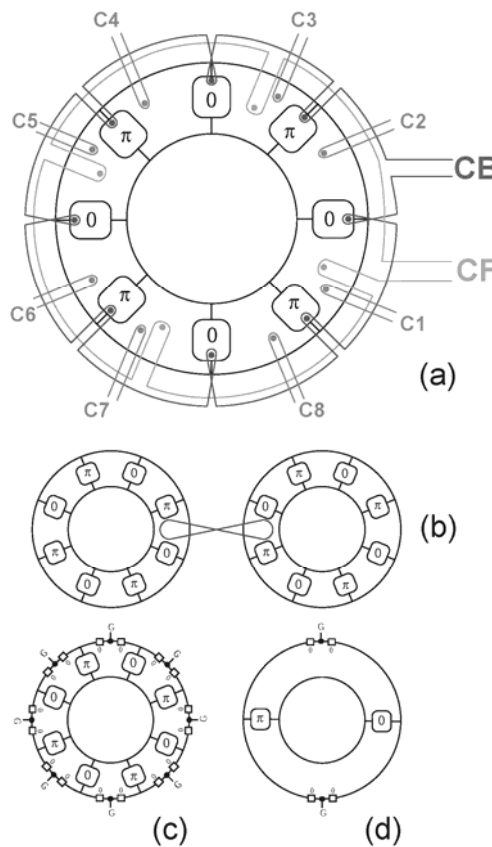


Figure 21. Configurations for a qubit ring unconventional array: (a) basic configuration with $N = 8$; (b) coupled ring arrays; (c) a mixed charge-flux device with $N = 8$; (d) a basic mixed charge-flux device with $N = 2$.

same, so using an area of $4/256 = 1.56 \cdot 10^{-2} \mu\text{m}^2$ the critical field for c -type is equal to $B_c = 33\text{G}$ for $\beta = 0.01$. However, such devices will be at nanometer scale and their fabrication still would be problematic at the present state of the art. In the long Junction approximation assuming λ_J of $100\mu\text{m}$ and λ_L around

10nm, we find $B_c = 5.27\text{G}$ for c -type control line and $B_c = 9.39\text{G}$ for s -type control line.

5. Discussion

Unconventional junction arrays with the properties described in the previous sections can be used as building blocks for qubit devices [8]. Other proposals are the use of annular configurations in advanced superconducting circuitry as memory elements [20] or plasma bandgap devices [36]. Here we briefly discuss the first possibility also in view of some recent progress reported in Ref. [32]. The use of multi-junctions devices is not new: the analysis of practical π -SQUID configurations for the qubit implementation often involves more than two junctions like the "quiet" qubit of Ioffe et al. [23]. The idea is simply to use the degenerate AF fundamental states as the qubit states $|0\rangle$ and $|1\rangle$. For a π AJJA with $n = 0$ a possible way to get the tunneling between fundamental states would be the creation and annihilation of (virtual) kink-antikink pairs $\uparrow\downarrow$ in which the kink annihilates over a negative magnetization state \downarrow flipping its magnetization to a positive state, i.e., $\uparrow + \downarrow = \uparrow$, and viceversa for the antikink, i.e., $\downarrow + \uparrow = \downarrow$ [32]. This flipping process involves creation and subsequent annihilation of kinks in the array which is a known classical process as shown in the previous section (see also Ref.s [19, 8, 20]). For example, for $N = 4$ and $N = 6$ the transition occurs via the following sequence of double flips:

$$\uparrow\downarrow\uparrow\downarrow \rightarrow \uparrow\uparrow\downarrow\downarrow \rightarrow \downarrow\downarrow\uparrow\uparrow$$

$$\uparrow\downarrow\uparrow\downarrow\uparrow\downarrow \rightarrow \uparrow\uparrow\downarrow\downarrow\uparrow\downarrow \rightarrow \uparrow\uparrow\downarrow\downarrow\uparrow\downarrow \rightarrow \downarrow\downarrow\uparrow\uparrow\downarrow\downarrow$$

In general there are $N/2$ double flips to pass from $|0\rangle$ to $|1\rangle$. But the above tunneling processes have $(N/2)!$ paths along which they can occur, so its rate should be roughly proportional to $(N/2 - 1)!\Omega_T$ where Ω_T is the tunneling rate of the single kink-antikink process [32].

Excited states above the fundamental state can interfere with the flipping quantum process if they are stable. The system could possibly flip out to an excited state if it is lower in energy. For fixed winding number this occurs toward $n = 0$ states which are also the lowest in energy. In addition to the "spectroscopical" interest, it would be better to have a device with a minimum number of excited states. Naturally, it is possible to exclude these states using low β arrays. This is relatively more easy to do in the all- π AJJA, where fabrication techniques can determine the β very accurately, than in k - π AJJA (or in long junctions) where the Josephson length depends on distributed

inductances along the array. Moreover, for all- π AJJA critical β for stability of the excited states is higher than in the k - π AJJA. In this last case the requirement of no-stable excited states implies a very low β which can be difficult to realize due to the stray inductance of superconducting films forming the array [38]. In all- π AJJA the most suitable configurations will be likely an $N = 16$ or $N = 64$ array with a β between 0.25 and 0.5. A higher number of loops or a lower β can render the requirement on the fabrication more difficult to achieve. Moreover, the local magnetization becomes very small for $\beta \rightarrow 0$ in both all- and k - π AJJA, so that the signature of fundamental state becomes more difficult to control and it is likely to be more sensitive to flux noise.

In an all- π AJJA, with the above β and N , the controls can be realized as depicted in Fig. 21a (see also Ref. [8]) for an $N = 8$ array. The **CF** coil applies the control field to the array. According to previous sections the control field can cause the system to flip between two fundamental states. So **CF** can be used to prepare the system in a known state before the quantum evolution takes place. The control field can be used also to read-out the system state controlling, after the quantum evolution is gone, if the state is the same of initial preparation or not.

Read-out could be also realized by means of the independent coils **CN**. One or more of these coils can be the input coils of external SQUID detector that can read the flux in selected array loops. Some of the same **CN** coils can be used to couple the ring array to other similar devices in order to build a multi-qubit device as shown in Fig. 21b. Quantum computing device with more than a single qubit have been realized and tested [39]. On the other hand, in recent years theoretical work on qubit candidates has continued with the proposal of new single qubit devices. For example, new tetrahedral configurations for qubit have been studied [40]. The coupling is schematically shown as an "eight" coil giving an antiferromagnetic coupling between qubits. This is the optimal configuration to form a C-NOT port, which is the basis of the quantum computing logic [41]. The coil was added just in two of the single qubit loops, this maybe the way to satisfy the requirement of "loosely" coupled qubits [42]. In fact, with the possibility to vary both N and the coil windings a large interval of couplings can be obtained. Naturally, if a good fabrication technique is able to produce a device of the type shown in Fig. 21a, then it should not be a problem to extend this procedure to have multi-qubits formed by different ring arrays. Finally, a **CB** coil is also depicted for the tuning of critical current of array junctions. As the energy scale of the system is $\Phi_0 I_0 (I_{CB})/2\pi$, where I_{CB} is the current in **CB** coil, the energy barrier for flipping is proportional to this factor. Due to the exponential dependence of the tunneling

rate on the energy scale, a control of barrier is needed in conventional qubits to permit fine adjustments of the tunneling rate. A way to realize the barrier tuning is described in Ref. [8]. This uses small SQUIDs instead of single junction in the array branches. In this case **CB** is a coil which puts flux in the small SQUIDs and so varies their critical current. Alternatives to the use of SQUIDs for controlling the junction currents can be also considered. An interesting combination would be a realization of a charge-flux device as depicted in Fig. 21c. In this configuration the additional degree of freedom is due to charge devices, i.e., Cooper pair boxes, on the external superconducting loop of the array. The Cooper pair boxes ring arrays were studied in Ref. [43]. Here this sub-system is integrated with an unconventional array to provide a flux degree of freedom. For $E_C \sim E_J$ the system could be considered a protected analog of the "quantronium" described in Ref. [44]. The simplest symmetric configuration is shown in Fig. 21d for $N = 2$.

The operation mode of single qubit π AJJA is the following. Firstly the system is prepared in one of its fundamental states by using the coil **CF**. Then the current in the coil is switched off and leads are possibly isolated from the external noise via thermal switches. Next stage is the quantum mixing phase: using **CB** coil the energy barrier is lowered until coherent oscillations set on. To make the mixing evident we can use **C1** (or **C1** and **C2**) coils to add a variable small local frustration to the system and sweep it across zero in order to maximize the mixing of two fundamental states. An optimal design of parameters will be necessary to reduce the needs of large currents via the **CB** coil. Finally, the read-out phase is accomplished using again **C1** (or **CF** itself as describe above).

Finally we consider the differences between an unconventional and a conventional ring array. Slightly different conventional AJJA was realized in Ref. [45] for the study of the breather solutions in ladder arrays. However, from a formal point of view these are very similar except for the four junction per loop instead of two junction per loop studied here. It is well known that a fully frustrated system, with $f = 1/2$, shows a checkerboard solution [46]. In large β one dimensional arrays this is nothing else but an alternating sequence of halfflux quanta along the array, i.e., a solution similar to fundamental state of unconventional arrays $\uparrow\downarrow\uparrow \dots$. Therefore, a fully frustrated conventional array should behave similarly to an unconventional one. However, AJJAs are not sensitive to an uniform field. To obtain a state similar to fundamental state of π AJJA, the frustration has to alternate from $-f$ to f along the array. This implies a relevant difference in the conventional case: the fundamental state is no longer degenerate for small values of β . In fact, to be flipped to its reversed counterpart $\downarrow\uparrow\downarrow \dots$ the conventional array *need the magnetic field to be reversed*. So the need for

unconventional junctions is justified by the zero field nature of degeneracy in unconventional AJJA.

The development of a reliable quantum device based on π -arrays rests on a detailed knowledge and reproducibility of results of systems containing π -junctions. There are three main ways to realize the π -junctions in the ring array. For the obvious reason that qubits should be quiet, non-equilibrium π -junctions based on SNS junctions are not mentioned as a possible alternative. Firstly, unconventional d -wave- I - d -wave biepitaxial junctions can be realized using YBCO [47]. The values of critical current range from about $1mA$ to $10mA$ and capacity is about $0.1pF$ [25, 47]. Dissipation effects are far from being completely analyzed in these systems. In the case of high- T_c junctions the normal resistance is typically low. However, we must ask ourselves whether these losses are important during qubit operation when no transport occurs through the junction. It can be argued (see [48]) that dissipation in high- T_c devices is smaller than indicated by its normal resistance. A recent indication of this behavior is the discovery of MQT effect in YBCO biepitaxial junctions with an estimated R of 600Ω in presence of rf-pump [25]. An alternative is the use of d -wave- I - s -wave junctions [16], which have similar current and capacity figures, but an apparently higher dissipation (about 20Ω for R_N). Finally, unconventional $S - F - S$ junctions can be realized using a ferromagnetic barrier (like $Ni - Cu$) between conventional s -wave superconductors [3].

Another important point to be raised is that 0 and π junctions should be symmetric, i.e., they should have roughly the same critical current for the system to be workable, otherwise a transition to a flat solution occurs [6]. This transition is induced by the larger (dominating) critical current junctions, which pull the whole array to a flat solution. In "zigzag" arrays realized in Ref. [16] this condition was easy to satisfy. However, a relatively high tolerance is possible up to 20% of difference in critical current for values of β between 0.1 and 1.0 in all- π AJJA case. These figures tend to be more tight for low β when the system is more rigid. A similar discussion is valid for the spread in critical currents: a maximum spread of about 15% is needed in all- π AJJA in order to have a well defined fundamental state.

6. Conclusion

π AJJAs are the simplest objects with a non-trivial topology and a degenerate fundamental state in which protection in Hamiltonian arises for large N . We have shown how the fundamental states, the excited states, and the spin flip process, both local and global, dominate the nature of both static and dynamic solutions on π AJJA. Lowest energy stable states can be classified, at

least as the configuration of a "spin chain", with different number of $k - ak$ at zero winding number ($n = 0$). Also higher energy state exists for winding number n different from zero. Finally, the emergent classical dynamics of unconventional junctions is an important recent topic. The basic process of half-flux quanta flipping via addition of full kink appears to be the basic mechanism for the flip between different states of ring array. Both for current driven arrays [20] and for frustration driven arrays (see the previous Section). The quantum behavior of a "macroscopic" chain of spins along an unconventional array is a completely new topic which in principle would permit quantum experiments in the coupling of "macroscopic spins". The "quantum spectroscopy" of macroscopic spin chains allows to see if and how the excited states form band and bandgaps structures with increasing energy and it is of great interest for developing both classical and quantum devices based on unconventional arrays [36]. The particular problem of quantum mixing between the two fundamental states is of primary interests also for a qubit device based on ring unconventional arrays [32],[49].

Acknowledgments

I warmly thank S. Sergeenkov, F. Lombardi, A. Leo, A. Barone, F. Tafuri, M. Lisitskii, C. Nappi, A. Tagliacozzo, A. Naddeo and E. Goldobin for useful discussions and suggestions. We acknowledge financial support from MIUR COFIN2007 project 'Sistemi Quantistici Macroscopici-Aspetti Fondamentali ed Applicazioni di strutture Josephson Non Convenzionali'.

References

1. Bulaevskii, L.N., Kuzii, V.V., and Sobyenin, A.A. 1977, JETP Lett., 25, 290.
2. Kirtley, J.R. and Tsuei, C.C. 2000, Rev. Mod. Phys., 72, 969.
3. Ryazanov, V.V., Oboznov, V.A., Rusanov, A.Yu., Veretennikov, A.V., Golubov, A.A., and Aarts, J. 2001, Phys. Rev. Lett., 86, 2427.
4. Van Harlingen, D.J. 1995, Rev. Mod. Phys., 67, 515.
5. Hilgenkamp, H., Smilde, H.J.H., Blank, D.H.A., Rijnders, G., Rogalla, H., Kirtley, J.R., and Tsuei, C.C. 2003, Nature, 422, 50.
6. Chandran, M. and Kulkarni, R.V. 2003, Phys. Rev. B, 68, 104505.
7. Rotoli, G. 2003, Phys. Rev. B, 68, 052505.
8. Rotoli, G. 2005, IEEE Trans. Supercond., 15, 852.
9. Ryazanov, V.V., Oboznov, V.A., Veretennikov, A.V., and Rusanov, A.Yu. 2001, Phys. Rev. B, 65, 020501(R).
10. Schultze, V., Jsselsteijn, R., Boucher, R., Meyer, H.G., Oppenlander, J., Haussler, Ch., and Schopohl, N. 2003, Supercond. Sci. Technol., 16, 1356.
11. De Leo, C. and Rotoli, G. 2002, Supercond. Sci. Technol., 15, 1711.
12. Kirtley, J.R., Chaudhari, P., Ketchen, M.B., Khare, N., Lin, Sh. Yu., and Shaw, T. 1995, Phys. Rev. B, 51, R12057; Mannhart, J., Hilgenkamp, H., Mayer, B.,

- Gerber, Ch., Kirtley, J.R., Moler, K.A., and Sigrist, M. 1996, *Phys. Rev. Lett.*, 77, 2782; Tafuri, F. and Kirtley, J.R. 2000, *Phys. Rev. B*, 62, 13934.
13. Chesca, B., Schulz, R.R., Goetz, B., Schneider, C.W., Hilgenkamp, H., and Mannhart, J. 2002, *Phys. Rev. Lett.*, 88, 177003.
 14. Goldobin, E., Sterk, A., Gaber, T., Koelle, D., and Kleiner, R. 2004, *Phys. Rev. Lett.*, 92, 057005.
 15. Kirtley, J.R., Moler, K.A., and Scalapino, D.J. 1997, *Phys. Rev. B*, 56, 886.
 16. Smilde H.J.H. et al. 2002, *Phys. Rev. Lett.*, 88, 057004.
 17. Goldobin, E., Koelle, D., and Kleiner, R. 2002, *Phys. Rev. B*, 66, 100508.
 18. Goldobin, E., Koelle, D., and Kleiner, R. 2003, *Phys. Rev. B*, 67, 224515.
 19. Lazarides, N. 2004, *Phys. Rev. B*, 69, 212501.
 20. Goldobin, E., Stefanakis, N., Koelle, D., and Kleiner, R. 2004, *Phys. Rev. B*, 70, 094520.
 21. De Leo, C. and Rotoli, G. 2002, *Phys. Rev. Lett.*, 89, 167001.
 22. Bertet, P., Chiorescu, I., Burkard, G., Semba, K., Harmans, C.J.P.M., Di Vincenzo, D.P., and Mooij, J.E. 2005, *Phys. Rev. Lett.*, 95, 257002.
 23. Ioffe, L.B., Geshkenbein, V.B., Feigel'man, M.V., Fauchere, A.L., and Blatter, G. 1999, *Nature*, 398, 679; Blatter, G., Geshkenbein, V.B., and Ioffe, L.B. 2001, *Phys. Rev. B*, 63, 174511.
 24. Frolov, S.M., Van Harlingen, D.J., Bolginov, V.V., Oboznov, V.A., and Ryazanov, V.V. 2006, *Phys. Rev. B*, 74, 020503.
 25. Bauch, T., Lombardi, F., Tafuri, F., Rotoli, G., Barone, A., Delsing, P., and Cleason, T. 2005, *Phys. Rev. Lett.*, 94, 087003; Bauch, T., Lindström, T., Tafuri, F., Rotoli, G., Delsing, P., Cleason, T., and Lombardi, F. 2006, *Science*, 311, 5757.
 26. Jin, X.Y., Lisenfeld, J., Koval, Y., Lukashenko, A., Ustinov, A.V., and Mueller, P. 2006, *Phys. Rev. Lett.*, 96, 177003.
 27. Kitaev, A.Yu. 1997, preprint quant-ph/9707021.
 28. Ioffe, L.B., Feigel'man, M.V., Ioselevich, A., Ivanov, D., Troyer, M., and Blatter, G. 2002, *Nature*, 415, 503.
 29. Doucot, B., Feigel'man, M.V., and Ioffe, L.B. 2003, *Phys. Rev. Lett.*, 90, 107003.
 30. Wallraff, A., Lukashenko, A., Lisenfeld, J., Kemp, A., Fistul, M.V., Koval, Y., and Ustinov, A.V. 2003, *Nature*, 425, 155.
 31. Kemp, A., Wallraff, A., and Ustinov, A.V. 2002, *Phys. Stat. Sol.(b)*, 233, 472.
 32. Naddeo, A., Rotoli, G., Lucignano, P., and Tagliacozzo, A. 2005, extended abstract booklet ISEC2005.
 33. De Leo, C. and Rotoli, G. 2002, in *Studies of Josephson Junctions Arrays I*, A.V. Narlikar (Ed.), NOVA Science Publishers, New York, 140.
 34. Zenchuk, A. and Goldobin, E. 2004, *Phys. Rev. B*, 69, 024515.
 35. Tinkham, M. 1996, *Introduction to Superconductivity*, McGraw-Hill, New York.
 36. Susanto, H., Goldobin, E., Koelle, D., Kleiner, R., and van Gils, S.A. 2005, *Phys. Rev. B*, 71, 174510.
 37. Lee, S.-G., Huh, Y., Park, G.-S., Kim, I.-S., Park, Y.K., and Park, J.-C. 1997, *IEEE Trans. Appl. Supercond.*, 7, 3347.
 38. Petraglia, A., Filatrella, G., and Rotoli, G. 1996, *Phys. Rev. B*, 53, 2732.

39. Yamamoto, T., Pashkin, Yu.A., Astafiev, O., Nakamura, Y., and Tsai, J.S. 2003, *Nature*, 425, 941; Pashkin, Yu.A., Yamamoto, T., Astafiev, O., Nakamura, Y., Averin, D.V., and Tsai, J.S. 2003, *Nature*, 421, 823.
40. Yukon, S.P. 2002, *Physica C*, 368, 320; Feigel'man, M.V., Ioffe, L.B., Geshkenbein, V.B., Dayal, P., and Blatter, G. 2004, *Phys. Rev. Lett.*, 92, 098301.
41. Makhlin, Y., Schon, G., and Shnirman, A. 2001, *Rev. Mod. Phys.*, 73, 357.
42. Orlando, T.P., Mooij, J.E., Tian, L., van der Wal, C.H., Levitov, L.S., Lloyd, S., and Mazo, J.J. 1999, *Phys. Rev. B*, 60, 15398.
43. Ivanov, D.A., Ioffe, L.B., Geshkenbein, V.B., and Blatter, G. 2001, *Phys. Rev. B*, 65, 024509.
44. Vion, D., Aassime, A., Cottet, A., Joyez, P., Pothier, H., Urbina, C., Esteve, D., and Devoret, M.H. 2002, *Science*, 296, 886.
45. Binder, P., Abraimov, D., Ustinov, A.V., Flach, S., and Zolotaryuk, Y. 2000, *Phys. Rev. Lett.*, 84, 745; Binder, P. and Ustinov, A.V. 2002, *Phys. Rev. E*, 66, 016603.
46. Dang, E.K.F. and Györfy, B.L. 1993, *Phys. Rev. B*, 47, 3290.
47. Lombardi, F., Tafuri, F., Ricci, F., Miletto-Granozio, F., Barone, A., Testa, G., Sarnelli, E., Kirtley, J.R., and Tsuei, C.C. 2002, *Phys. Rev. Lett.*, 89, 207001.
48. Fominov, Ya.V., Golubov, A.A., and Kupriyanov, M.Yu. 2003, *JEPT Lett.*, 77, 587; Amin, M.H.S. and Smirnov, A.Yu. 2003, *cond-mat/0304255*.
49. Fistul, M.V., Wallraff, A., Koval, Y., Lukashenko, A., Malomed, B.A., and Ustinov, A.V. 2003, *Phys. Rev. Lett.*, 91, 257004; Monaco, R., Mygind, Y., and Rivers, R.J. 2002, *Phys. Rev. Lett.*, 89, 080603; Gaitan, F. and Shenoy, S.R. 1996, *Phys. Rev. Lett.*, 76, 4404.

Transworld Research Network
37/661 (2), Fort P.O., Trivandrum-695 023, Kerala, India



New Developments in Josephson Junctions Research, 2010: 83-105
ISBN: 978-81-7895-328-1 Editor: Sergei Sergeenkov

4

Josephson junctions as a prototype for synchronization of nonlinear oscillators

G. Filatrella

Laboratorio Regionale SuperMat CNR-INFM Salerno and Dipartimento di Scienze Biologiche ed Ambientali, Università del Sannio, Via Port'Arsa 11, I-82100 Benevento, Italy

Abstract

Josephson junctions can be considered as nonlinear oscillators which, for obvious practical purposes, should be synchronized. Synchronization of coupled Josephson junctions can be described by using an analog of the Kuramoto model for nonlinear coupled oscillators. The connection between the superconducting elements and a well established framework for synchronization offers a unique possibility for experimental verification of the model predictions.

Correspondence/Reprint request: Dr. G. Filatrella, Laboratorio Regionale SuperMat CNR-INFM Salerno and Dipartimento di Scienze Biologiche ed Ambientali, Università del Sannio, Via Port'Arsa, 11, I-82100 Benevento Italy. E-mail: filatrella@unisannio.it

In this review paper, we will present our recent results on the practical consequences of the Kuramoto model as far as the experimentally accessible information is concerned. As an important application example, we will also discuss the modeling of the utility grid for transmission of electrical power via Josephson junctions based systems of synchronized nonlinear oscillators.

1. Introduction

Synchrony of periodic phenomena does not occur in the linear world. On the other hand, in Nature we often encounter periodic signals that spontaneously entrain. From these two observations one syllogizes the nonlinear character of many natural oscillators, even if the underlying dynamical model is not known. Examples of spontaneous synchronization are numerous [40], from the now classic case of far east fireflies that blink simultaneously to the more technological examples of Josephson Junctions (JJ) elements, that are the main subject of this Chapter. In the latter case the underlying dynamical model is well known, and therefore it is an actively studied model for scholars of synchronization. JJ possess some features that are generic for coupled nonlinear oscillators and make them one of the favorite playground for nonlinear scientists. The general character stems from the single JJ electrical behavior and the consequent dynamical equations for coupled elements. In fact, it is possible to couple JJ among themselves in a somewhat obvious scheme: series connection to a resonant cavity [8, 10]. The series coupling approach leads to a correspondence with a well known paradigm for coupled oscillators, the Kuramoto Model (KM) [1]. The interplay between KM and JJ physics is most interesting for the wide applicability of the KM model and the experimental availability of JJ. Moreover, JJ are, as circuit elements, flexible enough to be arranged in very different schemes including such common experimental set-ups as, for instance, ladders [11] or two-dimensional arrays [8, 10]. It has also been proposed [38] that there is a link between JJ and the problem of synchronization of oscillators over a network of connections with topologies that are not simply related to the two fundamental schemes of series or parallel connections [2]. Moreover, JJ are believed to be in relation with other systems such as the utility electrical power grid [23]. These relationships will be explored in this Chapter which is organized as follows. In Section 2, I will present the basic dynamics of JJ to establish a common language and to emphasize the physical aspects that are relevant for synchronization. In Section 3, I will show how JJ are coupled via a resonant cavity, and, in Section 4, I will sketch the mapping of such scheme on the KM and the most relevant (for JJ physics) mathematical properties of the KM. In Section 5, I will discuss some of the connections between JJ and other physical systems, while the concluding remarks are presented in Section 6.

2. Basic dynamics of Josephson junctions

Josephson junctions are nonlinear elements that convert a constant current into an ac term, which is the key feature that determines the capability of JJ to be synchronized by each other. But let me start with the basic equation:

$$I = I_c \sin \varphi. \quad (1)$$

Eq. (1) describes a nonlinear relation between the current and the gauge invariant phase difference $\varphi = \vartheta_1 - \vartheta_2$ across two superconductors, see Fig. 1. Indirectly, eq. (1) also determines a nonlinear IV characteristic since V is related to the voltage through the second Josephson equation:

$$V = \frac{\hbar}{2e} \frac{d\varphi}{dt}. \quad (2)$$

From these equations it is immediate to see why a JJ is a dc-ac converter, and therefore an *oscillator*: if one applies a constant voltage V in eq. (2), the differential equation dictates that:

$$\varphi = \varphi_0 + \frac{2e}{\hbar} V t = \varphi_0 + \omega t, \quad (3)$$

which, inserted into (1), gives an oscillating current

$$I(t) = I_c \sin(\varphi_0 + \omega t). \quad (4)$$

It should be noticed that such discussion is mostly mathematical and not yet physical for a number of practical problems that are hidden by the mere equation manipulation performed in (3,4). First, JJ are superconducting elements, and it is practically impossible to apply an ideal voltage generator to the leads of fig. 1, for it would require an internal impedance of the generator much lower than the resistance of the superconductors. Second, the sandwich of superconductors separated by the insulator that forms a JJ constitutes also unavoidably a capacitance, hence a displacement current is to be considered for the ac treatment. Third, in a superconductor at finite temperature there are not only Cooper's pairs that tunnel through the junction obeying eqs. (1,2), but also normal electrons that cross the discontinuity for a voltage difference: JJ is a resistance, as far as the normal electrons are concerned. The three channels, displacement current and tunnel of Cooper's pairs and normal electrons, contribute to the total current as shown in fig. 2.

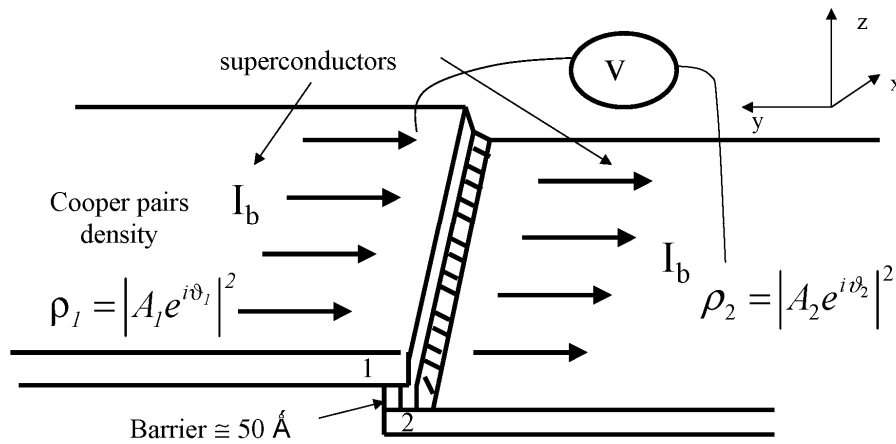


Figure 1. Sketch of a single JJ (out of scale). The superconductors 1 and 2, separated by a thin barrier, are described by two macroscopic wave functions that determine the Cooper's pairs densities. The Josephson phase difference φ is the difference between the two phases: $\varphi = \vartheta_1 - \vartheta_2$.

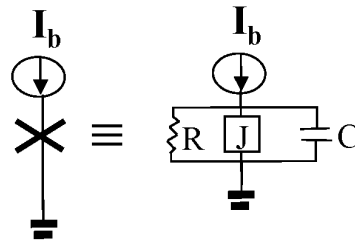


Figure 2. Lumped elements description of a JJ: the cross stands for the physical element, while the J in the rectangle rd presents the ideal Josephson effect as described by eqs. (1,2).

The lumped elements are described concisely by the current balance equation:

$$I_b = I_c \sin \varphi + \frac{1}{R} \frac{\hbar}{2e} \frac{d\varphi}{dt} + C \frac{\hbar}{2e} \frac{d^2 \varphi}{dt^2}. \quad (5)$$

If one applies a current generator I_b the solution of (5) for the phases determines the voltage through eq. (2). The very first general character of a JJ oscillator stems from the inspection of eq. (5), that is formally the same as a driven pendulum, a foremost oscillator studied by Galileo. If one is not content with historical preeminence, I would also like to draw the attention to another feature of eq. (5): it is an oscillator with a trigonometric nonlinearity. One might therefore speculate that eq. (5) is the first order truncation of a generic periodic nonlinear oscillator.

The utility of a dc-ac converter is evident. Unfortunately when one plugs in the figures for typical JJ at, say, about 500GHz , one gets:

$$V \simeq 1\text{mV}$$

$$I_b \simeq 1\text{mA}$$

Even for a 100% dc-ac conversion efficiency one obtains about a $1\mu\text{W}$ of emitted power, much less than the power required for many practical applications. Here the obvious idea: to synchronize several junctions to sum up the voltages (or the currents) and to reach the desired power output [8, 10].

Synchronization of several JJ is hindered by the differences in the characteristic parameters of the junctions [33]. The critical current I_c can change significantly even from device to device in the same production batch: spreads of 5% are considered ambitious achievements. Specifically the tunnel currents (both the supercurrent that determines I_c and the normal current that determines R) depend exponentially upon the thickness t of the barrier that separates the two superconductors, and are therefore very sensitive to the fabrication parameters. Because of the relation between I_c , R , and the superconducting gap Δ , the product of the two parameters is roughly constant [9]:

$$I_c R \propto \Delta \simeq \text{constant}. \quad (6)$$

Consequently, one wants to synchronize oscillators that have different natural frequencies. It is relatively easy to see the effect of the changes of I_c and R on the frequency in the overdamped case (i.e., with negligible capacitance $\beta_c \simeq 0$; the analysis of the underdamped case is mathematically more involved, but it leads to the same qualitative result). If we denote with I_c^j and R^j the parameters of the j^{th} element, its rotation speed j can be obtained from eq. (5):

$$\Omega_j = \frac{2e}{\hbar} R^j \sqrt{I_b^2 - (I_c^j)^2}. \quad (7)$$

So if for instance in a particular junction R^j is larger than the average resistance, then I_c^j is smaller because of the relationship (6) and the frequency (7) is increased with respect to the average velocity of the other junctions; the opposite is true if the junction resistance R^j is larger. One can therefore speak of a collection of oscillators with some average rotation velocity Ω_0 and some distribution of values that will depend on the fabrication procedure.

To treat the interaction mechanism that might lead to synchronization, it is useful to introduce normalized units [9]. One defines the Josephson frequency ω_j

$$\omega_j = \sqrt{\frac{2eI_c}{\hbar C}} \quad (8)$$

via the normalized time: $\tau = \omega_j t$. It is also useful to adopt the dissipation parameter α

$$\alpha = \frac{1}{R} \sqrt{\frac{\hbar}{2eI_c C}} \quad (9)$$

It is also common to use the McCumber parameter $\beta_c = \alpha^{-2}$, thus the overdamped case of negligible capacitance corresponds to $\beta_c \simeq 0$. With the definition of the normalized bias current:

$$\gamma_b = \frac{I_b}{I_c} \quad (10)$$

eq. (5) finally reads:

$$\frac{d^2\varphi}{d\tau^2} + \alpha \frac{d\varphi}{d\tau} + \sin\varphi = \gamma_b \quad (11)$$

3. Coupling schemes for Josephson systems

One can couple several JJ by connecting them with some geometry, for instance in parallel (as shown in fig. 3) or in series (as shown in fig. 4). The first coupling leads to the Frenkel-Kontorova model [13], which corresponds to a chain of pendula coupled by springs (see fig. 5).

The physical origin of the restoring "force", analogous to the Hooke elastic response, is the fluxoid quantization [29, 31]:

$$\frac{\Phi}{\Phi_0} = \frac{\varphi_{i+1} - \varphi_i}{2\pi} \quad (12)$$

In eq. (12) $\Phi_0 = h/2e$ is the elementary flux quantum, and Φ is the total flux in a cell, due to the flux induced by the external magnetic field minus the flux generated by the screening current I_i^s circulating in the i^{th} cell, see fig. 3. So eq. (12) reads:

$$\frac{1}{\Phi_0} (\Phi^{\text{ext}} - LI_i^s) = \frac{\varphi_{i+1} - \varphi_i}{2\pi} \quad (13)$$

From eq. (13) one retrieves the screening current I_i^s that contributes to the bias current of eq.(11). The presence of the screening currents thus forces the

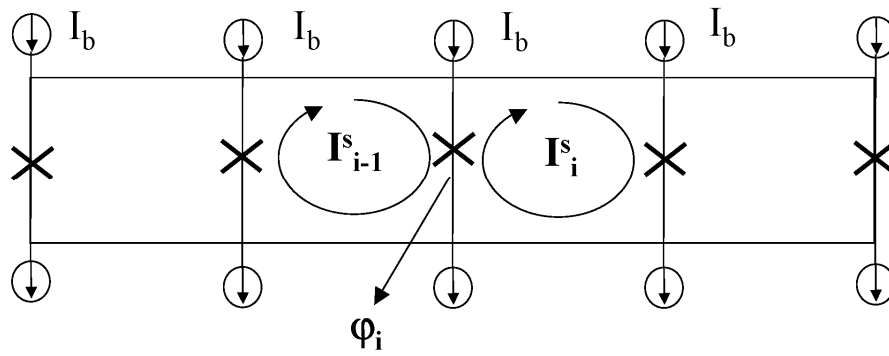


Figure 3. Schematic picture of a parallel array of JJ. The screening currents I^s circulate in a superconducting path and couple the junctions through fluxoid quantization.

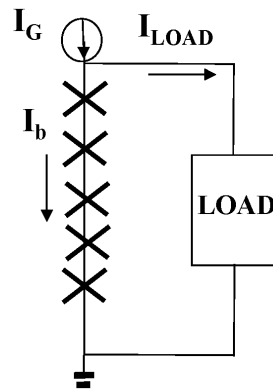


Figure 4. Electrical scheme for the series connection of JJ through an external load. The current I_{LOAD} deviated in the load couples the junction through the current balance (14).

junctions in a parallel array to have the same average speed, because the difference in the LHS of eq. (13) cannot increase indefinitely. Synchronization, at least on average, is therefore guaranteed in parallel arrays. This property has been exploited [48, 19, 51] to reduce the behavior of two-dimensional arrays, that are a combination of parallel rows connected in series, to the behavior of series connected arrays, see fig. 6.

Series coupling is due to the current balance, i.e. the current flowing through the junctions is the same for all junctions and amounts to the generator current I_G minus the current deviated through the load, I_L , see fig. 4:

$$I_b = I_G - I_{LOAD} = I_G - \frac{V_{LOAD}}{Z_{LOAD}} \quad (14)$$

The voltage applied to the load (V_{LOAD}) is due to the sum of all voltages of the individual junctions:

$$V_{LOAD} = \sum_i^N \frac{\hbar}{2e} \frac{d\varphi_i}{dt}. \quad (15)$$

In eq. (15) all terms are treated on an equal footing: the load cannot distinguish which junction occupies which position. This is the basic feature for the *global coupling* of all junctions coupled by each other. Inserting (15) in (14) and the resulting bias in eq. (11) one gets for a generic junction j :

$$\frac{d^2\varphi_j}{d\tau^2} + \alpha \frac{d\varphi_j}{d\tau} + \sin \varphi_j = \gamma_G - \frac{1}{Z_{LOAD}} \frac{\hbar}{2e} \frac{\omega_j}{I_c} \sum_i^N \frac{d\varphi_i}{d\tau} \quad (16)$$

Eq. (16) is peculiar: all junctions are coupled to all other junctions in the same manner and through the same term, the current deviated through the shunt. Putting it in another way, eq. (16) tells us that each junction is affected by the *average* velocity of the array, or that a sort of mean field approach is *exact* for series connected JJ. According to the vivid narrative of [40] when Wiesenfeld showed to Strogatz that a series arrays of JJ realizes the mean field *exactly*, Strogatz replied that a whole set of tools developed to treat the interaction among oscillators with an average approach had found a preferred system of application. Before describing the chief mean field approach, the Kuramoto Model [1], let me comment on two special properties of the global coupling (16). First, the very symmetry of the equations leads to the *attractor crowding* [47]. Suppose one finds a solution of (16), for instance, the so-called *splay states*:

$$V_j(t) = V_0(t + jT/N) \quad j = 1, \dots, N. \quad (17)$$

For the symmetry of the system there will be other $(N - 1)!$ solutions obtained by permutations. Such enormous number of coexisting attractors is not a unique feature of JJ. If you insert your favorite oscillator in (16) instead of the sine nonlinearity, the factorial growth of the number of solutions will hold true.

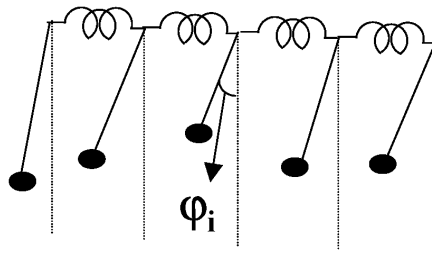


Figure 5. The mechanical analog of parallel arrays (see fig. 3): a chain of pendulums connected by springs corresponds to an harmonic lattice.

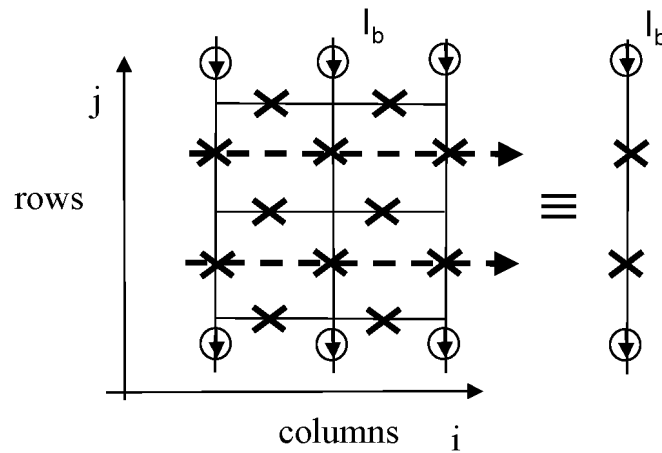


Figure 6. The logic of the reduction of two-dimensional array to one-dimensional series arrays: each row, being synchronized by the presence of screening currents, is assimilated to an effective single junction [51].

However, overdamped ($\beta_c \simeq 0$) JJ coupled through a resistor ($Z_{LOAD} = R_{LOAD}$) have a special property of their own, called "neutral stability" [32, 45, 46]: the maximum Liapunov exponent vanishes for a whole range of the parameters. This property is a consequence of the complete integrability of the overdamped eq. (16) with a pure resistive load. Notice that both properties are harmful for synchronization: the coherent state is neutrally stable (in the Liapunov sense) and the solutions (17) are metastable because they share the same energy.

4. Connection between Josephson arrays and the Kuramoto Model

As mentioned in the previous Section there exists a "mean field" model for synchrony. In 1975 Kuramoto has proposed a model for disordered oscillations [27], now known as the Kuramoto Model (KM):

$$\frac{d\theta_j}{dt} = \Omega_j + \frac{K}{N} \sum_{i=1}^N \sin(\theta_i - \theta_j) \quad (18)$$

There is a striking difference between JJ as described by eq. (16) and KM: in eq. (18) the oscillators are linear, while the coupling is nonlinear. However, the key nonlinearity is shared by both models, and in fact the mapping of JJ on the KM has been proved first with an averaging method [50] for the overdamped case and more recently with a simpler method that has allowed the mapping also in the underdamped case [16]. To be more specific, one usually assumes that the coupling load is a series *RLC* resonator [32], see fig. 7.

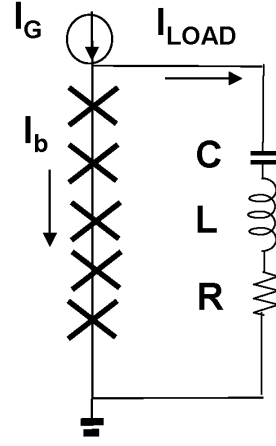


Figure 7. Electrical scheme for JJ series connected to an RLC resonator.

If we denote with q the charge (normalized to I_c/ω_j) on the capacitor and take into account the differences in the critical currents of the various junctions, eq. (16) can be rewritten as:

$$\frac{d^2\varphi_j}{d\tau^2} + \alpha \frac{d\varphi_j}{d\tau} + \frac{I_c^j}{I_c} \sin \varphi_j = \gamma_G - \frac{dq}{d\tau}. \quad (19)$$

The resonator dynamics is governed by the linear equation:

$$d\theta_j = \frac{\Omega_j d\varphi_j}{\gamma_G - \sin \varphi_j} \quad (20)$$

Here Q is the quality factor and Ω the resonance frequency. The parameter β_L describes the intensity of the coupling of the resonator with the array. Eqs. (19,20) are not obvious. The approach proposed by [50] is to consider the overdamped ($\beta_c \simeq 0$) case of eq. (11) since the analytical solution of the isolated junction is relatively simple. In fact if one performs the change of variables [50]:

$$d\theta_j = \frac{\Omega_j d\varphi_j}{\gamma_G - \sin \varphi_j} \quad (21)$$

the phases θ_j perform a uniform rotation, with Ω_j being the frequency of the j^{th} unperturbed oscillator that depends upon the value of I_c^j . However, the coupling among the junctions, when plugged into the new variables, is not as simple as in (16). In an approximate treatment based on averaging, it amounts to the sum of the sine of the difference of the θ variables, exactly the same structure as in eq. (18). The average procedure supplies the required change

from the nonlinear oscillators with linear coupling of eq. (16) to the linear rotators and nonlinear coupling as in eq. (18). The mathematical procedure of the mapping on the KM introduces also an important formal difference, the appearance of a phase θ_0 in the transformed variables:

$$\frac{d\theta_j}{d\tau} = \Omega_j + \frac{K}{N} \sum_{i=1}^N \sin(\theta_i - \theta_j + \theta_0). \quad (22)$$

However, the qualitative behavior of eq. (22) is very similar to the original model (18). The analytical procedure also provides the correspondence between JJ and KM parameters, namely the coupling constant K :

$$\cos(\theta_0) = \frac{Q/\Omega(\gamma_G^2 - 1 - \Omega^2)}{\left[\frac{Q^2}{\Omega^2} (\gamma_G^2 - 1 - \Omega^2)^2 + \left(1 + \frac{NR}{R_L}\right)^2 \right]^{1/2}} \quad (23)$$

and the phase angle θ_0 :

$$\cos(\theta_0) = \frac{Q/\Omega(\gamma_G^2 - 1 - \Omega^2)}{\left[\frac{Q^2}{\Omega^2} (\gamma_G^2 - 1 - \Omega^2)^2 + \left(1 + \frac{NR}{R_L}\right)^2 \right]^{1/2}} \quad (24)$$

Using a different approach, Dhamala and Wiesenfeld have extended the correspondence to underdamped JJ. It turns out that underdamped JJ can be mapped onto the massless KM eq. (18), and also in this case the explicit transformation

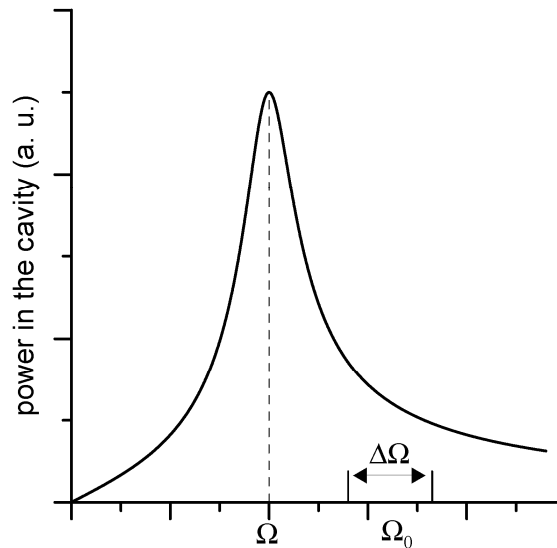


Figure 8. The resonance figure of the lumped circuit RLC whose frequency is denoted by Ω . The rotation frequencies of the JJ are spread around Ω_0 in an interval $\sim \Delta\Omega$.

of the parameters is available [16]. A key property of the system is the position of the average frequency of the JJ, $\Omega_0 = \langle \Omega_j \rangle$ with respect to the frequency of the resonator Ω , see fig. 8. The junctions are oscillating in the interval $\Delta\Omega$ if no resonator is coupled. The averaging approach [50] assumes that the coupling is weak enough to not alter significantly the relative position of Ω_0 and Ω , or that the two frequencies are close enough to remain unchanged by the interaction.

As mentioned several times the mapping of the JJ onto KM brings hopes of an experimental verification of the analytical predictions of the KM. Therefore, let me summarize the most preeminent feature of the KM, the transition to a synchronized state, referring to [1] for a detailed analysis. A way to describe the degree of synchrony of a dynamic state is to compute a sort of an order parameter, r :

$$r = r_0 e^{i\psi} = \frac{1}{N} \sum_{k=1}^N e^{i\theta_k} \quad (25)$$

Its meaning is rather obvious in the two limiting cases. Suppose one starts with many uncoupled oscillators, $K = 0$ in eq. (18), then all θ_j are randomly spread and for $N \rightarrow \infty$ one obtains $r \rightarrow 0$. In the opposite case, if all θ_j are synchronous and identical, eq. (25) gives $|r| = r_0 = 1$ for $K \rightarrow \infty$, this limit is intuitively reasonable for one expects that with increasing the coupling more and more all rotators will be eventually forced to move synchronously. The most interesting feature of the Kuramoto analysis is the analytical prediction of

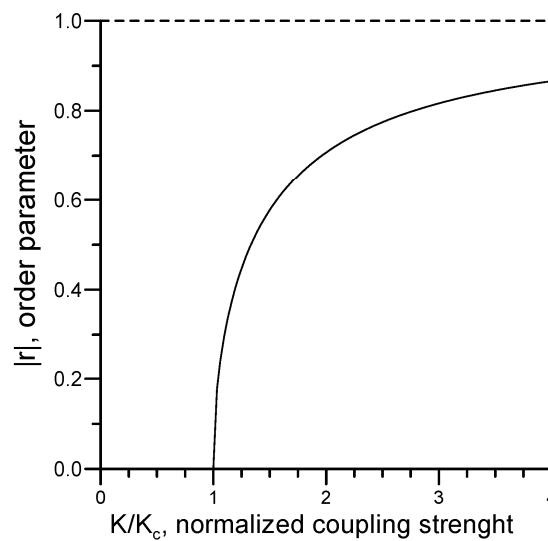


Figure 9. Behavior of the modulus of the order parameter $|r|$ as a function of the coupling strength K (normalized to the critical coupling K_c) for the KM (18).

the transition from $|r| = 0$ for uncoupled ($K = 0$) oscillators to completely synchronized system $|r| = 1$ for strongly coupled ($K \rightarrow \infty$) oscillators. For unimodal and symmetric distributions $g(\Omega)$ of the natural frequencies the prediction says that up to a critical value $K_c = 2/\pi g(\Omega_0)$ the system stays incoherent, or $|r| = 0$. For a Lorentzian distribution of the frequencies

$$g(\Omega) = \frac{(\Gamma/\pi)}{\Gamma^2 + (\Omega - \Omega_0)^2} \quad (26)$$

one gets $K_c = 2\Gamma$. The other nontrivial prediction is the smooth behavior of $|r|$ above K_c :

$$r = \sqrt{1 - \frac{K_c}{K}} \quad (27)$$

This behavior thus results in a second order phase transition, and is represented in fig. 9. Notice that the full synchronized state is only reached asymptotically for infinite coupling, in contrast with the observation that natural systems do reach a synchronous state also for a finite value of the coupling [17].

By comparing the analytical results with the experiments on JJ one should consider the translation of the analytical properties into experimentally available, or realistically manageable, information. The first difficulty is the measure of the degree of synchrony, or the order parameter r . Josephson elements are very rapid, they operate typically around 1mV and therefore through eq. (2) at hundreds of GHz. It is hence impossible to sample the waveform and to directly evaluate r through eq. (25). To circumvent this difficulty one measures the irradiated power, because the power emitted by the junctions is indirectly related to the degree of coherence. An incoherent not emitting array should be characterized by a low r , while "perfect" coherent emission with optimal power delivered should be characterized by a high value of r , possibly approaching 1. The second difficulty stems from the tenability of the coupling constant K . Inspection of its expression (23) in terms of the JJ parameters reveals that the only parameter that can be changed externally during an experiment is the generator current. In Ref. [50] it has been predicted that the degree of coherence should change dramatically sweeping the bias, see fig. 10. One should be able to observe a reentrant behavior: first the power sharply increases above the critical current, up to a maximum value; if one keeps increasing the bias the degree of synchronization returns to 0. However, to my knowledge, nobody has yet tried an experimental verification of this

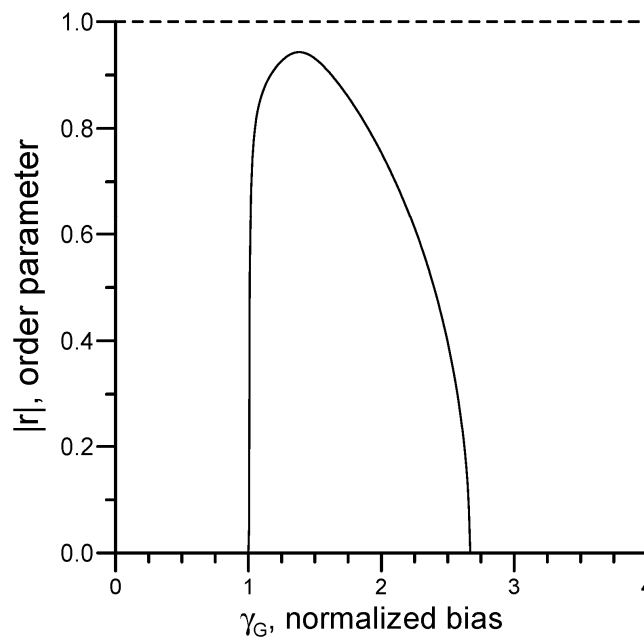


Figure 10. Sketch of the dependence of the modulus of the order parameter $|r|$ upon the external normalized bias for a series array of JJ coupled to an *RLC* cavity, eq. (27).

prediction. I believe that the main difficulty in the experimental verification of this behavior of $r(\gamma_G)$ is possibly the change in frequency that comes along the bias sweep. Microwave circuits are not easily realized with uniform properties in such a wide range of frequencies. Putting it in another way, the lumped circuit element equivalent of an actual distributed structure would not have the same parameters during the bias sweep.

However, for one reason or another, the experiments have followed a rather different path. The main results have been found by the Maryland group using arrays that are twodimensional and underdamped [8]. It has been shown that the extra dimension does not alter significantly the mapping on the KM [21, 48], and we have already mentioned that the mapping of the underdamped arrays can be performed onto the KM (18). The point is that for underdamped arrays the high slope of the IV characteristics fixes the frequency, and one cannot explore a whole range of bias current as in fig. 10. Instead Barbara et al [8] have tried another interesting approach exploiting the hysteretic behavior of low dissipation arrays to modify the coupling between the junctions: to change the number of active oscillators. Due to hysteretic dynamics, there are in fact two stable states, one corresponding to a rotating solution and another to a static solution. Because of the voltage relation, eq. (2), by measuring the voltage it is possible to recognize the fraction of active oscillators, while recording the output power one can infer on the order parameter, to surmise on the degree of synchronization. The conclusions of Ref. [8] are striking: the

power output stays at zero (or below detection) for a certain number of active junctions, then suddenly increases up to the almost perfect synchronized state above such threshold. This is partially in contrast with the effect predicted by eq. (27), that describes a smooth, or second order (in the language of phase transitions) passage from the disordered to the ordered state. To verify if the observed behavior is in agreement with the general features of the KM one should discuss the role of the number of active oscillators on the coupling. In eq. (23) we do have N dependence, but the results are derived in the $N \rightarrow \infty$ limit, therefore a naive translation to finite (and small) N would have a rather shaky ground. Recently the finite N behavior has been investigated by Pazó [37]. Unfortunately the analysis fails just around the transition from the disordered to the ordered state, and it is limited to compact support distributions of the natural frequencies Ω_j , for which the transition is expected to be first order also in the infinite N limit. So the behavior of KM at low N with non-compact distributions remains an open question. While the Maryland experiment was performed I had the good fortune to be collaborating with Pedersen and Wiesenfeld, and we came up with a rather different approach [20], admittedly much less rigorous. We speculate that the key difference is in the hypothesis of weak coupling assumed in the traditional mapping of JJ onto the KM model. In [50] it is supposed that the JJ are oscillating around the peak of the resonance, and that the resonator forces the junctions to compromise to the same frequency, but does not pull them away from their natural frequencies. Seen from the resonator point of view, whether a junction is in a synchronized state or not will make little difference: it will anyway excite the cavity with roughly the same frequency, close to the optimal resonant mode. We assume a different point of view: suppose that the oscillators are displaced with respect to the cavity (and at higher frequency otherwise the system would never lock-in [49]). Suppose also one drops in the oscillators one by one. At the beginning the cavity is weakly excited because the driving terms act on the outskirts of the resonance; until the cavity is feebly oscillating the frequency of the junctions will also be little affected. However, at a critical value the exciting terms are enough to move the frequencies of the junctions towards the resonance, and then a positive feedback mechanism is triggered: the more the junctions move, the stronger the answer of the resonator, the larger the effect on the junctions and so forth.

The resulting behavior is shown in fig. 11, and it is in qualitative agreement with the findings of [8]. The transition of the order parameter resembles a first order transition: the modulus stays almost at zero up to a critical value of 15 active junctions. At such value the order parameter suddenly jumps to almost 1, and the power delivered to the cavity starts

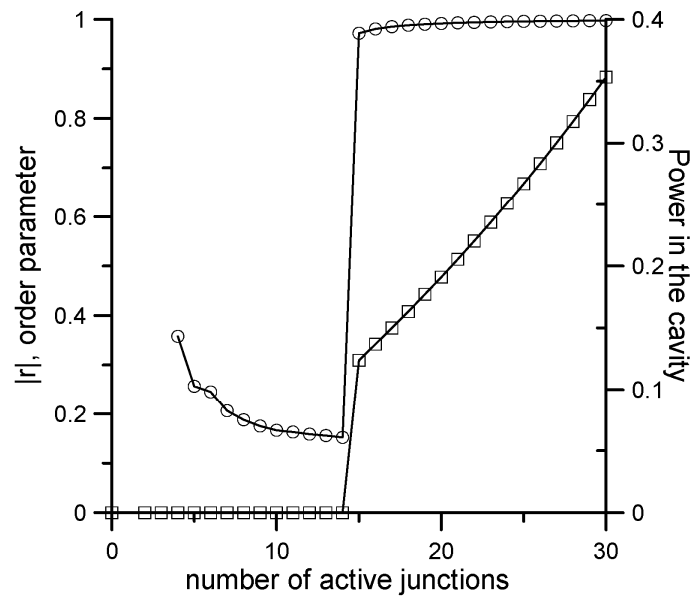


Figure 11. Order parameter r (squares, left axis) and power emitted (crosses, right axis) as a function of the number of active junctions for the system in fig. 7. The Q of the cavity is 100, the McCumber parameter reads $\beta_c = 10$, the critical currents are Lorentzian distributed with $\Gamma = 0.002$ and detuning $\delta = 0.075$.

increasing (a similar approach has also been used by [25]). The simulations are performed with eqs. (16,20), assuming a positive detuning:

$$\delta = \Omega_0 - \Omega \quad (28)$$

In view of the success of the numerical experiments, we have tried to map the behavior on the KM following an heuristic approach [22]. A logical consequence of the basic assumption that the interaction is strong, should be that the coupling strength depends upon the degree of synchronization. Being unable to treat analytically the strong interaction we employed the argument in a phenomenological manner. To show how we did it, first let me rewrite the KM (18) in the following equivalent form [1, 39] [here r and ψ are the same as in eq. (25)]:

$$\frac{d\theta_j}{d\tau} = \Omega_j + Kr \sin(\psi - \theta_j) \quad (29)$$

Let us assume that the coupling K has the property that the strength depends upon the dynamical state: the larger is the fraction of synchronous oscillators the larger is the resonator response because the oscillators move towards the peak of the resonance:

$$K \propto r^z, \quad z > 0. \quad (30)$$

The parameter z is a new phenomenological parameter that describes this tendency of the phase locked states to favor the coupling. The standard KM is recovered for $z = 1$. The assumption leads to a modified Kuramoto model inserting eq. (30) in eq. (29):

$$\frac{d\theta_j}{d\tau} = \Omega_j + K_0 r^z \sin(\psi - \theta_j). \quad (31)$$

This model can be obviously expressed in terms of the rotators variables:

$$\frac{d\theta_j}{d\tau} = \Omega_j + \frac{K_0}{N} \left[\frac{1}{N} \sum_{k=1}^N e^{i\theta_k} \right]^{z-1} \sum_{k=1}^{\infty} \sin(\theta_k - \theta_j). \quad (32)$$

The model is surprisingly tractable. In particular it predicts a first order phase transition for $z > 1$, and no phase transition for $z < 1$, see fig. 12.

The special case $z = 1$ is the only one to have a bona fide second order phase transition, while for $z < 1$ the behavior is only a resemblance of the second order phase transition, but is a smooth transition from the mathematical point of view. Assuming a Lorentzian distribution (26) the analytical prediction for the critical value of the coupling strength K_0 above which (partial) synchronization occurs reads:

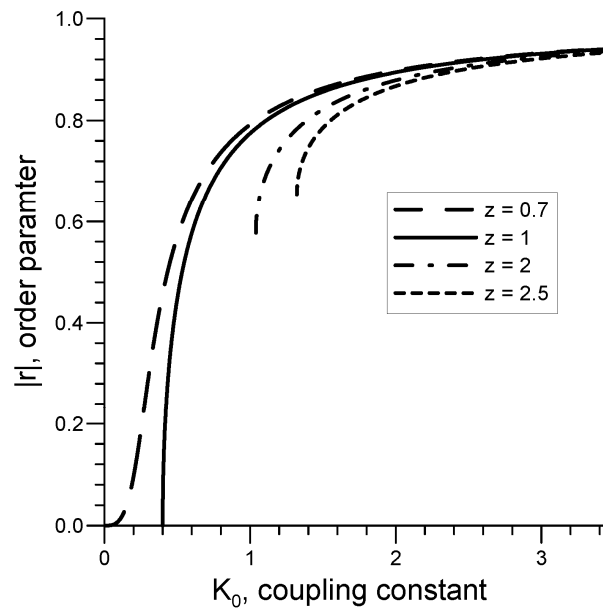


Figure 12. Behavior of the modified KM given by eq. (32) for different values of the exponent z .

$$K_c = \Gamma(z + 1) \left[\frac{z - 1}{z + 1} \right]^{\frac{z-1}{2}} \quad (33)$$

Above the value (33), the order parameter r jumps to

$$r_c = \left[\frac{z - 1}{z + 1} \right]^{\frac{1}{2}} \quad (34)$$

Moreover, the system in presence of noise has been investigated in [24], thus supplying a complete picture of this generalized version (32). Unfortunately, at the moment of this writing the value of z still cannot be derived from the Josephson junctions parameters.

5. Connections with other systems

The idea to insert the oscillators one at a time is not only confined to the JJ arrays described in the experiment of [8]. Actually, the very same idea was investigated for *long* JJ, i.e. for structures that are enough extended to allow the phase difference φ to be spatially modulated [9, 35, 36]. The system is very similar [30, 34], but instead of the small point contacts here described, it is based on the spatially extended junctions (in the x direction in the sketch of fig. 1). A completely different analysis of the basic oscillators (that are modeled via a nonlinear return map derived with an energetic argument [28]) gave a threshold value for synchronization [18]. More recently, laser oscillators have been synchronized in the same manner, adding the pumping elements one by one [14]. Even if the system is rather different, the route to synchrony seems analogous. Also the much discussed problem of the oscillations of the "London Millennium Bridge" (at the opening in the summer of 2000) has been related to the more and more people crowding on the passage of pedestrians (the event is recorded for instance on [5]). The sudden transition to large oscillations has been ascribed to the slow increase of the number of "oscillators", woman and man walking on the resonant structure above the Thames [41]. The reduction of the mechanical bridge oscillations and of the physiological (the pedestrians gait) systems to a version of the Kuramoto model seems to describe the phenomenon with a certain degree of accuracy, although, as one can easily imagine, human gait can be modeled only phenomenologically.

So far I have underlined the importance of the global coupling in the analysis of the KM. However, research has also been directed towards models that retain some memory of the individual bonds between the oscillators. In the KM framework, the following generalization has been proposed:

$$\frac{d\theta_j}{dt} = \Omega_j + \sum_{i=1}^N \frac{K_{i,j}}{N} \sin(\theta_i - \theta_j). \quad (35)$$

The matrix K_{ij} contains the information about the coupling between the i^{th} and the j^{th} oscillator, thus the original KM, eq. (18) is the particular case with $K_{ij} = K$. This model, often referred as *Local Kuramoto Model* (LKM) is relevant for JJ that are connected in parallel [15], often referred as *ladders*, see fig. 3. In fact it has been demonstrated, again with the averaging method, that parallel arrays can be mapped onto a nearest neighbor version of the LKM [15]. Also in this case JJ are thus a practical realization [11, 12, 44] of a generic model for synchronization.

More recently the LKM has been proposed [6, 38] to describe also oscillators coupled over a network of connections with novel topological properties [2]. In this category we can speculate about the stability of the so-called utility power grids that distribute electrical energy to consumers [23]. The main point of the analogy is the observation that energy flows from a generator to an utilizer only if there is a phase difference between the corresponding rotators. If one describes each machine with a phase angle, the power balance for the simplest system of just one generator θ^G and one utilizer θ^U (see fig.13) reads [26]:

$$P_{\text{source}}^M = I^G \frac{d^2\theta^G}{dt^2} \frac{d\theta^G}{dt} + K_D \left(\frac{d\theta^G}{dt} \right)^2 + P^{\text{MAX}} \sin(\theta^G - \theta^U), \quad (36)$$

$$P_{\text{utilizer}}^M = I^U \frac{d^2\theta^U}{dt^2} \frac{d\theta^U}{dt} + K_D \left(\frac{d\theta^U}{dt} \right)^2 + P^{\text{MAX}} \sin(\theta^U - \theta^G). \quad (37)$$

Here I is the moment of inertia, K_D a dissipation parameter, and P^{MAX} the maximum power that the transmission line can deliver between the two machines. These equations can be manipulated in normalized units and under the hypothesis of slow perturbation of the frequency of the distribution grid (50

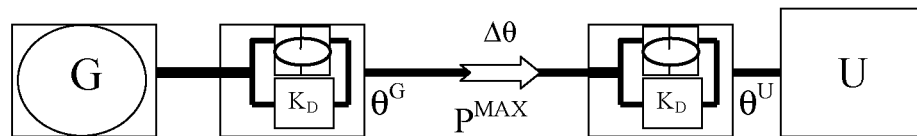


Figure 13. Schematic picture of a generator θ^G and utilizer θ^U machines in the power grid system. Both systems are rotating masses described by an angular variable θ with dissipation K_D . The power transmitted depends upon the phase difference $\Delta\theta = \theta_2 - \theta_1$, and cannot exceed some maximum value P^{MAX} .

or 60 Hz), to arrive at the equations (dissipation is assumed to be the same in the two systems):

$$\ddot{\theta}^G = W^G - \alpha \dot{\theta}^G + T \sin(\theta^U - \theta^G) \quad (38)$$

$$\ddot{\theta}^U = W^U - \alpha \dot{\theta}^U - T \sin(\theta^U - \theta^G) \quad (39)$$

If one was to consider a more complicated network of utilizers and generators, eqs. (38,39) were to be extended to assume the general form of eq. (35). Interestingly, in the simplest case of eqs. (38,39) the sum of the phases $S = \theta^G + \theta^U$ follows a linear equation:

$$\ddot{S} = W^G - W^U - \alpha \dot{S}. \quad (40)$$

The difference of the phases $D = \theta^G - \theta^U$, that describes the stability of the system, has the same structure as a JJ, see eq. (11):

$$\ddot{D} = W^G - W^U - \alpha \dot{D} + 2T \sin(D). \quad (41)$$

So the analogy between JJ and power grids is twofold. Indirectly, through the LKM because both systems can be mapped onto such general model. More directly, because the stability of the most elementary connection, fig.13, is described by an equation that is formally the same as a single JJ.

Regarding the connections with other systems, I would like to mention another important analogy: the similarity between JJ and lasers. It was pointed out long ago that the coherent behavior of several JJ could be described with the same tools as the coherent behavior of quantum mechanical particles in a laser, adopting a semi-classical approximation [7, 42]. The quantum mechanical treatment of JJ in a cavity has been recently developed by Almaas and Stroud [3, 4], and it essentially confirms the dynamical picture of the classical treatments [20, 25]. Also the existence of the threshold has an analogy with laser behavior. Suppose one realizes a laser mixing of two kinds of molecules in a resonant cavity, see fig. 14. Suppose also that one of the two species is capable to resonate with the cavity, while the other is not (i.e., one spectrum contains two levels whose energy spacing is close enough to the cavity resonance to allow for the population inversion, while the other spectrum does not). One could think of the two gases as either "active" oscillators or "absorbing" oscillators. The equivalent experiment depicted in fig. 11 (see ref.[8]), should be performed varying the proportion of the two gases. Below a certain threshold of the concentration of the active molecules the amplification mechanism does not work: too much power is absorbed by

the passive molecules. The question about the order of the phase transition for such a system would translate as follows: above the threshold, a finite amount of power is available immediately (first order transition) or the power continuously increases from zero (second order transition)?

6. Conclusion

In this Chapter I have tried to explain the rationale behind the preference the scholars of synchronization have granted to JJ as model systems. Nonlinear scientists appreciate the general trigonometric periodic function that appears in the model equation, a property shared by many other systems, from mechanically coupled pendulums to practical applications, such as the utility power grid. However, I have underlined my point of view that JJ have another special property: as circuit elements they can be coupled together in such a way that each junction is only affected by the average dynamical state of the other junctions. The average mediated effect of the coupling is particularly useful in studies of the route towards synchronization where the main analytical technique, the Kuramoto model, is based on a mean field approach (and, of course, on a sinusoidal periodic function). The approximated equivalence of the JJ model equations and of the Kuramoto model is one of the principal reasons for the fame of JJ in the synchronization research. As a practical realization of the Kuramoto model, JJ have their advantages and disadvantages. For instance take the speed: it is surely useful to quickly reach the steady state, but somehow JJ are too fast: their dynamics is not actually available in the experiments and only average properties can be recorded. Another example of a double side characteristic is the fact that JJ are superconducting elements. On one hand, at low temperatures the noise level is low, on the other hand, it demands cryogenics facilities. Finally, let me touch upon another point, practical applications of synchronized JJ for microwave and THz electronics. I have focused on the theoretical usefulness of JJ, but I do not want to shadow the importance of their practical applications. Most of the research on JJ is powered by the needs of the technology, not by the curiosity of the theoreticians. However, hopes are that each side helps the other to achieve even more cooperation (one might say, synchronization of the efforts) on tackling the same issues.

Acknowledgments

I wish to thank the financial support from the ESF network-programme "Arrays of Quantum Dots and Josephson Junctions" and from the project "Fabrication and Characterization of High- T_c Superconducting Thick Films" funded by the Regione Campania, Italy.

References

1. Acebrón, J. A., Bonilla, I. L., Perez Vicente, C. J., Ritrot, F., and Spigler, R. 2005, *Rev. Mod. Phys.*, 77, 137.
2. Albert, R. and Barabási, A. 2002, *Rev. Mod. Phys.*, 74, 47.
3. Almaas, E. and Stroud, D. 2001 *Phys. Rev. B*, 63, 144522.
4. Almaas, E. and Stroud, D. 2002 *Phys. Rev. B*, 65, 134502.
5. ARUP website: <http://www.arup.com/millenniumbridge/indepth/video.htm>
6. Barahona, M. and Pecora, L.M. 2002, *Phys. Rev. Lett.*, 89, 054101.
7. Bonifacio, R., Casagrande, F., and Milani, M. 1982, *Lett. Nuovo Cimento Soc. Ital. Fis.*, 34, 520.
8. Barbara, P., Cawthorne, A. B., Shitov, S. V., and Lobb, C. J. 1999, *Phys. Rev. Lett.*, 82, 1963.
9. Barone A. and Paternò, G. 1982, *Physics and application of the Josephson effect*, Wiley, New York.
10. Benz, S.P. and Burroughs, C.J. 1991, *Appl. Phys. Lett.*, 58, 2162.
11. Binder, P., Caputo, P., Fistul, M. V., Ustinov, A. V., and Filatrella, G. 2000, *Phys. Rev. B*, 62, 8679.
12. Binder, P., Abraimov, D., Ustinov, A.V., Flach, S., and Zolotaryuk, Y. 2000, *Phys. Rev. Lett.*, 84, 745.
13. Braunm O.M. and Kivshar, Y. 1998, *Phys. Rep.*, 306, 3.
14. Brusselbach, H., Cris Jones, D., Mangir, M. S., Minden, M., and Rogers, J. L. 2005, *Opt. Lett.*, 30, 1339.
15. Daniels, B. C., Dyssanayake, S.T.M., Trees, B.R. 2003, *Phys. Rev. E*, 67, 026216.
16. Dhamala, M. and Wiensefeld, K. 2002, *Phys. Lett. A*, 292, 269.
17. Ermentrout, G.B. 1991, *J. Math. Biol.*, 29, 571.
18. Filatrella, G., Rotoli, G., Grønbech-Jensen, N., Parmentier, R.D., and Pedersen, N.F. 1992, *J. Appl. Phys.*, 72, 3179.
19. Filatrella, G. and Wiesenfeld, K. 1995, *J. Appl. Phys.*, 78, 1878.
20. Filatrella, G., Pedersen, N. F., and Wiesenfeld, K. 2000, *Phys. Rev. E*, 61, 2513.
21. Filatrella, G., Pedersen, N. F., and Wiesenfeld, K. 2001, *IEEE Trans. Appl. Sup.*, 11, 1184.
22. Filatrella, G., Pedersen, N. F., and Wiesenfeld, K. 2006, *Phys. Rev. E*, 75, 017201.
23. Filatrella, G., Nielsen, A.H., and Pedersen, N.F. 2007, e-print cond-mat/07051305.
24. Giannuzzi, F., Marinazzo, D., Nardulli, G., Pellicoro, M., and Stramaglia, S. 2007, *Phys. Rev. E*, 75, 051104.
25. Grib, A. N., Seidel, P., and Scherbel, J. 2002, *Phys. Rev. B* 65, 094508.
26. Kundur, P. 1993, *Power system stability and control*, McGraw Hill.
27. Kuramoto, Y. 1975, in *International Symposium on Mathematical Problems in Theoretical Physics*, edited by H. Araki, *Lecture Notes in Physics*, 30, Springer, New York.
28. McLaughlin, D.W. and Scott, A.C. 1978, *Phys. Rev. A*, 18, 1652.
29. Miller, J.H., Guratne, H.H., Huang, J., and Golding, T.D. 1991, *Appl. Phys. Lett.*, 59, 3330.
30. Monaco, R., Pagano, S., and Costabile, G. 1988, *Phys. Lett. A* 131, 122.
31. Nakajima, K. and Sawada, Y. 1981, *J. Appl. Phys.*, 52, 5732.

32. Nichols S. and Wiesenfeld, K. 1992, *Phys. Rev. A*, 45, 8430.
33. Octavio, M., Whan, C.B., and Lobb, C.J. 1990, *Appl. Phys. Lett.*, 60, 766.
34. Pagano, S., Monaco, R., and Costabile, G. 1989, *IEEE Trans. Magn.*, 25, 1080.
35. Parmentier, R. D. 1978, Fluxons in long Josephson junctions, in *Solitons in action*, edited by K. Lonngren and A. C. Scott, Academic, New York.
36. Parmentier, R. D. 1993, Solitons and long Josephson junctions, in *The New Superconducting Electronics*, edited by H. Weinstock and R. W. Ralston, Kluwer, Dordrecht.
37. Pazò, D. 2005, *Phys. Rev. E*, 72, 046211.
38. Trees, B. R., Saranathan, V., and Stroud, D. 2005, *Phys. Rev. E*, 71, 016215.
39. Strogatz, S. H. 1993, *Lecture Notes in Biomathematics*, Springer, 100, 122.
40. Strogatz, S. H. 2003, *Sync: The emerging Science of spontaneous order*, Hyperion, New York.
41. Strogatz, S. H., Abrams, D. M., Mcrobie, A., Eckhardt, B., and Ott, E. 2005, *Nature (London)*, 438, 43.
42. Tilley, R.D. 1970, *Phys. Lett. A*, 33, 205.
43. Tornes, I. and Stroud, D. 2005, *Phys. Rev. B*, 71, 144503.
44. [Trías, E., Mazo, J.J., and Orlando, T.P. 2000, *Phys. Rev. Lett.*, 84, 741.
45. Watanabe, S. and Strogatz, S.H. 1993, *Phys. Rev. Lett.*, 70, 2391.
46. Watanabe, S. and Strogatz, S.H. 1994, *Physica D*, 74, 197.
47. Wiesenfeld, K. and Hadley, P. 1989, *Phys. Rev. Lett.*, 62, 1335.
48. Wiesenfeld, K., Benz, S., and Booi, P.A. 1994, *J. Appl. Phys.*, 76, 3835.
49. Wiesenfeld, K. and Swift, J.W. 1995, *Phys. Rev. E*, 51, 1020.
50. Wiesenfeld, K., Colet, P., and Strogatz, S. H. 1996, *Phys. Rev. Lett.*, 76, 404; *ibid*, *Phys. Rev. E*, 57, 1563.
51. Wiesenfeld, K., Landsberg, A., and Filatrella, G. 1997, *Phys. Lett. A*, 233, 373.



Current-voltage characteristics and breakpoint phenomenon in intrinsic Josephson junctions

Yu.M. Shukrinov^{1,2} and F. Mahfouzi³

¹BLTP, JINR, Dubna, Moscow Region, 141980, Russia; ²Physical Technical Institute, Dushanbe, 734063, Tajikistan; ³Institute for Advanced Studies in Basic Sciences, 45195-1159, Zanjan, Iran

Abstract

We review here our latest results on the investigation of the current-voltage characteristics and breakpoint phenomenon in the stacks with finite number of intrinsic Josephson junctions in layered superconductors.

Introduction

Strongly anisotropic high- T_c superconductor (HTSC) is a natural stack of intrinsic Josephson junctions (IJJ) and shows the intrinsic Josephson effect [1, 2]. The phase

dynamics in the IJJ have attracted a much attention because of its rich and interesting physics from one side and perspectives of its applications from the other side. Different couplings between junctions, like inductive coupling in the presence of magnetic field [3], capacitive [4, 5, 6], charge-imbalance [7] and phonon [8, 9] couplings determine a variety of current-voltage characteristics (IVC) observed in HTSC. Individual junction's area, its oxygen content and different coupling barrier layers could play an important role as well [10].

Due to the coupling, the equations for phase-differences in IJJ form a non-linear coupled differential equation. Its solution is classified by the number of rotating phases. The change of its number occurs intrinsically in this nonlinear equation, which leads to formation of branches in IVC. Although the number of rotating phases is the same, different patterns of distribution of rotating phases lead to slightly shifted branches. It is still an open question and a future problem which patterns are more easily realized among many possible patterns.

Capacitive mechanism of coupling between intrinsic Josephson junctions is based on the charging of the superconducting layers in the stack. The tunneling current creates the charge fluctuations on the superconducting layers which is related [4, 5, 6] to the gauge invariant scalar potential. The thickness of superconducting CuO_2 layers is extremely small and comparable to the charge screening length μ , which becomes incomplete within the single superconducting layers. The charging of the superconducting layers can not be neglected and it leads to the generalized Josephson relation (GJR) between the gauge-invariant phase difference $\varphi_l(t)$ and voltage $V_l(t)$ between layers l and $l + 1$. GJR takes into account that electric field generated inside a junction site affects the neighboring junctions and shows a coupling between Josephson oscillations in different barriers. This CCJJ model was used to analyze the current-voltage characteristics (IVC) of Bi-2212 superconductor, to explain the branch structure in IVC and the details of hysteresis jumps [4, 5, 6, 9, 10]. The equation for the interlayer phase difference was derived in [4] and solved numerically for finite system with 100 junctions to simulate the IVC.

It has been stressed [8] that capacitive coupling takes various values in HTSC and layered organic superconductors, that is, the capacitive coupling is tunable in this systems. Based on this fact, a systematic study for the dynamics of the CCJJ model, focusing on the dependence of phase dynamics on the strength of the capacitive coupling constant from weak to strong coupling regimes has been presented. A conclusion have been made that the dynamics of the localized rotating modes primarily determines the IVC of IJJ. Since the energy required to excite the localized rotating modes is increased with the capacitive coupling parameter, several junctions collectively rotate. As a

result, the equidistant multiple-branch structure disappears in the strong coupling systems.

As was shown in Ref.[7, 11], diffusion current plays an important role in the charge imbalance effect in the stack of IJJ. The CCJJ model including diffusion current was derived in Ref.[12] based on Euler-Lagrange equations obtained from effective action for system of IJJ. But the authors considered that a term corresponding to the diffusion current might be neglected. We investigated the total branch structure in the IVC of eleven IJJ in a stack and the coupling dependence of the branch slopes at different boundary conditions. Then we included the diffusion current in the total tunneling current and demonstrated that the equidistance of the branch structure could be restored.[13]

A simulation of the current-voltage characteristics (IVC) of a stacks of intrinsic Josephson junctions (IJJ)[1] at different values of the model parameters such as the coupling and dissipation parameters is a way to predict the properties of the IJJ. McCumber and Steward have investigated the return current as a function of dissipation parameter in a single Josephson junction a long time ago.[14] In the case of the system of junctions, the situation is cardinally different. The IVC of IJJ is characterized by a multiple branch structure and branches have a breakpoint region with its breakpoint current (BPC) and transition current to another branch. [15, 16] The BPC is determined by the creation of the longitudinal plasma waves (LPW) with a definite wave number k , which depends on the parameters α and β , the number of junctions in the stack, and boundary conditions. If we neglect the coupling between junctions, the branch structure disappears, and the BPC coincides with the return current.

In this Chapter, we review our recent results based on the description of IVC of the IJJ in the framework of CCJJ, CCJJ+DC and CIB models. We show that IVC have a breakpoint in their branches.[17] The BPC I_{bp} on the outermost branch as a function of the coupling α and dissipation β parameters for the stacks with a different number of IJJ is presented and demonstrated to possess a plateau with BPC oscillation. We show that the $\alpha\beta$ -dependence of the BPC is an instrument to determine the mode of LPW created at the breakpoint in the stacks with a different number of junctions.

2. Coupling between junctions in the stack of IJJ in layered superconductors

2.1. Generalized Josephson relation

Tunnel junction is the capacitor at the same time, i.e. it has a charge $Q = CV$, where $C = \epsilon S/4\pi d$. Because a thickness of S-layers in HTSC is very small,

this charge is not screened and this fact leads to the coupling between junctions. The origin of coupling is the capacity of the junction, that is why such kind of coupling is called "capacitive".

We consider a system of superconducting layers with indices l and order parameter $\Delta_l(t) = |\Delta| \exp(i\chi_l(t))$ with time-dependent phase $\chi_l(t)$. We define the gauge invariant phase difference as:

$$\gamma_l(t) = \chi_l(t) - \chi_{l+1}(t) - \frac{2e}{\hbar} \int_l^{l+1} dz A_z(z, t), \quad (1)$$

where $A_z(z, t)$ is the vector potential in the barrier. Here e denotes the elementary charge. The charge of the electron is $-e$.

For the time derivative of $\gamma_{l,l+1}$ we obtain the generalized Josephson relation:

$$\frac{d\gamma_l}{dt} = \frac{2e}{\hbar} (V_l + \Phi_{l+1} - \Phi_l). \quad (2)$$

Here

$$V_l = \int_l^{l+1} dz E_z(z, t) \quad (3)$$

is the voltage and $\Phi_l(t)$ is the so-called gauge invariant scalar potential defined by

$$\Phi_l(t) = \phi_l(t) - \frac{\hbar}{2e} \dot{\chi}_l(t), \quad (4)$$

where $\phi_l(t)$ is the electrical scalar potential.

The quantity $\hbar\dot{\gamma}_l = 2e(V_l + \Phi_{l+1} - \Phi_l)$ is the total energy required to transfer a Cooper pair from layer l to $l + 1$, $e\Phi_l$ can be considered as the shift of the chemical potential of the superconducting condensate with respect to an average chemical potential μ , i.e. the number of particles in the condensate is controlled by $\mu + e\Phi_l$. For equilibrium superconductors $\hbar\dot{\chi}_l = 2e\phi_l$, $\Phi_l = 0$, and one has the usual Josephson relation $\hbar\dot{\gamma}_l = 2eV_l$.

Relation between the charge ρ_i and the potential Φ_i is

$$\rho_i = -\frac{1}{4\pi r_D^2} \Phi_i \quad (5)$$

where Φ_i is expressed through a scalar potential ϕ_i and derivative of phase θ by

$$\Phi_i(t) = \phi_i - \frac{\hbar}{2e} \frac{\partial \theta_i}{\partial t} \quad (6)$$

From (6) we come to the modified Josephson relation

$$\frac{d\phi_{i,i+1}}{dt} = \frac{2e}{\hbar} V_{i,i+1} + \frac{2e}{\hbar} (\Phi_{i+1} - \Phi_i) \quad (7)$$

Using (5) and (7) we find

$$\frac{\hbar}{2e} \frac{d\phi_{i,i+1}}{dt} = V_{i,i+1} - 4\pi r_D^2 (\rho_{i+1} - \rho_i) \quad (8)$$

We can express ρ through the V by Maxwell equations

$$\text{div} D = 4\pi\rho \quad D = \varepsilon E \quad E = V/d \quad (9)$$

and write

$$\begin{aligned} \rho_i &= \frac{\epsilon_0}{4\pi d_0 d} (V_{i,i+1} - V_{i-1,i}) \\ \rho_{i+1} &= \frac{\epsilon_0}{4\pi d_0 d} (V_{i+1,i+2} - V_{i,i+1}) \end{aligned} \quad (10)$$

Then MJR has a form

$$\frac{\hbar}{2e} \frac{d\phi_{i,i+1}}{dt} = V_{i,i+1} - \alpha (V_{i+1,i+2} + V_{i-1,i} - 2V_{i,i+1}) \quad (11)$$

where $\alpha = \epsilon r_D^2 / d_0 d$. This formula shows the coupling between junctions: phase difference in the junction depends on the voltages in the nearest ones.

2.2. Coupled system of equations

Taking the derivative and multiplying by C we find

$$\frac{\hbar C}{2e} \partial^2 \phi_{i,i+1} / \partial t^2 = \partial V_{i,i+1} / \partial t - \alpha C (\partial V_{i+1,i+2} / \partial t + \partial V_{i-1,i} / \partial t - 2\partial V_{i,i+1} / \partial t) \quad (12)$$

We can find $C\partial V/\partial t$ from

2.3. Numerical procedure

We solve this system for stacks with different numbers N of intrinsic junctions. The numerical procedure has been done as follows. For a given set of model parameters N, α, β, γ we simulate the IVC of the system, i.e., $V_l(I)$, increasing I from zero up and then down. A change in the parameters N, α, β, γ changes the branch structure in the IVC essentially. Their influence on the IVC in the CCJJ and CCJJ+DC models was discussed in Refs.[19, 13, 18]. To calculate the voltages $V_l(I)$ in each point of the IVC (for each value of I), we simulate the dynamics of the phases $\varphi_l(t)$ by solving the system of equations (15) using the fourth-order Runge-Kutta method. After simulation of the phase dynamics we calculate the dc voltages on each junction as

$$\partial\varphi_l/\partial t = \sum_{l'} A_{ll'} V_{l'} \quad (18)$$

where V_l is normalized to $V_0 = \hbar\omega_p/(2e)$. The average of the voltage \bar{V}_l is given by

$$\bar{V}_l = \frac{1}{T_{max} - T_{min}} \int_{T_{min}}^{T_{max}} V_l dt \quad (19)$$

where T_{min} and T_{max} determine the interval for the averaging. After completing the voltage averaging for current I , the current I is increased or decreased by a small amount δI to calculate the voltages at the next point of the IVC. We use the distribution of phases and their derivatives achieved in the previous point of the IVC as the initial distribution for the current point.

Numerical stability was checked by doubling and dividing in half the temporal discretization steps Dt and checking the influence on the IVC. Finally we can obtain the total dc voltage V of the stack by

$$V = \sum_{l=1}^N \bar{V}_l \quad (20)$$

At some current I some junction (or junctions) switches to the nonzero voltage state and gives some branch of the IVC. We plot the total IVC at different parameters of the problem. The details concerning the numerical procedure are given in [6, 18].

3. IVC in CCJJ model

The CCJJ model was described in detail in Ref.[18]. Let us consider the $N + 1$ superconducting layers (S-layers), numbered from 0 to N . The widths of

0-th and N-th S-layers are extended due to the proximity effect into attached normal metals. In cases of no applied magnetic field and small sample size in the a-b direction, the physical quantities are spatially homogeneous on each layer. In the framework of this model the resistive state in IJJ is realized as a state with definite number of rotating (R) or oscillating (O) junctions. If the l-th junction ($\varphi_l \equiv \varphi_{l,l+1}$) has a rotating phase, then

$$\langle \partial\varphi_l/\partial\tau \rangle = \text{const} \quad (21)$$

$$\langle \sin \varphi_l \rangle = 0 \quad (22)$$

If the l-th junction has a oscillating phase, then

$$\langle \partial\varphi_l/\partial\tau \rangle = 0 \quad (23)$$

$$\langle \sin \varphi_l \rangle = \text{const} \quad (24)$$

The O-state is one of the new elements which appears in IJJ in comparison with one JJ. The O-state can be realized if number of junctions in the stack is more than 2. According to the GJR, the Josephson oscillation frequency $\frac{\partial\varphi_l}{\partial t}$ is determined not only by the voltage in the same junction but also by the voltages in neighboring junctions. Total voltage is not a sum of voltages on R-junctions, but it is distributed among other junctions in the stack. The hysteresis jumps in the IVC are associated with the change of the distribution pattern of rotating phase motions.

In the CCJJ model the dynamics of the gauge-invariant phase difference φ_l between superconducting layers l and $l+1$ is described by the equation:

$$\begin{aligned} \partial^2\varphi_l/\partial t^2 = & \frac{I}{I_c} - \beta\partial\varphi_l/\partial t - \sin \varphi_l \\ & + \alpha(\sin \varphi_{l+1} + \sin \varphi_{l-1} - 2 \sin \varphi_l) \end{aligned} \quad (25)$$

where I and I_c are the external dc current and the Josephson critical current, respectively.

To simulate an experiment which investigates the IVC of IJJ we should choose some initial conditions for phases and their derivatives and perform the current increasing and decreasing many times. Influence of value of the current step δI on the branch structure of IVC imply [6] that several bifurcation points are distributed in a very narrow region for controlling parameter I of equation (25). Results of such simulation are shown in Fig. 1b for the same stack as in Fig. 1a. To determine the state corresponding to the chosen branch, we analyze

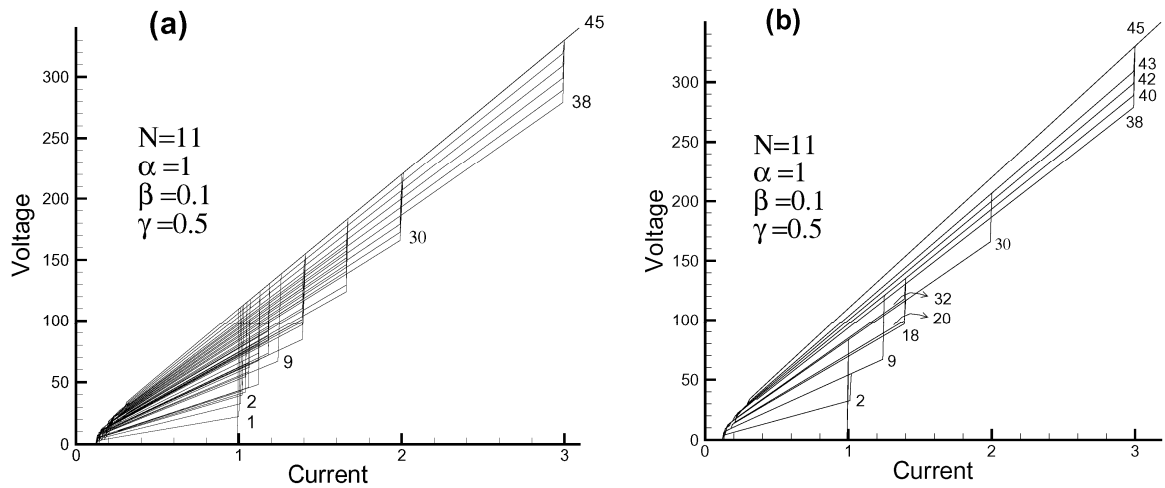


Figure 1. The total branch structure in the IVC of IJJ (a) and result of simulation of IVC at fixed initial conditions (b). The branch numbers correspond to the states with definite number and positions of the R- and O-junctions in the stack, presented in the Table of the Ref.[19].

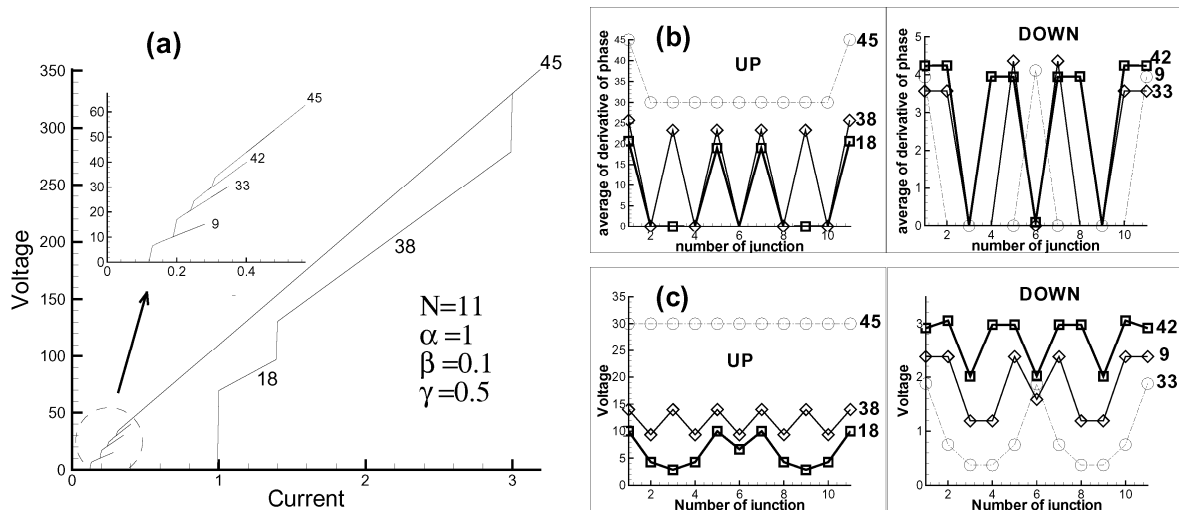


Figure 2. IVC for one current increasing and decreasing process (a) and corresponding phase (b) and voltage (c) distributions (From Ref.[19]).

the voltage and the average of the phase derivative distributions. Fig. 2a presents the IVC for $\delta I = 0.01$ for one increasing and decreasing circle. The current is gradually increased up to $I/I_c = 3.2$ and then gradually decreased. In the current increasing process, the IVC shows the jumps at $I/I_c = 1.0, 1.4$ and 3.0 . In the current decreasing process, there appear three jumps when the current becomes smaller than 0.3 .

In order to explain this branch structure, we show in Fig. 2b average of the phase derivative, and in Fig. 2c the voltage distributions on each junction just after the jumps for the current increasing and decreasing processes. For the

branch 18, four junctions have highest voltage. The phases of the junctions with highest voltage increase approximately linearly in time, correspondingly to the phase rotating motion, while the other junctions have oscillating phase motion. When the time average of the derivative of phase is plotted in Fig. 2b, junctions with rotating and oscillating phases are clearly identified [18]. As we can see, the number of phase rotating junctions is six for branch 38 and eleven for branch 45. For the branches 33, 8 and 42 the number of junctions in rotating state is equal to 3, 6 and 8, respectively. As it was discussed in detail in Ref. 7 the hysteresis jumps are associated with the change of the distribution pattern of rotating phase motion.

The branches in the IVC of IJJ in CCJJ model demonstrate the breakpoint. In Fig. 3(left) we show the breakpoint on the outermost branches at different values of the coupling parameter α by arrows.[19]

The "breakpoint region" (BPR) on the IVC of the stack of IJJ was demonstrated in Ref.[15] and it is explained as a result of resonance between Josephson and plasma oscillations. Simulation of the IVC of IJJ by different groups using different models shows the BPR on the outermost branch as well, but the authors did not mention it (see Fig. 4). To our knowledge, no precise experiments to observe the BPR have been done yet. The equation for the Fourier component of the difference of phase differences $\delta_l = \varphi_{l+1,l} - \varphi_{l-1,l}$ between neighboring junctions is[15, 16, 17]

$$\delta_k'' + \beta(k)\delta_k' + \cos(\Omega(k)\tau)\delta_k = 0, \quad (26)$$

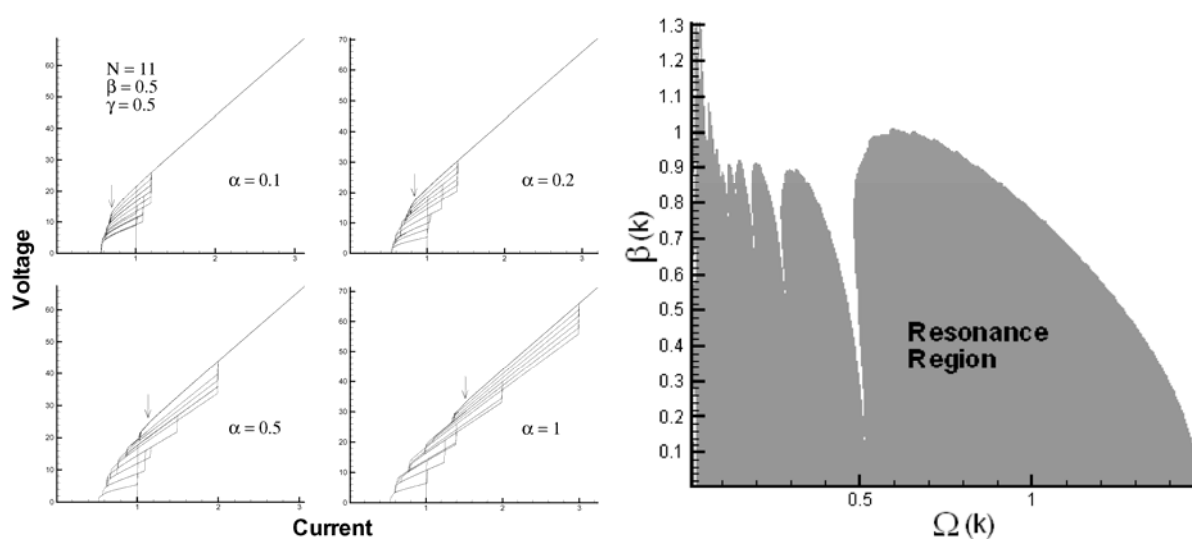


Figure 3. On the left: Breakpoint on the outermost branches in the IVC of IJJ in CCJJ model at different values of the coupling parameter α ; on the right: Phase diagram in $\Omega(k) - \beta(k)$ space for the stack of IJJ at $\alpha = 1$, $\beta = 0.2$ and $\gamma = 0$;

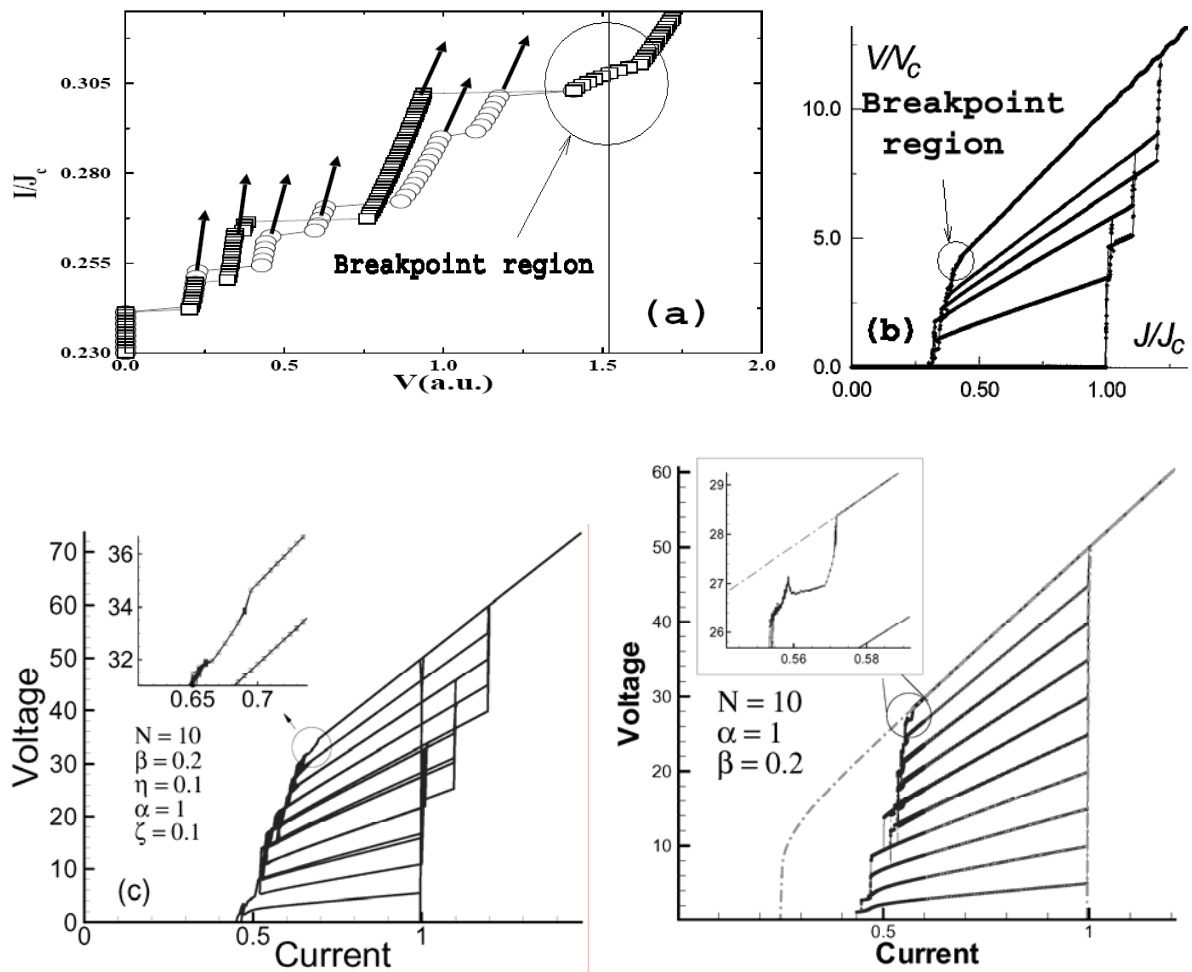


Figure 4. Demonstration of the breakpoint on the outermost branch in simulated IV characteristics in different models: (a) CCJJ model (Cf. Fig.3a in [6]); (b) charge imbalance (CIB) model (Cf. Fig.1 in [7]); (c) CIB model (Cf. Fig.2(left) in [20]); (d) CCJJ+DC model (Cf. Fig.1 in [15]).

where $\tau = \omega_p(k)t$, $\omega_p(k) = \omega_p C$, $\beta(k) = \beta/C$, $\Omega(k) = \Omega/C$ and $C = \sqrt{1 + 2\alpha(1 - \cos(k))}$. This equation shows a parametric resonance with changing its parameters $\beta(k)$ and $\Omega(k)$. We note that in comparison with CCJJ+DC model, where $\beta(k) = \beta C$, the effective dissipation parameter $\beta(k)$ in this model is less than β . We may conclude that with increase in α it is more favorable for the system to have the plasma waves. We solved the Eq. (26) numerically and result is presented in Fig. 3(right), where the resonance region for the stack of IJJ at $\alpha = 1$, $\beta = 0.2$ and $\gamma = 0$ is shown. For $\Omega(k)$ and $\beta(k)$ inside of the resonance regions the solution of the equation increases in time. It means that we observe a parametric resonance in this region. Outside of this region, starting from any initial condition, the solutions attenuate in time to zero.

4. IVC in CCJJ+DC model

In the CCJJ model with diffusion current

$$J_D^l = -\frac{\Phi_l - \Phi_{l+1}}{R}. \quad (27)$$

the total external current is equal to

$$J = C \frac{dV_l}{dt} + J_c^l \sin(\varphi_l) + \frac{\hbar}{2eR} \dot{\varphi}_l \quad (28)$$

To obtain the equation (28) we used the GJR

$$\frac{d\phi_l}{dt} = \frac{2e}{\hbar} V_l + \frac{2e}{\hbar} (\Phi_{l+1} - \Phi_l) \quad (29)$$

Total external current (28) in CCJJ+DC model differs from the current in CCJJ model (15) by third term in the right hand side. In CCJJ model it is equal to V_l/R . Finally, in CCJJ+DC model we obtain the next equation for the gauge-invariant phase difference

$$\ddot{\varphi}_l = \sum_{l'=1}^n A_{ll'} [I - \sin(\varphi_{l'}) - \beta \dot{\varphi}_{l'}] \quad (30)$$

where $I = J/J_c$ and we consider that critical current is the same for all junctions $J_c^l = J_c$.

To simulate an experiment which investigates the IVC of IJJ we define the initial conditions for phases and their derivatives and perform the current increasing and decreasing many times. The total branch structure in the IVC in framework of the CCJJ+DC model for the stack of 11 junctions at $\alpha = 1$, $\beta = 0.2$ and $\gamma = 0$ is shown in Fig. 5(left).

As we can see, the inclusion of the diffusion current in the CCJJ model leads to the equidistant branch structure. Changes in α and β do not effect the equidistance of the branch structure. We investigated the influence of the parameter γ and found that the increase in γ leads to the appearance of the additional branches and breaks the equidistance. At periodic boundary conditions the branch structure is equidistant. Fig. 5(right) shows the IVC for 10 IJJ calculated by the equation Eq.(30) at $\alpha = 1$, $\beta = 0.2$ and periodic boundary conditions. The parameter β is related to the conductivity of the insulating layer and determines the slope of the IVC. Variation in β in the framework of the CCJJ model [19] changes the hysteresis loop of IVC but preserve

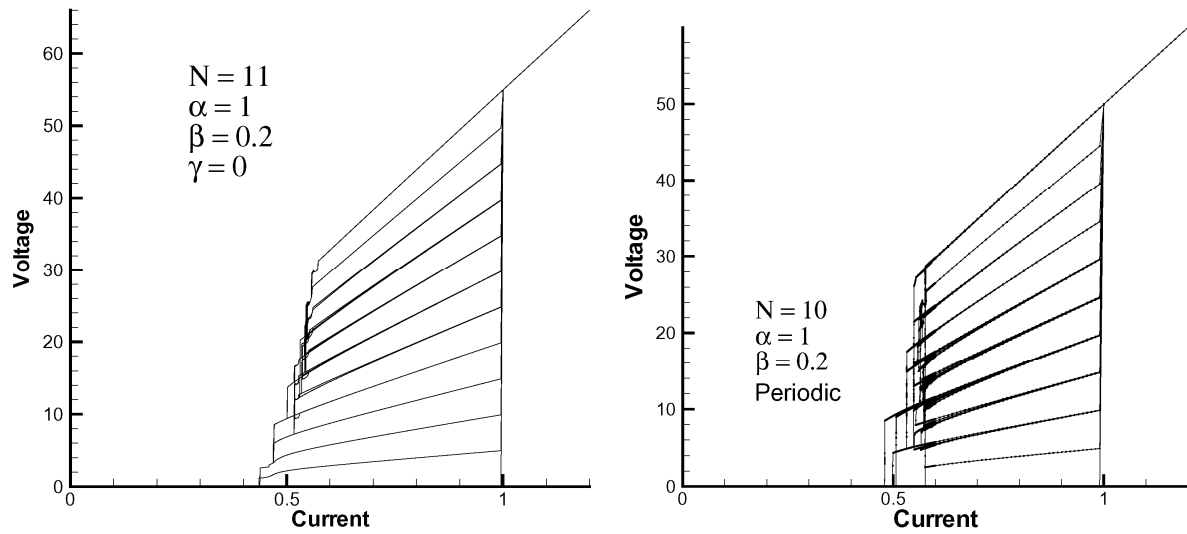


Figure 5. The branch structure in IVC in CCJJ model with diffusion current at $\gamma = 0$ (left) and at periodic boundary conditions (right) (From Ref.[13]).

the main features of the branch structure. The nonequidistance of the branch structure cannot be removed by variation in β . In CCJJ+DC model change in β does not have effect on the equidistance of the branch structure. The coupling parameter α determines the nonlinear effects among phase differences. In the CCJJ+DC model in the parameters range we study here, the coupling parameter changes the return current of the branches. We consider that the origin of such behavior is a term in Eq.(30) proportional to the product of the coupling and McCumber parameters which is absent in the CCJJ model. In the CCJJ+DC model the value of the endpoints of the branches is the same for all branches and does not depend on β . Situation is changed [20] if we take into consideration the nonequilibrium effects created by tunneling current injection [7]. In this case the new branches appear and the current endpoints for branches depend in different way on disequilibrium parameter. At small value of the disequilibrium parameter the branch structure is close to the equidistant one and just a small splitting of some branches exists [20].

5. IVC in Charge Imbalance Model

In the CIB model the dynamics of the gauge-invariant phase difference $\varphi_{l,l+1}$ between superconducting layers l and $l+1$ is described by the equation

$$\frac{d^2\varphi_{l,l+1}}{d\tau^2} = (1 - \alpha\nabla^2)(J - \sin(\varphi_{l,l+1}) - \psi_l + \psi_{l+1} - \beta\frac{d\varphi_{l,l+1}}{d\tau}) - \frac{\dot{\psi}_l - \dot{\psi}_{l+1}}{\beta} \quad (31)$$

and kinetic equations

$$\begin{aligned}
\zeta \dot{\psi}_0 &= \eta \gamma_d (bJ - \beta \dot{\phi}_{0,1} + \psi_1 - \psi_0) - \psi_0 \\
\zeta \dot{\psi}_l &= \eta (\beta (\dot{\phi}_{l-1,l} - \dot{\phi}_{l,l+1}) + \nabla^{(2)} \psi_l) - \psi_l \\
\zeta \dot{\psi}_n &= \eta \gamma_d (\beta \dot{\phi}_{n,n+1} - bJ + \psi_{n-1} - \psi_n) - \psi_n
\end{aligned} \tag{32}$$

In these equations J is the external current in J_c units, parameter b determines the injection of quasiparticles from boundaries, ψ_l - the charge imbalance potential on superconducting layers [7], α - the coupling parameter, β is related with the McCumber parameter β_c as $\beta = 1/\sqrt{\beta_c}$, η - the nonequilibrium parameter, $\zeta = \omega_p \tau_{qp}$, ω_p - the plasma frequency, τ_{qp} - the charge imbalance relaxation time, $\gamma_d = s/s_0 = s/s_N$ and s_0, s_N are the thickness of the first and last S -layers, respectively. The Laplacian on the boundaries is defined as $\nabla^{(2)} f_{0,1} = f_{1,2} - (1 + \gamma)f_{0,1}$, $\nabla^{(2)} f_{N-1,N} = f_{N-2,N-1} - (1 + \gamma)f_{N-1,N}$.

To obtain the voltage we use the generalized Josephson relation

$$\frac{V_{l,l+1}}{\beta J_c R} = (1 - \alpha \nabla^{(2)})^{-1} (\dot{\phi}_{l,l+1} + \frac{\psi_l - \psi_{l+1}}{\beta}) \tag{33}$$

We have solved numerically this system of equations using fourth order Rounge-Kuta method in the presence of very small noise with maximum 10^{-10} . Results of two simulations of the total branch structure for the stack of 10 IJJ at different values of η and ζ are shown in Fig. 6. The structure in the IVC is close to the equidistant one and the both IVC demonstrate the breakpoint regions

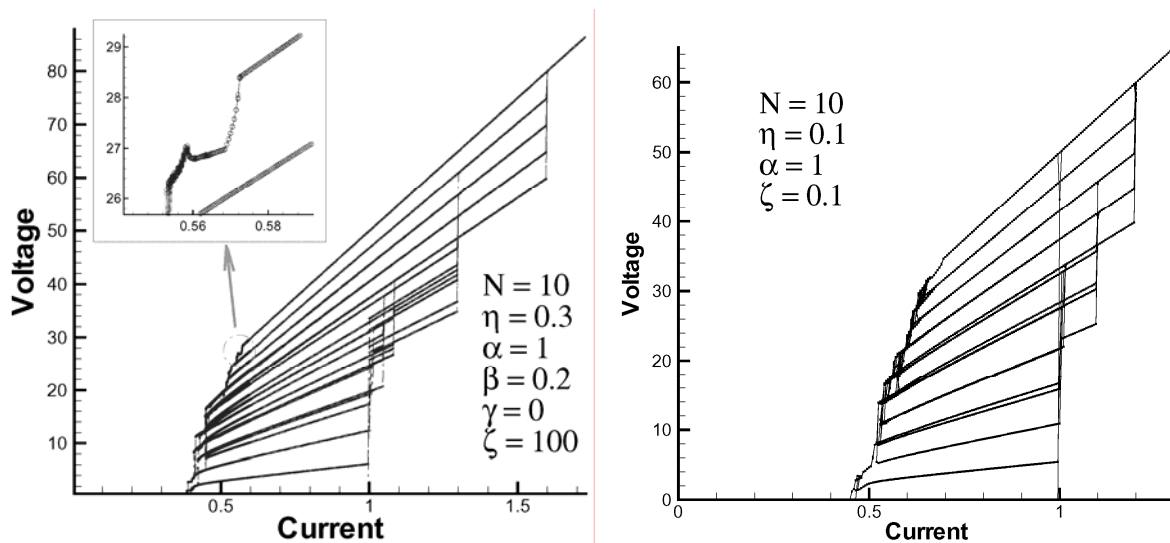


Figure 6. The total branch structure in the IVC of 10 IJJ for different values of nonequilibrium parameter η .

on their outermost branches. The detailed investigation of the influence of the model parameters on the vortex structure in the CIB model will be presented somewhere else.

In the CIB model we find the equation for the Fourier component of the difference of phase differences $\delta_l = \varphi_{l+1,l} - \varphi_{l,l-1}$ between neighboring junctions

$$\ddot{\delta}_k + \cos(\varphi)\delta_k + (\beta(k) - \frac{\eta(k)}{\zeta})\dot{\delta}_k + (1 + \frac{\eta(k)+1}{\zeta\beta(k)})\eta(k)\beta(k) \int_0^\tau dt \delta_k e^{\frac{1+\eta(k)}{\zeta\beta(k)}(t-\tau)} + \Delta\psi_0 e^{-\frac{1+\eta(k)}{\zeta\beta(k)}\tau} = 0 \quad (34)$$

where the dimensionless parameters ψ' and $\eta(k)$ are defined as $\psi' = 2(1 - \cos(k))\psi$ and $\eta(k) = 2(1 - \cos(k))\eta$. Other parameters have the same form as in CCJJ model. As we can see, the dynamical equations are different for different modes k even at $\alpha = 0$. To find the resonance regions for parameters of the system, we have solved the equation (34) numerically. The results of calculations are presented in Fig. 7. The decrease in $\Omega(k)$ means the decrease in the voltage, so we may conclude from the Fig. 7(left) that for $\beta(k)$ smaller than some value β_0 , the increase in $\eta(k)$ increases the voltage value of the breakpoint, while for $\beta(k)$ bigger than β_0 , the increase in η decreases the breakpoint voltage. Fig. 7(right) demonstrates a decrease of the breakpoint voltage with the increase in β .

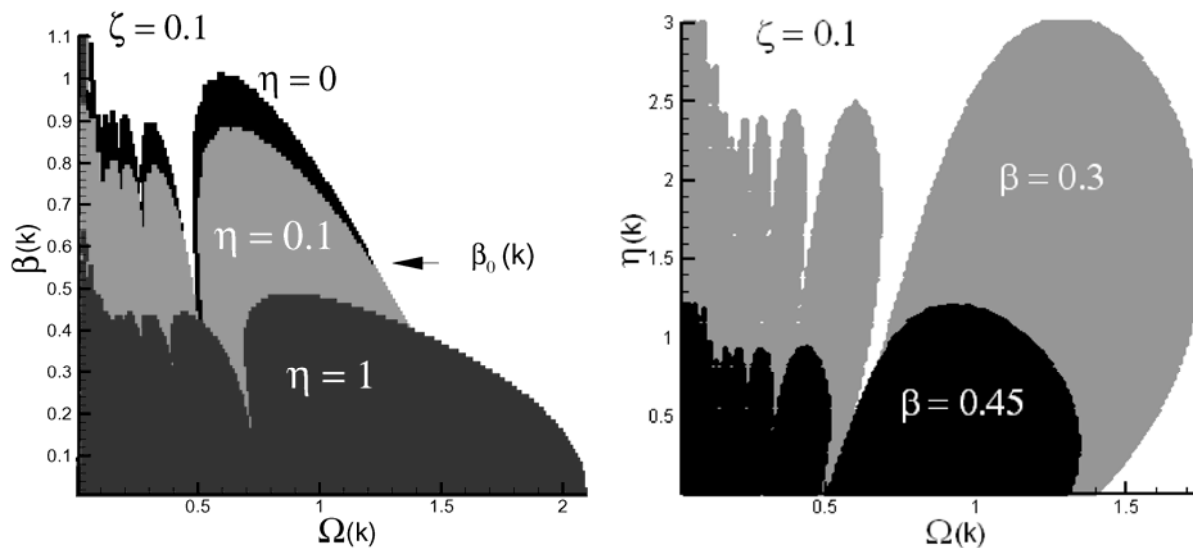


Figure 7. Left - Resonance regions $\Omega(k) - \beta(k)$ diagram at different values of the nonequilibrium parameter; Right - Resonance regions $\Omega(k) - \eta(k)$ diagram at different values of β .

6. Breakpoint Phenomenon

6.1. Breakpoint in the IVC

Fig. 8 shows the IVC of a stack of 10 IJJ at $\alpha = 1$, $\beta = 0.2$ and $\gamma = 0$. The dash line corresponds to the result of calculations without noise (round of error less than 10^{-15}), while the solid line corresponds to the result of calculations with a small noise in the current with its maximum in the interval $(-10^{-8}, +10^{-8})$. As we can see, a branch structure is not observed without noise at these values of model parameters. Opposite, in case with noise the branching of IVC with equidistant branch structure is observed. Later we will return to the discussion of the noise effect on the branching in the IVC.

In the inset of Fig. 8 we have shown the outermost branch near the breakpoint where the curves with noise and without noise separate from each other.

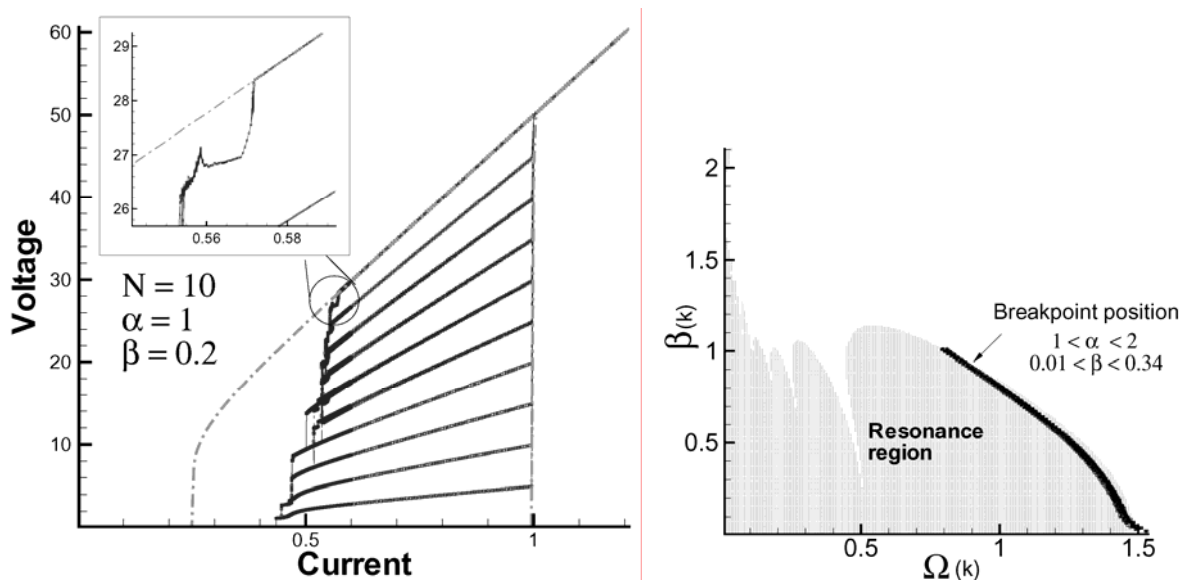


Figure 8. (a) IV-characteristic of a stack of 10 IJJ at $\alpha = 1$, $\beta = 0.2$ and $\gamma = 0$. From Ref.[15]; (b) Parametric resonance region in $\Omega(k) - \beta(k)$ diagram. Black dots (stripe) correspond to the breakpoint current I_{bp} in the IVC for $k = \pi$ at different values of parameters α and β . (From Ref.[16])

6.2. The origin of the breakpoint on the outermost branch

To explain the observed features of the finite-stack IVC let us discuss the origin of the breakpoint on the outermost branch. The hysteresis jump in the IVC is associated with a change of the distribution pattern of rotating phase motions.[18] But the question of why a change in the current leads to a change in the distribution pattern of the rotating phase motions is still open.

As we mentioned above, the outermost branch in the IVC corresponds to the state of the stack with all junctions in the rotating state. Let us write an equation for the difference of the phase differences $\delta_l = \varphi_{l+1} - \varphi_l$ for the outermost branch.

By subtracting Eq. (15) for the $(l+1)$ th from that for the (l) th junction we get

$$(\ddot{\varphi}_{l+1} - \ddot{\varphi}_l) + (1 - \alpha \nabla^{(2)}) \{ \sin(\varphi_{l+1}) - \sin(\varphi_l) + \beta(\dot{\varphi}_{l+1} - \dot{\varphi}_l) \} = 0 \quad (35)$$

Here $\nabla^{(2)} f_l = f_{l+1} + f_{l-1} - 2f_l$ is the discrete Laplacian. Consider the linear approximation $\sin(\varphi_{l+1}) - \sin(\varphi_l) \approx \delta l \cos(\varphi)$, where $\varphi \simeq \Omega t = \frac{1}{N} V t$, Ω is the Josephson frequency, and V is the total voltage of the stack, we obtain

$$\ddot{\delta}_l + (1 - \alpha \nabla^{(2)}) (\cos(\varphi) \delta_l + \beta \dot{\delta}_l) = 0 \quad (36)$$

Expanding $\delta_l(t)$ in the Fourier series

$$\delta_l(t) = \sum_k \delta_k e^{ikl} \quad (37)$$

the linearized equation for the Fourier component of the difference of the phase differences δ_k between neighbor junctions can be written in the form[15]

$$\ddot{\delta}_k + \beta(k) \dot{\delta}_k + \cos(\Omega(k)\tau) \delta_k = 0, \quad (38)$$

where $\tau = \omega_p(k)t$, $\omega_p(k) = \omega_p C_\alpha$, $\beta(k) = \beta C_\alpha$, $\Omega(k) = \Omega/C_\alpha$ and $C_\alpha = \sqrt{1 + 2\alpha(1 - \cos(k))}$.

The important fact for us is that this linearized equation manifests a parametric resonance in the system of IJJs. In Fig. 8(left) we plot the resonance region for this equation on the $\beta(k) - \Omega(k)$ diagram. The dark stripe on this figure is actually the distribution of the dots, corresponding to the positions of the breakpoints of the outermost branch. Using the breakpoint values of the voltage in the equation $\Omega(k) = \Omega/C_\alpha = V/NC_\alpha$, we obtain this distribution of the breakpoints by the variation of the coupling parameter α in the interval (1,2) with a step 0.1 and the dissipation parameter β in the interval (0.01,0.34) with the step 0.01 at each value of α . The breakpoints are inside the resonance region, i.e., the resonance between the Josephson and plasma oscillations is approached at the breakpoint current I_{bp} . As a result, the plasma mode is excited by the Josephson oscillations. We can prove this statement directly. By the Maxwell equation, $\text{div}(E/d) = 4\pi\rho$, we express the charge ρ_l on the superconducting (S) layer l by the voltages $V_{l,l-1}$ and $V_{l,l+1}$ in the neighboring

insulating layers $\rho_l = \frac{\epsilon_0}{4\pi d_0 d} (V_{l,l+1} - V_{l-1,l})$. The investigation of the time dependence of ρ_l demonstrates that with periodic BCs in the stacks with 10 IJJs a LPW with $k = \pi$ is realized. The wavelengths of the standing LPWs that can be realized in a stack with N junctions are N/n lattice units in the z direction, where n changes from 1 to $N/2$ for stacks with an even number of junctions and from 1 to $(N-1)/2$ for odd N . The voltage of the stack at the breakpoint is related to the wave number k of the LPW by the formula $V = N\Omega(k)\sqrt{1 + 2\alpha(1 - \cos(k))}$, so the largest breakpoint voltage V in the current decreasing process corresponds to the creation of a LPW with k equal to π (π mode) for stacks with even numbers of IJJs and modes with $k = (N-1)\pi/N$ for stacks with odd N .

6.3. IVC for stacks with different numbers of IJJs

The outermost branch corresponds to the state of the stack with all junctions in the rotating (R) state [18] and it is the upper branch in the IVC. The values of the breakpoint current I_{bp} and transition current I_j (the jumping point to the next branch in the IVC) on the outermost branch are shown by arrows in Fig. 9a. The distance between these two values we call as the width w_{bp} of the BPR. We have found that the breakpoint current I_{bp} and BPR width w_{bp} depend on the parameters α and β , the boundary conditions, and the number of junctions in the stack. Let us first describe the main features of the BPR which follow from the results of the simulation. As we can see in Fig. 9a, at $\gamma = 0$ both I_{bp} and I_j increase with N , but the increase of I_{bp} is monotonic. The IVC of the stacks with even N has larger w_{bp} at small N . The width of the

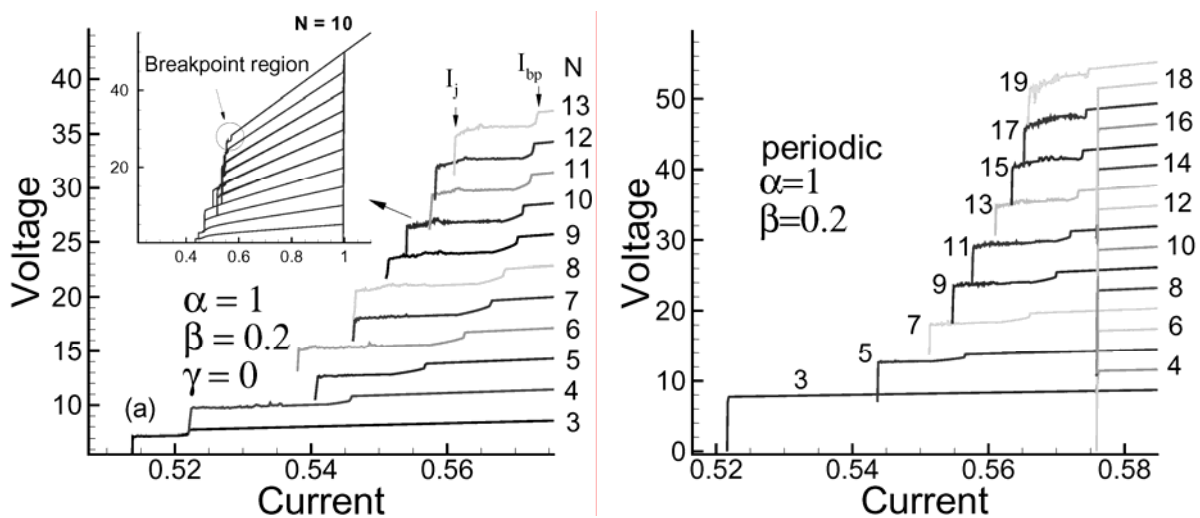


Figure 9. (a) IVC of the outermost branch for stacks with different numbers N of IJJs at $\gamma = 0$; (b) the same at periodic BCs. (From Ref.[16])

BP region is decreased with N . There is a saturation of N -dependence of the I_{bp} at large N . The IVC with periodic boundary conditions (Fig. 9b) shows the same behavior for the I_{bp} and BPR width w_{bp} for the stacks with odd N as in the nonperiodic case, but for the stacks with even N the value of I_{bp} does not depend on N and the BPR for these stacks is absent. In the stack with 10 IJJs a LPW with $k = (N - 1)\pi/N$ is created and it leads to an increase of I_{bp} with N and its saturation to a value corresponding to the π mode. As Fig. 9 shows, with periodic BCs we observe the same value of I_{bp} in all the stacks with even N . This is in agreement with our suggestion that in this case a LPW with $k = \pi$ is created. We check it directly as well, by the time dependence of ρ_l . We find that at periodic BCs in the stacks with even N the charge on the nearest neighbor layers has the same value and opposite sign which means that a LPW with $k = \pi$ is realized. In the stacks with odd N the π -mode cannot exist, so the LPW with the largest k equal to $(N - 1)\pi/N$ is created. The creation of different modes of the LPW leads to different I_{bp} , and this fact explains the difference in the IVC with periodic BCs of the stacks with even and odd numbers of IJJs. With increase in N the wave number k reaches the limiting value π and it leads to the increase in I_{bp} that we observe in Fig. 9(right). Finally, we note that in the case of coupling between junctions the parameter β cannot be determined in the usual way by the return current, because it depends now on two parameters β and α . The dependence of I_{bp} and the BPR width w_{bp} on the dissipation and coupling parameters opens an opportunity to develop a new method for determination of these parameters for stacks of IJJs.

6.4. The α and β dependence of the breakpoint current

A system of dynamical equations in the capacitively coupled Josephson junctions model with diffusion current (CCJJ+DC model)[12, 13]

$$\begin{aligned} \frac{d^2}{dt^2}\varphi_l = & (I - \sin \varphi_l - \beta \frac{d\varphi_l}{dt}) + \alpha(\sin \varphi_{l+1} + \sin \varphi_{l-1} \\ & - 2 \sin \varphi_l) + \alpha\beta(\frac{d\varphi_{l+1}}{dt} + \frac{d\varphi_{l-1}}{dt} - 2\frac{d\varphi_l}{dt}) \end{aligned} \quad (39)$$

for the gauge-invariant phase differences $\varphi_l(t)$ between superconducting layers (S-layers) for the stacks with a different number of intrinsic junctions has been numerically solved.

The CCJJ+DC model is different from the CCJJ model[4, 18, 19] by the last term on the right hand side. This coupled Ohmic dissipation term might be derived by the microscopic theory[12] or phenomenologically by the inclusion of the diffusion current between S-layers and leads to the equidistant branch

structure in the IVC.[13] The details concerning the system (39) are presented in Ref.[13] Here we use the periodic boundary conditions considering the first S-layer as a neighbor of the last one. The simulated IVC have the breakpoint on their outermost branches. We have calculated the β -dependence of the BPC I_{bp} at fixed value of α , changing β in the interval (0,1) by step 0.005. The result of the calculation at $\alpha = 0, 1$ and 5 is presented in Fig. 10a.

At $\alpha = 0$, the IVC does not manifest the multibranch structure, and the breakpoint coincides with the return current. The curves at $\alpha \neq 0$ have new features in comparison with the case without coupling. Particularly, they show a stronger increase of the I_{bp} at small β , a plateau at $I_{bp} \simeq 0.83$ and the oscillation of the I_{bp} on this plateau, and a transition to the non-hysteretic regime (second plateau) at smaller β . These features are discussed below. We change the coupling parameter α in the interval (0,8) by step 0.1 and repeat the calculations of the β -dependence of I_{bp} . By this method, we build the three-dimensional picture of the $\alpha\beta$ -dependence of the I_{bp} for a stack with 10 IJJ, which is shown in Fig. 10b. We see two plateaus on this dependence and the oscillations of the I_{bp} on the first one as a function of α and β . We note the next features for the β -dependence : i) At α equal to zero, our results for β -dependence of the I_{bp} coincide with the previous simulation of the β -dependence of the return current[14]; ii) at small β , the β -dependence is getting sharper with the increase in α ; iii) the oscillations of the I_{bp} are getting stronger at larger α ; iiiii) with the increase in α , the transition to the non-hysteretic regime (to the second plateau) is approached at smaller β . For the α -dependence

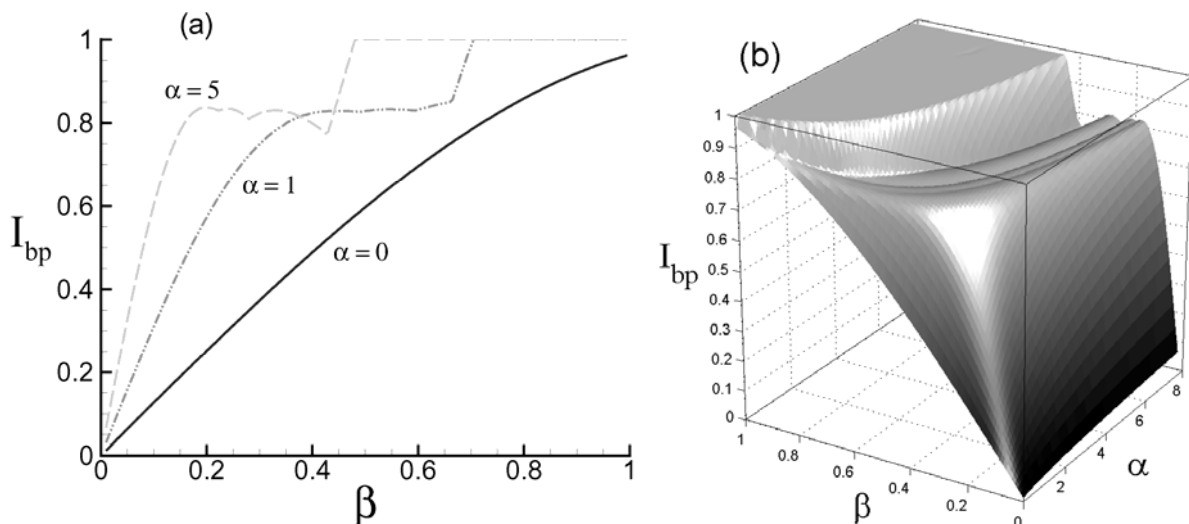


Figure 10. (a) The β -dependence of the BPC I_{bp} of the outermost branch in the IVC at different values of coupling parameter α ; b) The $\alpha\beta$ -dependence of the I_{bp} for a stack of 10 IJJ. (From Ref.[17])

of the I_{bp} we may note: i) At small β , the α -dependence is monotonic, and I_{bp} is increasing with α ; ii) at some β , the oscillations of I_{bp} appear, iii) with the increase in β , the transition to the non-hysteretic regime is observed at smaller α . The value of the I_{bp} changes strongly at small α and β . On the first plateau, the variation of the I_{bp} consists of $\simeq 3 \div 4$ percent of the value of I_c for $N = 10$. As we can see below, it depends on the number of junctions in the stack and decreases with N .

Let us analyze in more detail the α - and β -dependence of the I_{bp} . Fig. 10a demonstrates the general features of β -dependence of the I_{bp} at different values of the coupling parameter. To clearly show these features, we demonstrate in Fig. 11a in an increased scale the β -dependence of the I_{bp} at $\alpha = 3$. We can see clearly four maximums of I_{bp} on this curve. Using the Maxwell equation $\text{div}(E/d) = 4\pi\rho$, we express the charge ρ_i on the superconducting layer i by the voltages $V_{i,i-1}$ and $V_{i,i+1}$ in the neighbor insulating layers $\rho_i = \frac{\epsilon_0}{4\pi d_0 d} (V_{i,i+1} - V_{i-1,i})$. Solution of the system of equations (39) gives us the voltages $V_{i,i+1}$ in all junctions in the stack, and it allows us to investigate the time dependence of the charge on each S-layer. We analyze the time dependence of the charge oscillations on S-layers at β equal to 0.24, 0.27, 0.3 and 0.4 (around each maxima).

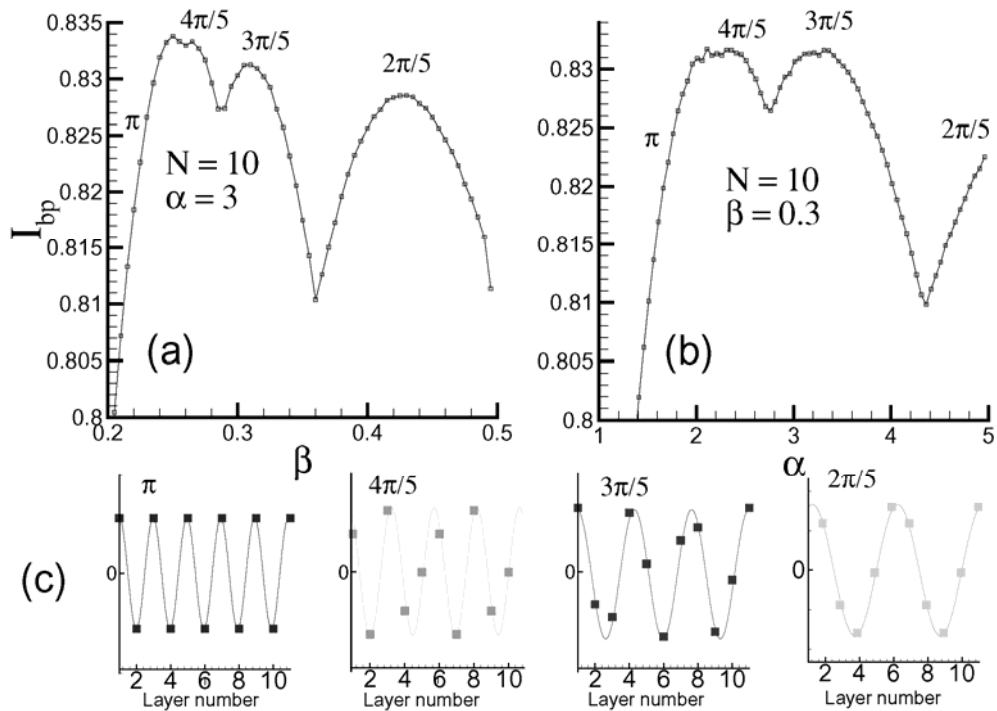


Figure 11. a) The β -dependence of the I_{bp} for a stack with 10 IJJ at $\alpha = 3$; b) The α -dependence of the I_{bp} at $\beta = 0.3$; c) The charge distribution among the layers corresponding to the different plasma modes in the stack of 10 IJJ at $\alpha = 3$ and $\beta = 0.24, 0.27, 0.3, 0.4$. (From Ref.[17])

The charge distributions among the S-layers in the stack at a fixed time moment at the breakpoint of the outermost branch are presented in Fig. 11c. The charge oscillations on S-layers correspond to standing LPW with k equal to π , $4\pi/5$, $3\pi/5$ and $2\pi/5$, relating to the four different intervals of the β with four maximums in this region. Fig. 11b shows the α -dependence of I_{bp} at $\beta = 0.3$, and it demonstrates four regions corresponding to the different modes of LPW.

The ideas and results presented above have strong support from the results of investigation of the α - and β -dependence of the I_{bp} in the case of a different number of IJJ in the stack. The minimal wavelength λ which might be realized in the discrete lattice at periodic boundary conditions is two lattice units. So, in the stack with N junctions, the LPW with $k = 2\pi n/N$ may exist, where n is an integer from 1 to $N/2$ for even N and from 1 to $(N-1)/2$ for odd N . Because of the term $(1 - \cos k)$ in (40), the LPW with k corresponding to the highest I_{bp} in the decreasing current process is created. In Ref.[16], we showed that, at small values of α and β at periodic boundary conditions for stacks with even N , the π -mode of LPW is created, but for stacks with odd N the LPW with $k = (N-1)\pi/N$ is observed. Here we consider a case of strong coupling between junctions, and the results are different from the previous consideration.

6.5. Modeling of the α and β dependence of the BPC

To prove our results and test the idea that at the breakpoint a parametric resonance is approached and plasma mode is excited by Josephson oscillations, we have modeled the $\alpha\beta$ -dependence of the I_{bp} in the CCJJ+DC model. The equation for the Fourier component of the difference of phase differences $\delta\varphi_l = \varphi_{l+1,l} - \varphi_{l,l-1}$ between neighbor junctions is[15] $\ddot{\delta}_k + \beta(k)\dot{\delta}_k + \cos(\Omega(k)\tau)\delta_k = 0$, where $\tau = \omega_p(k)t$, $\omega_p(k) = \omega_p C$, $\beta(k) = \beta C$, $\Omega(k) = \Omega/C$ and $C = \sqrt{1 + 2\alpha(1 - \cos(k))}$. This equation shows a resonance with changing its parameters $\beta(k)$ and $\Omega(k)$.

In Fig. 12a, we have plotted the parametric resonance region for this equation on the diagram $\beta(k) - \Omega(k)$. Using this diagram, we determine the curve which corresponds to the edge of the resonance region. This curve is shown in Fig. 12a by dots. We consider that the point on this curve corresponding to $\max\Omega(k)$ at a fixed value of $\beta(k)$ gives us the value of the $\Omega_{bp}(k)$ which corresponds to the breakpoint voltage. Taking into account the relations for the outermost branch $\Omega_{bp}(k) = V_{bp}/(N\sqrt{1 + 2\alpha(1 - \cos k)})$ and $V_{bp}/N = I_{bp}/\beta$, we get

$$I_{bp}(\alpha, \beta, k) = \beta\sqrt{1 + 2\alpha(1 - \cos k)}\Omega_{bp}(k, \beta). \quad (40)$$

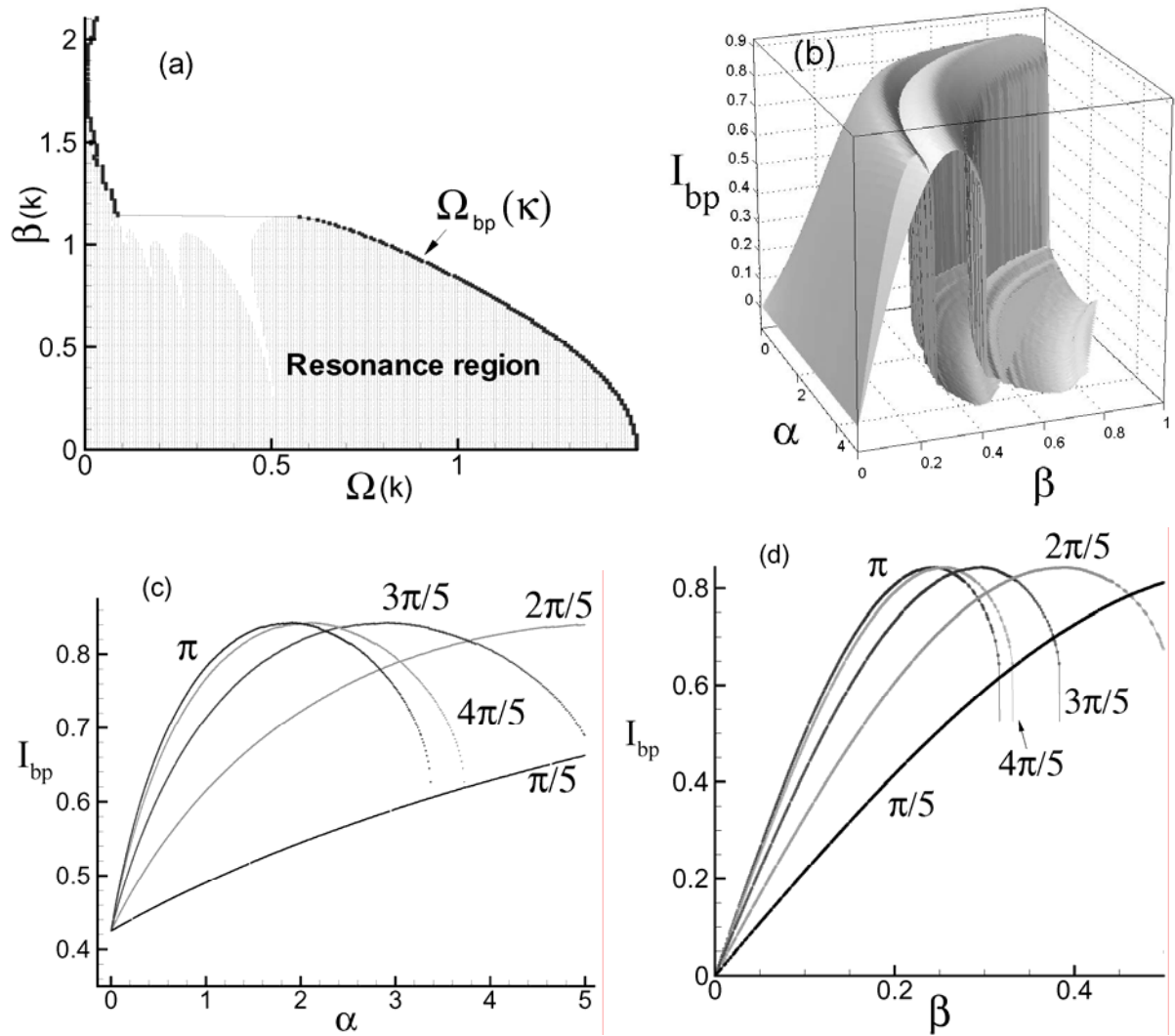


Figure 12: a) Parametric resonance region in $\Omega(k)$ – $\beta(k)$ diagram. The value $\Omega(k) = \Omega_{bp}(k)$ corresponds to the breakpoint voltage on the outermost branch; b) Result of modeling of the $\alpha\beta$ -dependence of the I_{bp} for plasma modes with $k = \pi$ and $k = 2\pi/5$ for a stack of 10 IJJ; c) The modeled α -dependence of I_{bp} for stack with 10 IJJ at $\beta = 0.3$ corresponding to the creation of the LPW with different k ; d) The modeled β -dependence of I_{bp} at $\alpha = 3$. From Ref.[17]

As an example, using the expression (40) for I_{bp} , we have plotted in Fig.12b the three-dimensional $\alpha\beta$ -dependence of the I_{bp} for two plasma modes with $k = \pi$ and $k = 2\pi/5$ for a stack with 10 IJJ. Using the formulas (40), we have calculated the α -dependence of the I_{bp} at $\beta = 0.3$ for plasma modes with different wave numbers k . The corresponding curves are presented in Fig. 12c. We will see that these results of modeling coincide qualitatively with the results of simulation presented Fig.10 and Fig.11. Both kinds of curves show the same behavior. We can see the increase in the distance between the maximums of I_{bp} and their sloping with increase in k in simulated and modeled

curves. Fig. 12d shows the modeled β -dependence of I_{bp} at $\alpha = 3$. This dependence is in agreement with the results of simulation as well, and it demonstrates the oscillations of the I_{bp} , but it does not reflect the decrease in the values of I_{bp} maximums, which is shown in Fig. 11a. This is a result of the approximations we have used to obtain the linearized equation for the Fourier component of the difference of phase differences for neighbor junctions.[15] The theoretical considerations which we use to model the $\alpha\beta$ -dependence of the I_{bp} , lead to the conclusion that there are regions on the $\alpha\beta$ -dependence of I_{bp} which correspond to the creation of the LPW with a different wave number k and explain the origin of the I_{bp} oscillations.

6.6. Group behavior. The $k - \alpha\beta$ method

Fig. 13 shows the result of simulation of the outermost branch in the IVC near the breakpoint for a stack with $\alpha = 3$, $\beta = 0.3$ and N from $N = 3$ to $N = 15$.

We can see that the value of I_{bp} depends on the number N of IJJ in the stack, excluding the stack with $N = 3n$, where n is an integer number. Time dependence analysis of the charge oscillations on the S-layers shows that, at the breakpoint in the stacks with $N = 3n$, the LPW with $k = 2\pi/3$ is created. In the stack with $N = 4$, we observe the LPW with $\lambda = 4$. We will not touch the question concerning the breakpoint region in the IVC presented in Fig. 13. It will be considered in detail somewhere else. We may note another interesting group behavior of the IVC, presented in Fig. 13. There is a monotonic increase of the I_{bp} with N for stacks with $N = 3n + 1$, $n \geq 1$. The same monotonic behavior

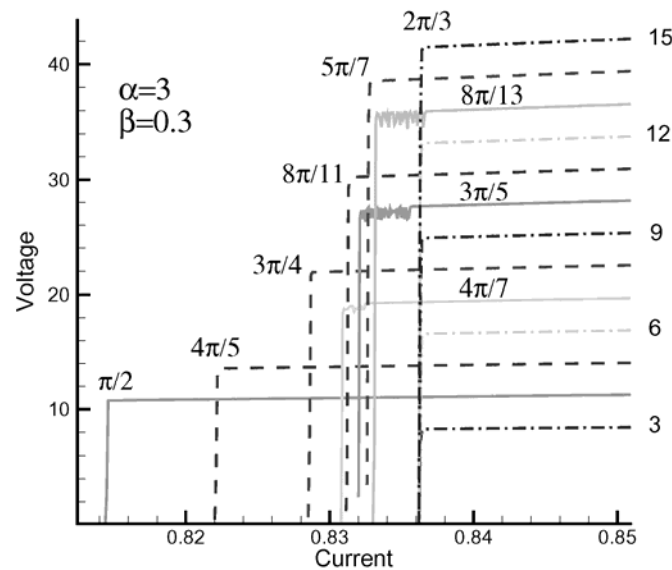


Figure 13. The simulated IVC of the outermost branch in the stacks with a different number of junctions at $\alpha = 3$, $\beta = 0.3$. (From Ref.[17])

was observed for stacks with $N = 3n + 2$. Below, we explain these results using the idea of LPW creation at the breakpoint. Comparison of the α - or β -dependence of the I_{bp} for stacks with a different number of IJJ give us a simple method to determine the wave numbers k of the LPW.

Fig. 14a shows the β -dependence of the I_{bp} at $\alpha = 3$ for the stacks with 3, 6, 9 and 12 IJJ. It demonstrates that, in some intervals of β , the stacks with different N have the equal value of the I_{bp} . Particularly, all stacks have the equal values of the I_{bp} in some interval around $\beta = 0.3$. According to the results of modeling for the stack with given N , the intervals on the curves of the α - and β -dependence corresponding to the different modes of the LPW, follow in decreasing order in k . Because the interval around $\beta = 0.3$ corresponds to the regions around the maximum on the β -dependence of the I_{bp} for stack with $N = 3$, the second maximum for the stacks with $N = 6$ and $N = 9$, and the third maximum for the stack with $N = 12$, we may conclude that in this interval the LPW with $k = 2\pi/3$ is created. For stacks with $N = 6$ this interval is continued until $\beta = 0.365$. Using this method of the wave number determination, which we call as $k - \alpha\beta$ -method, we can determine all modes of LPW which might be created in stacks with different parameters α and β and a different number of IJJ. Particularly, we find that on the β -dependence the interval $(0, 0.27)$ and the region $\beta > 0.41$ correspond to the creation of the π - and $\pi/3$ - modes of LPW, respectively. From the α -dependence of the I_{bp} which is presented in

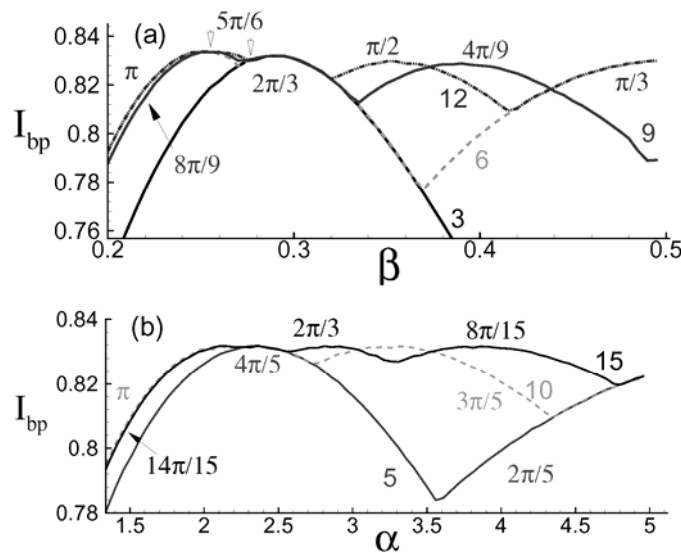


Figure 14. a) The simulated β -dependence of the I_{bp} for the stacks with 3, 6, 9 and 12 IJJ at $\alpha = 3$. The region corresponding to the creation of the LPW mode with wave number $k = 5\pi/6$ is shown by arrows. b) The simulated α -dependence of the I_{bp} for the stacks with 5, 10 and 15 IJJ at $\beta = 0.3$. (From Ref.[17])

Fig. 14b for stacks with 5, 10 and 15 IJJ, we find that the interval around the maximum with 2.35 and the region $\alpha > 4.82$ correspond to the creation of the $4\pi/5$ - and $\pi/5$ - modes of LPW, respectively. Using the $k - \alpha\beta$ -method, we find the values of k for IVC presented in Fig. 13. In the stacks with $N = 3n$ (dash-dotted curves in Fig. 13), the LPW with the same wave number $k = 2\pi/3$ are created. For the stacks with $N = 3n + 1$ (solid curves), we obtain $k = 2(N - 1)\pi/3N$. This value limits to $2\pi/3$ with an increase in N from the side of smaller values of k . In the stacks with $N = 3n+2$ (dash curves), we get $k = 2(N + 1)\pi/3N$, which limits to $2\pi/3$ from the side of bigger values of k . So, the idea of the LPW creation at the breakpoint explains the group behavior of IVC in Fig. 13. The value of I_{bp} depends on k , but does not depend on N at chosen parameters α and β ; i.e., the creation of the same mode in the stacks with different N leads to the same value of I_{bp} . We may predict a different commensurability manifestation in the IVC of stacks with a different number of IJJ. This is a generalization of the commensurability effect we have observed in Ref.[16] at small α and β .

Let us now discuss this group behavior of the outermost branches in IVC of the stacks with a different number of IJJ in the layered superconductors with $\alpha = 3$ and $\beta = 0.35$. [21] Fig. 15 shows the result of simulation of the outermost branch in the IVC near the breakpoint for a stack with N from $N = 3$ to $N = 30$. We can see that the value of I_{bp} depends on the number N of IJJ in the stack, excluding the stack with $N = 4n$, where n is an integer number. The $k - \alpha\beta$ -method and time dependence analysis of the charge oscillations on the S-layers show that, at the breakpoint in the stacks with $N = 4n$, the LPW with $k = \pi/2$ is created. There is a different monotonic increase of the I_{bp} with N for stacks with $N = 4n+1$, $N = 4n+2$ and $N = 4n+3$, $n \geq 1$, which demonstrate a group behavior of the IVC, presented in Fig. 15. These results find the explanation in the framework of the idea of LPW creation at the breakpoint.

In agreement with time dependence analysis we find that in the stacks with $N = 4n$, the LPW with the wave number $k = \pi/2$ are created and all outermost branches in Fig. 15a have the same value of BPC. For the stacks with $N = 4n+1$, which outermost branches of IVC are shown in Fig. 15b, we obtain $k = (N - 1)\pi/2N$. This value limits to $k = \pi/2$ with an increase in N from the side of smaller values of k . In the stacks with $N = 4n + 2$, which IVCs are shown in Fig. 15c, we get $k = (N + 2)\pi/2N$, which limits to $k = \pi/2$ from the side of bigger values of k . And finally, for the stacks with $N = 4n + 3$ (see Fig. 15d), we obtain $k = (N + 1)\pi/2N$, which limits to $k = \pi/2$ from the side of bigger values of k as well. So, all outermost branches of IVC in the stack with $\alpha = 3$ and $\beta = 0.35$ are distributed in four groups and the idea of the LPW creation at the breakpoint explains this group behavior of IVC in Fig. 15.

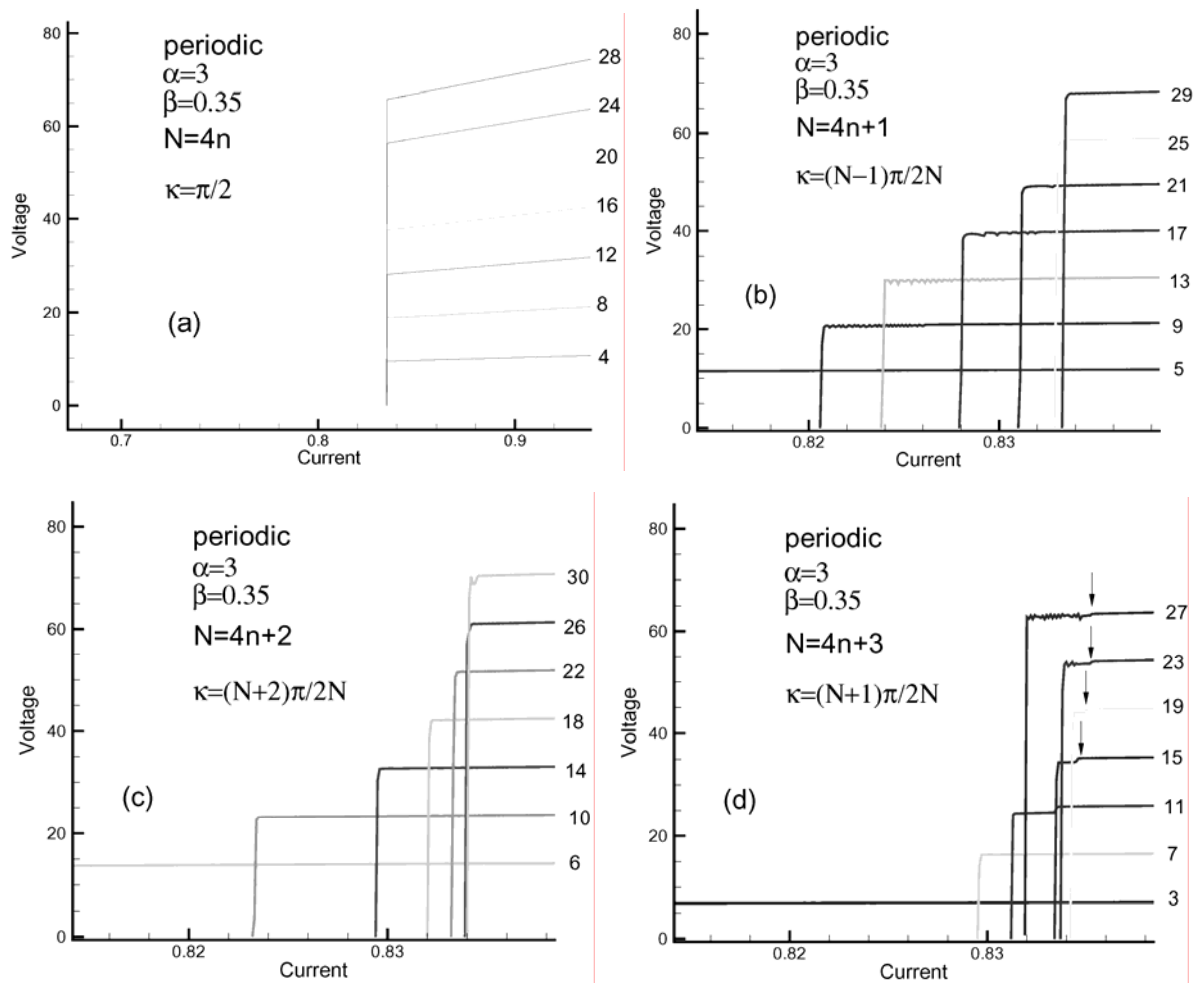


Figure 15. The simulated IVC of the outermost branch at $\alpha = 3$, $\beta = 0.35$ in the stacks with a different number of junctions: (a) $N=4n$; (b) $N=4n+1$; (c) $N=4n+2$; (d) $4n+3$, where n is integer number. (From Ref.[21])

6.7. Breakpoint on the other branches. One oscillating junction

Let us now discuss briefly the breakpoints on the other branches of the IVC. As we mentioned above, the resistive state in the system of IJJs is realized as a state with different numbers of R and O junctions.[18, 19] The different positions of R and O junctions in the stack (different configurations) correspond to different states of the IJJs system. Equidistant positions of the O junction from the ends of the stack (for example, stacks with first or tenth O junction) lead to the same state. So there are five different states in the stack with one O junction corresponding to the different position of this junction. Figure 16 shows the BPR on the branches of the IVC of stacks with one O junction in the case of ten IJJs at $\alpha = 1$, $\beta = 0.2$, and $\gamma = 0$. Equidistant positions of the O junction from the ends of the stack lead to the same value of

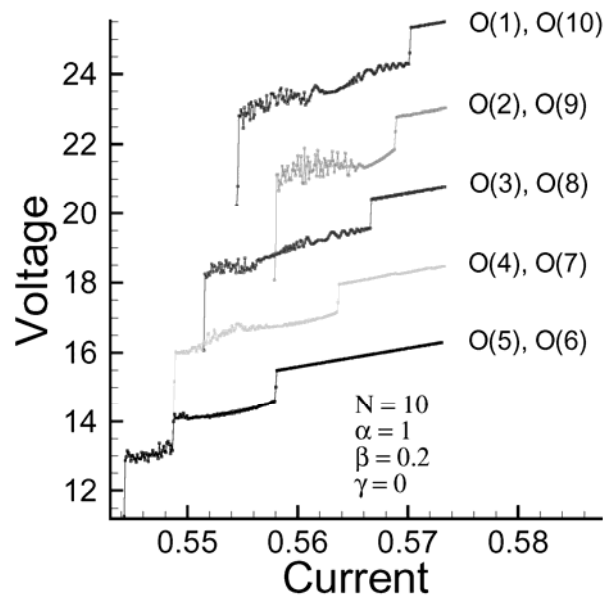


Figure 16. BPR on the branches of the IVC of stacks with one oscillating junction in the case of ten IJJs at $\alpha = 1$, $\beta = 0.2$, and $\gamma = 0$. The top curve corresponds to the real scale of voltage, but the others are shifted down for clarity by two units. (From Ref.[17])

I_{bp} and the same width of the BPR. The shift of the O junction from the end of the stack to its center decreases the I_{bp} of the corresponding state. We can establish a delay of LPW creation in the current-decreasing process when the position of the O junction is shifted to the center of the stack.

We consider that the origin of such behavior is as follows. This one oscillating junction separates the stack into two parts with different numbers of R junctions which are weakly coupled through the O junction. With a decrease in current, the first LPW is created in the part with the largest I_{bp} (with the largest number of junctions). The shift of the O junction and the decrease in the number of R junctions in this part lead to a decrease of I_{bp} as Fig. 10 demonstrates. The increase of the number of junctions in the second part might manifest a second breakpoint which is related to the creation of a LPW in this second part of the stack. This situation is observed for $N = 10$ when the O junction occupies the fifth or sixth site in the stack. The width of the BPR in the other branches of the IVC depends essentially on the state of the stack. For the other branches, the increase in the number of O junctions in the stack decreases the number of effective junctions for creation of the LPW and leads to a decrease of the return current. This fact explains why we can obtain a total branch structure in the hysteresis region, because in the other case we would not be able to observe it in the simulation. The correspondence between the position of the O junction in the stack and the value of I_{bp} opens the possibility

for junction diagnostics, i.e., by measuring the value of I_{bp} we can answer the question of which junction in the stack goes into the R or O state. From the other side, the monitoring of the transitions between branches is useful for understanding the phase dynamics in a system of IJJs.

7. Conclusion

In this review we presented the results of the numerical calculations of the current-voltage characteristics of intrinsic Josephson junctions to clarify their dependence on the coupling constant and dissipation parameter β ($\beta^2 = 1/\beta_c$, where β_c is McCumber parameter). We showed that coupling between junctions changes crucially the dependence of the return current on a dissipation parameter. Particularly, it leads to the appearance of the plateau on the β -dependence of the BPC on the outermost branch and the oscillation of the BPC as a function of β . Using the idea that at the breakpoint the parametric resonance is approached and a longitudinal plasma wave is created, we modeled the α - and β -dependence of the BPC and obtained good agreement with the results of the numerical simulation. We demonstrated that the study of the α - and β -dependence of the BPC for the stacks with a different number of IJJ gives us the instrument to determine the wave number of the LPW.

Acknowledgments

We thank P. Müller, R. Kleiner, A. Ustinov, T. Koyama, M. Machida, A. Yurgens, Yu. Latyshev, A. Irie, G. I. Oya, M. Suzuki, T. Hatano, H. Wang, N.F. Pedersen, P. Seidel, M. Sargolzaei, T. L. Boyadjev, N. M. Plakida, Y. Sobouti, M. R. H. Khajepour for stimulating discussions and support of this work.

References

1. Kleiner, R., Steinmeyer, F., Kunkel, G., and Müller, P. 1992, Phys. Rev. Lett., 68, 2394.
2. Oya, G., Aoyama, N., Irie, A., Kishida, S., and Tokutaka, H. 1992, Jpn. J. Appl. Phys., 31, L829.
3. Bulaevskii, L.N., Dominguez, D., Maley, M., Bishop, A., Ivlev, B. 1996, Phys. Rev. B, 53, 14601.
4. Koyama, T. and Tachiki, M. 1996, Phys. Rev. B, 54, 16183.
5. Machida, M., Koyama, T., and Tachiki, M. 1998, Physica C, 300, 55.
6. Machida, M., Koyama, T., and Tachiki, M. 1999, Phys. Rev. Lett., 83, 4816.
7. Ryndyk, D.A. 1998, Phys. Rev. Lett., 80, 3376; Ryndyk, D.A., Keller, J., and Helm, Ch. 2002, J. Phys.: Condens. Matter, 14, 815.

8. Helm, Ch., Preis, Ch., Forsthofer, F., Keller, J., Schlenga, K., Kleiner, R., and Muller, P. 1997, *Phys. Rev. Lett.*, 79, 737; Preis, Ch., Helm, Ch., Schmalzl, K., Keller, J., Kleiner, R., and Muller, P. 2001, *Physica C*, 362, 51.
9. Shukrinov, Yu.M., Nasrulaev, Kh., Sargolzaei, M., Oya, G., and Irie, A. 2002, *Supercond. Sci. Technol.*, 15, 178.
10. Seidel, P., Grib, A.N., Shukrinov, Yu.M., Scherbel, J., Hubner, U., and Schmidl, F. 2001, *Physica C*, 362, 102.
11. Ryndyk, D.A. and Keller, J. 2005, *Phys. Rev. B*, 71, 054507.
12. Machida, M., Koyama, T., Tanaka, A., and Tachiki, M. 2000, *Physica C*, 330, 85.
13. Shukrinov, Yu.M., Mahfouzi, F., and Seidel, P. 2006, *Physica C*, 449, 62.
14. McCumber, D.E. 1968, *J.Appl.Phys.*, 39, 3113; Steward, W.C. 1968, *Appl.Phys.Lett.*, 12, 277.
15. Shukrinov, Yu.M. and Mahfouzi, F. 2007, *Supercond. Sci.Technol.*, 19, S38-S42.
16. Shukrinov, Yu.M., Mahfouzi, F., and Pedersen, N.F. 2007, *Phys. Rev. B*, 75, 104508.
17. Shukrinov, Yu.M. and Mahfouzi, F. 2007, *Phys. Rev. Lett.*, 98, 157001.
18. Matsumoto, H., Sakamoto, S., Wajima, F., Koyama, T., and Machida, M. 1999, *Phys. Rev. B*, 60, 3666.
19. Shukrinov, Yu.M. and Mahfouzi, F. 2006, *Physica C*, 434, 6.
20. Shukrinov, Yu.M. and Mahfouzi, F. 2006, *J. Phys. Conf. Ser.*, 43, 1143.
21. Shukrinov, Yu.M. and Mahfouzi, F. 2007, *Materials of SNS2007, Sendai, Aug.20-24.*